

1983

A mathematical model for small tidal streams capable of simulating both short-term and long-term water quality variations

Stephen Anthony Williams

College of William and Mary - Virginia Institute of Marine Science

Follow this and additional works at: <https://scholarworks.wm.edu/etd>



Part of the [Applied Mathematics Commons](#), [Environmental Sciences Commons](#), and the [Hydrology Commons](#)

Recommended Citation

Williams, Stephen Anthony, "A mathematical model for small tidal streams capable of simulating both short-term and long-term water quality variations" (1983). *Dissertations, Theses, and Masters Projects*. William & Mary. Paper 1539617542.

<https://dx.doi.org/doi:10.25773/v5-g25z-9653>

This Thesis is brought to you for free and open access by the Theses, Dissertations, & Master Projects at W&M ScholarWorks. It has been accepted for inclusion in Dissertations, Theses, and Masters Projects by an authorized administrator of W&M ScholarWorks. For more information, please contact scholarworks@wm.edu.

A MATHEMATICAL MODEL FOR SMALL TIDAL STREAMS
CAPABLE OF SIMULATING BOTH SHORT-TERM
AND LONG-TERM WATER QUALITY VARIATIONS

A Thesis

Presented to

The Faculty of the School of Marine Science
The College of William and Mary

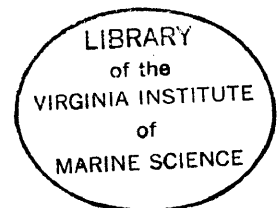
In Partial Fulfillment

Of the Requirements for the Degree of
Master of Arts

by

Stephen Anthony Williams

1983



X

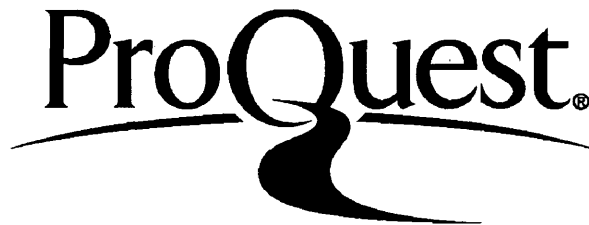
ProQuest Number: 10626453

All rights reserved

INFORMATION TO ALL USERS

The quality of this reproduction is dependent upon the quality of the copy submitted.

In the unlikely event that the author did not send a complete manuscript and there are missing pages, these will be noted. Also, if material had to be removed, a note will indicate the deletion.



ProQuest 10626453

Published by ProQuest LLC (2017). Copyright of the Dissertation is held by the Author.

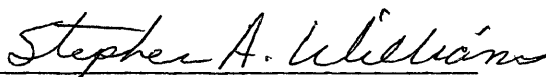
All rights reserved.

This work is protected against unauthorized copying under Title 17, United States Code
Microform Edition © ProQuest LLC.

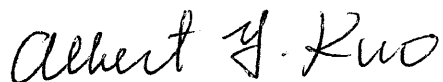
ProQuest LLC.
789 East Eisenhower Parkway
P.O. Box 1346
Ann Arbor, MI 48106 - 1346

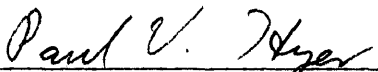
APPROVAL SHEET

This thesis is submitted in partial fulfillment of
the requirements for the degree of
Master of Arts in Marine Science

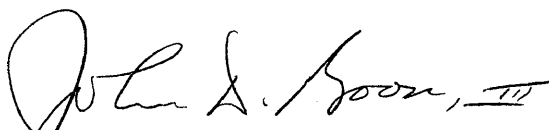

Stephen Anthony Williams

Approved, April 1983


Albert Y. Kuo, Ph.D.


Paul V. Hyer, Ph.D.


Ching Seng Fang, Ph.D.


John D. Boon, III, Ph.D.

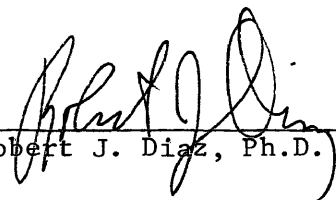

Robert J. Diaz, Ph.D.

TABLE OF CONTENTS

	PAGE
ACKNOWLEDGEMENTS	iv
LIST OF TABLES	v
LIST OF FIGURES	vi
ABSTRACT	x
CHAPTER I. INTRODUCTION	2
CHAPTER II. THE MATHEMATICAL FORMULATION OF THE MODEL	12
CHAPTER III. MATHEMATICS OF SOLUTION	34
CHAPTER IV. MODEL APPLICATION - A CASE STUDY	50
CHAPTER V. SUMMARY AND CONCLUSIONS	112
CHAPTER VI. DISCUSSION AND RECOMMENDATIONS	116
APPENDIX. RESULTS OF MODEL VALIDATION	119
REFERENCES	142
VITA	146

ACKNOWLEDGEMENTS

The author thanks the members of his committee and the faculty and students of the Department of Physical Oceanography and Hydraulics of the School of Marine Science for their help and guidance throughout this study. Special thanks are extended to Dr. Albert Y. Kuo for his patient encouragement and support.

Thanks are also extended to Shirley Crossley and Nancy Courtney for their help in the preparation of the manuscript.

This study was funded by the Virginia State Water Control Board through the Cooperative State Agencies Program.

Dedicated to my wife, Lisa.

LIST OF TABLES

Table	Page
I. Physical Parameters.....	55
II. STP Field Measurements (12 hour composite samples) and Corresponding Model Point Source Inputs.....	69
III. Nonpoint Source Loadings.....	70
IV. Concentrations of Nonpoint Runoff as Predicted by NVPDC Versus Field Measurements at Station 7.....	72
V. Downstream Boundary Conditions.....	73
VI. Calibration Parameters - Water Quality Submodel.....	75
VII. Point Source Loadings for Model Validation Run.....	89

LIST OF FIGURES

Figure	Page
1. Definition sketch - irregular channel.....	15
2. Schematic of Ecosystem Model.....	24
3. Schematization of a tidal creek.....	34
4. Time variations of tidal height and velocity at the channel entrance.....	46
5. Time variations of tidal height and velocity at the midpoint of the channel.....	46
6. Time variations of tidal height and velocity near the closed-end of the channel.....	47
7. Longitudinal distribution of tidal amplitude along a closed-end channel.....	48
8. Longitudinal distribution of the amplitude of tidal current along a closed-end channel.....	48
9. Little Hunting Creek sample stations.....	51
10. Model segmentation.....	54
11. Tidal simulation - station 5 (2.5 km).....	60
12. Current velocity simulation.....	61
13. Hour 4 (1900) of dye dispersion simulation.....	63
14. Hour 8 (2300) of dye dispersion simulation.....	63
15. Hour 12 (0300) of dye dispersion simulation.....	64
16. Hour 16 (0700) of dye dispersion simulation.....	64
17. Hour 20 (1100) of dye dispersion simulation.....	65
18. Hour 24 (1500) of dye dispersion simulation.....	65

Figure	Page
19. Cycle 3.5 (low slack) - dye dispersion simulation.....	66
20. Cycle 4.0 (high slack) - dye dispersion simulation.....	66
21. Cycle 6.0 (high slack) - dye dispersion simulation.....	67
22. Cycle 8.0 (high slack) - dye dispersion simulation.....	67
23. Calibration results - organic nitrogen.....	77
24. Calibration results - ammonia nitrogen.....	77
25. Calibration results - nitrite-nitrate nitrogen.....	78
26. Calibration results - organic phosphorus.....	78
27. Calibration results - inorganic (ortho) phosphorus.....	79
28. Calibration results - CBOD.....	79
29. Calibration results - chlorophyll 'a'.....	80
30. Calibration results - dissolved oxygen.....	80
31. Ammonia - field data (August, 1980 intensive survey) versus model results.....	81
32. Chlorophyll 'a' - field data (August, 1980 intensive survey) versus model results.....	83
33. Dissolved oxygen - field data (August, 1980 intensive survey) versus model results.....	85
34. Hydrodynamic submodel validation - predictions of upstream tidal heights versus field data.....	88
35. Model predictions versus field measurements of chlorophyll 'a' from the June, 1980 diurnal survey.....	94
36. Model predictions versus field measurements of DO from the June, 1980 diurnal survey - nonpoint DO set to 10.0 mg/l.....	96
37. Model predictions versus field measurements of DO from the June, 1980 diurnal survey - nonpoint DO set to 4.2 mg/l.....	97

Figure	Page
38. Results for ammonia nitrogen - point source inputs set to zero.....	99
39. Results for nitrite-nitrate nitrogen - point source inputs set to zero.....	101
40. Results for organic phosphorus - nonpoint source inputs set to zero.....	102
41. Results for inorganic (ortho) phosphorus - nonpoint source inputs set to zero.....	103
42. Results for chlorophyll 'a' - point source inputs set to zero.....	104
43. Results for chlorophyll 'a' - nonpoint source inputs set to zero.....	105
44. Results for dissolved oxygen - point source inputs for nitrogen, phosphorus and CBOD set to zero.....	106
45. Results for dissolved oxygen - nonpoint source inputs for nitrogen, phosphorus and CBOD set to zero.....	108
46. Results for dissolved oxygen - sediment oxygen demand set to zero.....	109
47. Results for chlorophyll 'a' - downstream boundary conditions set to zero.....	110
A1. Validation results for ammonia - station 2.....	120
A2. Validation results for ammonia - station 3.....	121
A3. Validation results for ammonia - station 4.....	122
A4. Validation results for ammonia - station 5.....	123
A5. Validation results for nitrite-nitrate nitrogen - station 4.....	124
A6. Validation results for nitrite-nitrate nitrogen - station 5.....	125
A7. Validation results for organic nitrogen - station 4.....	126
A8. Validation results for organic nitrogen - station 5.....	127

Figure	Page
A9. Validation results for inorganic phosphorus - station 4....	128
A10. Validation results for inorganic phosphorus - station 5....	129
A11. Validation results for organic phosphorus - station 4.....	130
A12. Validation results for organic phosphorus - station 5.....	131
A13. Validation results for CBOD - station 4.....	132
A14. Validation results for CBOD - station 5.....	133
A15. Validation results for chlorophyll 'a' - station 2.....	134
A16. Validation results for chlorophyll 'a' - station 3.....	135
A17. Validation results for chlorophyll 'a' - station 4.....	136
A18. Validation results for chlorophyll 'a' - station 5.....	137
A19. Validation results for dissolved oxygen - station 4.....	138
A20. Validation results for dissolved oxygen - station 5.....	139
A21. Long-term simulation: nonpoint DO set to 4.2 mg/l - station 4.....	140
A22. Long-term simulation: nonpoint DO set to 4.2 mg/l - station 5.....	141

ABSTRACT

A real time, one-dimensional mathematical model has been developed for use in small tidal streams to investigate both the short-term (intra-tidal and diurnal) fluctuations and the long-term (seasonal) variations in water quality. The model is composed of two submodels - a hydrodynamic submodel and a water quality submodel.

In the hydrodynamic submodel the equations of continuity and momentum are solved simultaneously through the use of a semi-implicit finite difference scheme. The solution of these equations provides information on velocity and surface elevation as functions of longitudinal distance and time. The velocity and surface elevation functions are used to solve the mass-balance equations of the water quality submodel. The solution of the mass-balance equations, via an implicit finite difference scheme, describes the longitudinal and temporal distribution of eight dissolved or suspended substances comprising an 'ecosystem'.

The model has been calibrated and validated using data from the Little Hunting Creek, a small tidal stream joining the Potomac River. The model successfully predicts both the short-term and long-term water quality variations measured in the creek. The model has also been applied as a diagnostic tool to assess the impact of such factors as sediment oxygen demand, sewage treatment plant discharge and nonpoint source wasteloadings on water quality conditions in the creek.

A MATHEMATICAL MODEL FOR SMALL TIDAL STREAMS
CAPABLE OF SIMULATING BOTH SHORT-TERM
AND LONG-TERM WATER QUALITY VARIATIONS

I. INTRODUCTION

The generation of voluminous amounts of wastes by mankind has had its effect on all the earth's water systems. Where large populations are centered or where industry has grown the effect has at times been dramatic. Estuarine systems in general have been greatly affected. Historically these systems are attractive as routes for trade and travel, sources of food and convenient receptacles for wastes. In the nineteenth century new industries situated along the estuaries to take advantage of these 'water roads' for the shipment of raw materials and finished products. The growing centralized population provided the labor force. And, of course, the estuary provided a convenient dumping site for wastes. At present, virtually every major estuary has been significantly polluted or faces pollution problems in the foreseeable future.

Mathematical modeling of water quality is over a half century old, the result of a growing concern with the preservation of our water resources. Over the years models have grown with our advancing knowledge of the complex processes which operate in a waterbody. In many instances water quality models were instrumental in the advancement of our understanding of the hydrographic, chemical and biological interactions in an estuary.

The bulk of the water quality modeling effort has centered on the major estuaries. The use of these water bodies affects large

populations, often spanning more than one county or state. Controversy resulted from the conflicting uses of the estuary by industry, finfish and shellfish harvestors and recreational concerns. Because of the economic benefits to be reaped or lost to a region or state the controversy has often taken on a political edge. It was in this atmosphere that water quality modeling was conceived and has grown, paid for by federal or state taxes or by the commercial concerns affected.

While modeling of the larger estuaries was ongoing, the fates of many smaller tidal streams were ignored and their conditions deteriorated. Often these smaller systems were sacrificed to industry or to the need to dispose of municipal wastes cheaply. In less urban areas, streams were the victims of the unforeseen effects of land runoff bearing excess fertilizer, pesticides or herbicides.

It has grown more apparent, in part due to advances in water quality modeling, that the health of large estuarine systems depends on the health of all its parts. From this fact together with the advances in computer capabilities and efficient numerical techniques, it is apparent that models applicable to water quality problems in small tidal streams are now both economically feasible and desirable. In view of this, mathematical models have been developed as a practical way to analyze factors affecting water quality in small tidal streams.

A mathematical model uses mathematical expressions and equations to represent actions and processes which occur in a real world system. Most of the early efforts at modeling water quality in estuaries were exercises in the rigorous manipulation of the governing equations with the goal of obtaining forms of the equations which would yield

analytical solutions. Since estuaries in general have irregular geometries and complex cause-and-effect relationships, few useful analytic solutions were obtained. Each simplifying assumption made in order to obtain such a solution diminished the model's resemblance to the prototype. As a result, models with analytical solutions usually produced only a rough approximation to the fate of pollutants and that only where the simplifying assumptions were approximately correct.

With the advent of modern digital computers and the refinement of numerical techniques, the length of time needed to produce solutions to complex differential equations has been greatly reduced. Although these techniques do not produce exact solutions, by virtue of the fewer simplifying assumptions involved such models more closely reproduce real world situations and are more generally applicable than estuarine models with analytical solutions.

An array of water quality models are available at present. Each type of model has its advantages and disadvantages and, thus, its own range of applicability. Numerous explanations and comparisons of these various modeling approaches can be found in the literature (e.g., Tracor, Inc., 1971; Nielson, 1977).

Water quality models can be categorized (after Kuo et al., 1979) by (1) the water quality components modeled, (2) the number of spatial dimensions represented, (3) the time scale and (4) the method of representing tidal influence.

Of the single component water quality models the most familiar are the salinity intrusion models (Harleman and Abraham, 1966; Thatcher and Harleman, 1972; Kuo and Fang, 1972). Any unusual movement in the position of the head of the salinity intrusion can have

significant effects on the distribution of ecologically important organisms and may jeopardize supplies of drinking water. Salinity intrusion models are often used to study the effects of proposed changes in the system. Salinity can be used as a natural tracer and salinity models employed as a means of evaluating the dispersion characteristics of a system in preparation for modeling other pollutant concentrations (Cox and Macola, 1967). Other water quality parameters modeled in single component models are excess heat (Koh and Fan, 1970) and hazardous substances (Onishi and Wise, 1978).

On the next level of complexity, and more generally associated with water pollution than are salinity models, are the DO - BOD models. One well known early modeling effort was that of Streeter and Phelps (1925), a first attempt to describe the relationship between dissolved oxygen, atmospheric reaeration and biological or chemical oxidation of the organic loading in a riverine system. This work was later expanded upon by Thomann (1963), Dobbins (1964) and O'Conner (1966) with the inclusion of additional sources and sinks.

In order of increasing complexity, models have been developed in which (1) the oxygen demanding material is separated into nitrogenous (NBOD) and carbonaceous (CBOD) components (Kuo et al., 1975) and (2) an 'ecosystem' is modeled. Included in the last category are models of phytoplankton populations (Thomann et al., 1970) and 'food chain' models which include zooplankton and other consumers (Kremer and Nixon, 1978). In the ecosystem models it is necessary to include the closed loops of the nutrients, nitrogen and phosphorus.

Algal blooms are a frequent result of excess nutrients entering a tidal stream. The presence of large algal populations often are a

major factor in the violation of minimum water quality standards for dissolved oxygen. Decaying algal mats produce undesirable odors. In these situations an ecosystem water quality model would more effectively reproduce system behavior and provide more information as to cause and effect.

The concentration of pollutants in real estuaries vary in the three spatial dimensions as well as in time. Until recently modeling water quality in three dimensions was economically unfeasible and averaging over one or more spatial dimensions was necessary.

Early efforts in estuarine pollution analysis employed the tidal prism concept (Tully, 1949). The classical tidal prism approach entailed the assumptions that a pollutant could be treated as being simultaneously diffused throughout the entire estuary and that none of the polluted water leaving the estuary on the ebb tide returned on the flood. Results are average concentrations over the entire water body for each tidal cycle. Later versions modified the flushing by allowance of some portion of the polluted water exiting on the ebb to return on the flood.

Because of the assumption of complete mixing throughout the system, the classical tidal prism models are limited in their applicability to small embayments and boat basins. Complete mixing at high tide is not possible in estuarine rivers and streams. Ketchum (1951) extended the zero-dimensional tidal prism concept to a one-dimensional approach by dividing the estuary into a number of segments with each segment undergoing complete mixing over a tidal cycle. Other modified tidal prism models are in use today (e.g., Kuo, 1976).

Another one-dimensional approach to water quality modeling employs the mass-balance equation derived by a spatial integration of the three-dimensional equation over the flow cross-section (Okubo, 1964; Holley and Harleman, 1965). This approach owes much to the works of Taylor (1953) and Aris (1956) on dispersion (transport due to spatial deviations of the velocity field).

The basic assumption inherent in one-dimensional models is that vertical and lateral gradients are negligible. These conditions are characteristic of tidal streams with intense tidal mixing. Where significant variations in the vertical and/or lateral directions exist, the modeler must employ either a two-dimensional or even a full three-dimensional representation.

Another aspect in which water quality models have grown increasingly sophisticated through the years is in the handling of the time scale. In early models a steady state (no change with time) was assumed (Thomann, 1963). Given the large variability in the inputs and forces affecting an estuary, a steady state is seldom approached and never achieved in a real system.

Others (Pritchard, 1952 and 1954; O'Conner and DiToro, 1964) formulated time varying models known as tidal average models and slack tide models, respectively. In these models the mass-balance equation is averaged over a time period equal to one tidal cycle. Thus, tidal advection is averaged out of the calculations and its effects appear in a time-averaged dispersion term. These models using intertidal time scales are useful in economically representing longterm fluctuations and large scale spatial gradients in water quality.

Models utilizing time steps of much less than a tidal cycle,

known as 'real time' or 'tidal time' models, have grown in use as computers have grown more sophisticated. Because of the shorter time step involved, these models are able to reproduce intratidal variations that cannot be reproduced by tidal prism, tidal average or slack tide models. It has become increasingly useful to be able to predict the range of concentrations of water quality parameters experienced during a tidal cycle as well as the average concentration. While real time models are able to predict variations within a tidal cycle and are good indicators of violations of minimum standards in water quality, their use has been generally to reproduce and predict short-term behavior on the order of days or weeks. Where the study of long-term seasonal variations is desired the use of real time models may be too costly, especially if the model estuary has to be divided into numerous segments. In those instances where an estuary can be modeled with relatively few segments and the time scale of calculations is not overly small it would be to the modeler's advantage to use a real time model. While a tidal average model cannot reproduce variations within a tidal cycle but only variations between cycles, a real time model can serve both purposes.

Tidal current is not calculated in the tidal prism, tidal average or slack tide models. However, in a real time model tidal current is modeled as advective velocity which is a function of space and time. In one-dimensional models during low freshwater flow conditions under which the tidal current is rather insensitive to the change in freshwater flow, a kinematic approach to calculating tidal currents may be used (Fang et al., 1973). In this approach the cross-sectional average tidal current may be calculated through field

measurements coupled with the continuity equation, and modeled as a periodic function of time.

The tidal velocity field may also be calculated with a separate hydrodynamic submodel which simultaneously solves the equations of momentum and continuity. The results of this dynamic tidal calculation are then fed into the water quality model (Thatcher and Harleman, 1972). Substantial effort is needed in the calibration and validation of this hydrodynamic submodel. However, this approach is necessary in two and three-dimensional models and in one-dimensional models under conditions of high freshwater inflow. The dynamic approach to tidal calculations requires a minimum of field measurements. And, as has been pointed out by Harleman (1971), the increased accuracy in the description of advective motion reduces the importance of the artificial longitudinal dispersion term.

In general, small tidal streams are high energy systems, undergoing drastic changes in volume, cross-sectional area and surface area within each tidal cycle. For this reason, these systems are likely to be well mixed and, therefore, can be studied using a one-dimensional representation. In these small streams storm runoff will have an irregular but significant effect on stream flow and cross-sectional area. Adequately accounting for the effects of high runoff calls for a dynamic approach to the modeling of the transport processes.

The deleterious effects of point source and nonpoint source loadings on water quality in small tidal streams is often exacerbated by the presence of excess algae. Large phytoplankton populations can lead to undesirable pH levels and large fluctuations in dissolved

oxygen within a twenty-four hour period. Where this situation exists, it is desirable to take into account the effect of phytoplankton on water quality measures. To do this, the model must include not only phytoplankton but also the cycling, sources and sinks of nutrients necessary for phytoplankton growth. Therefore, an 'ecosystem' approach to studying water quality is needed.

To address such problems as violations of minimum or maximum daily water quality standards, a real-time approach to modeling should be employed. In this way the effects of such phenomena as the reversal of flow within a tidal cycle and changes in solar radiation within a diurnal cycle can be taken into account. A tidal average or tidal prism model affords no insight into the interplay of these and other short-term influences. Employing a real-time model for the study of long-term seasonal changes in water quality is made economically viable through the use of an efficient numerical scheme of computation and by the relatively small number of model segments needed to adequately describe these systems. Therefore, a single model can be used to investigate both short-term and long-term water quality behavior. There is no need to develop and validate two separate models.

The following chapters detail the development and application of a real-time model suitable for simulating both short-term intra-tidal and diurnal variations in water quality and long-term seasonal behavior. The model is divided into two submodels - a hydrodynamic submodel and an 'ecosystem' water quality submodel. The hydrodynamic submodel is based on the one-dimensional equations of momentum and continuity as derived by Harleman (1971). This submodel simulates the effects of dispersion, advection and other physical processes on

dissolved constituents. A finite-difference approach is used in solving the momentum and continuity equations simultaneously for the velocity, surface elevation and dispersion coefficient as functions of distance and time. These parameters are supplied to the one-dimensional mass-balance equations in the water quality submodel. The water quality submodel combines the effect of physical transport with that of biogeochemical cycling of dissolved constituents including the processes of biological uptake, decay and biochemical transformation.

An implicit scheme is employed for the solution of the finite-difference forms of the governing equations. An implicit scheme is more stable and allows for the use of a longer time step of integration than is possible with a comparable explicit scheme and, thus, requires less overall computer time.

The model is calibrated and verified using data from a small tidal creek located along the upper Potomac River in Virginia.

II. The Mathematical Formulation of the Model

Water quality in a tidal system is a result of a complex series of biochemical substance transformations and physical transport processes. Nutrient exchanges between the surroundings and the water column, and wasteload inputs exert additional influences on the system. Under these circumstances, it is difficult to predict the ultimate effect of changes in the use, wasteload or hydraulic characteristics of the water body. A mathematical model is useful in this instance both to aid in understanding of the system and to provide consistent, rational forecasts of the response of the system to changes in specified factors.

A complete model would couple the three-dimensional momentum and continuity equations describing physical transport processes in the system with the mass-balance equations describing in detail the biochemical kinetics and sources and sinks of all dissolved constituents. Such a representation is neither economically feasible nor desirable. In practice, the modeller must isolate the dominant hydrodynamic terms, the dissolved constituents of interest, and the kinetic terms which influence these constituents and next must abstract these into a model consistent with tractability, economy and desired results.

In the approach presented here the modeling effort is divided between the development of two submodels - a hydrodynamic submodel and a water quality submodel. The hydrodynamic submodel consists of the

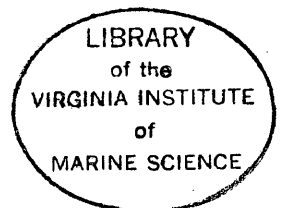
one-dimensional equations of continuity, momentum and mass-balance for a conservative substance. After calibration using available field measurements, the data generated by this submodel will be stored for use in the water quality submodel. The water quality submodel consists of the mass-balance equations for eight nonconservative parameters comprising an 'ecosystem' and will be calibrated and validated with the use of field data.

A. Hydrodynamic Submodel

Transport of dissolved constituents through a small tidal stream is highly variable in several different time scales. During each 12.4 hour tidal cycle flow in the system is completely reversed. Channel cross-sections change radically in the same period as the tide range is large in comparison to the mean depth of the system.

Storm runoff also influences the hydrodynamic transport on an irregular basis. Runoff is expected to occur as large pulses of short duration which increase the stream flow and conveyance area to a great extent during the runoff period.

Due to the transient nature of the transport processes in such a system, it is appropriate to apply an intra-tidal, real-time hydrodynamic submodel. A one-dimensional longitudinal approach is employed as vertical and lateral parameter variations in the stream are assumed to be small. The model is based on the one-dimensional momentum and continuity equations. Solution of these equations provides velocity and cross-section area parameters to the mass-balance equation which is the basis of the water quality submodel. The derivations of the one-dimensional equations applicable to unsteady, non-uniform flow in



tidal channels are well documented (Harleman and Lee, 1969; Harleman, 1971; Lin, 1975) and will not be detailed here.

Assuming incompressible flow, the three-dimensional equations necessary to completely describe water movement in the salinity intrusion region of an estuary are:

(i) the continuity equation (conservation of water mass)

$$\frac{\partial u}{\partial x} + \frac{\partial v}{\partial y} + \frac{\partial w}{\partial z} = 0 \quad (1)$$

(ii) the momentum equations

$$\begin{aligned} \frac{\partial u}{\partial t} + u \frac{\partial u}{\partial x} + v \frac{\partial u}{\partial y} + w \frac{\partial u}{\partial z} = & -\frac{1}{\rho} \frac{\partial P}{\partial x} + \nu \nabla^2 u + \frac{\partial}{\partial x} (\overline{-u'^2}) \\ & + \frac{\partial}{\partial y} (\overline{-u'v'}) + \frac{\partial}{\partial z} (\overline{-u'w'}) \end{aligned} \quad (2)$$

$$\begin{aligned} \frac{\partial v}{\partial t} + u \frac{\partial v}{\partial x} + v \frac{\partial v}{\partial y} + w \frac{\partial v}{\partial z} = & -\frac{1}{\rho} \frac{\partial P}{\partial y} + \nu \nabla^2 v + \frac{\partial}{\partial x} (\overline{-u'v'}) \\ & + \frac{\partial}{\partial y} (\overline{-v'^2}) + \frac{\partial}{\partial z} (\overline{-v'w'}) \end{aligned} \quad (3)$$

$$\begin{aligned} \frac{\partial w}{\partial t} + u \frac{\partial w}{\partial x} + v \frac{\partial w}{\partial y} + w \frac{\partial w}{\partial z} = & -\frac{1}{\rho} \frac{\partial P}{\partial z} - g + \nu \nabla^2 w + \frac{\partial}{\partial x} (\overline{-u'w'}) \\ & + \frac{\partial}{\partial y} (\overline{-v'w'}) + \frac{\partial}{\partial z} (\overline{-w'^2}) \end{aligned} \quad (4)$$

(iii) the salt balance equation (neglecting molecular diffusion)

$$\begin{aligned} \frac{\partial s}{\partial t} + u \frac{\partial s}{\partial x} + v \frac{\partial s}{\partial y} + w \frac{\partial s}{\partial z} = & \frac{\partial}{\partial x} (\overline{-u's'}) + \frac{\partial}{\partial y} (\overline{-v's'}) \\ & + \frac{\partial}{\partial z} (\overline{-w's'}) \end{aligned} \quad (5)$$

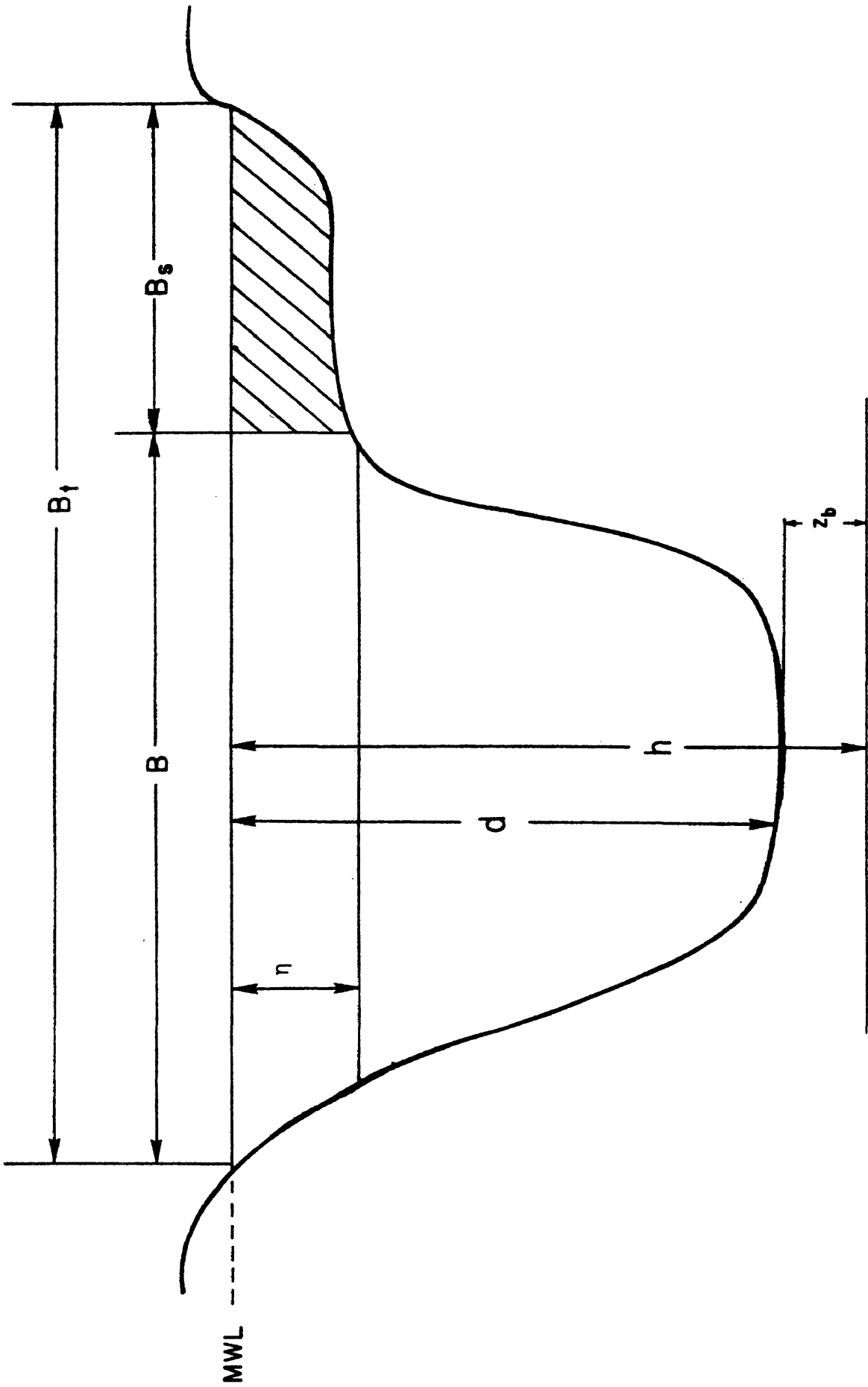


Figure 1. Definition sketch - irregular channel.

where t is time; u , v and w are the ensemble average velocity components in the x , y and z directions, respectively; u' , v' and w' are the turbulent velocity fluctuations; P is the pressure; g is gravitational acceleration; ρ is the water density; ν is the kinematic viscosity; ∇^2 is the Laplacian operator; s is the ensemble average salinity and s' is the turbulent salinity fluctuation. In practical application ensemble averages are replaced by time averages over an interval longer than the turbulent time scale but much shorter than a tidal cycle.

Inherent in the above equations is the assumption that the effect of pressure on density is negligible, that is, the flow field is incompressible. It is also assumed that the range of temperature encountered in an estuary at a given instant is generally narrow, thus the effect of temperature on density can be neglected. Therefore, density is defined in this development by the equation

$$\rho = \rho_0 (1 + ks) \quad (6)$$

where ρ_0 is the density of freshwater and k is an experimental constant equal to 0.00075.

The one-dimensional equations applicable to unsteady, non-uniform flow in tidal channels can be derived by integrating the three-dimensional equations over the transverse cross-sectional area (Lin, 1971) or by the material method (Harleman and Lee, 1969).

A cross-section of an irregular channel is depicted in Figure 1. The x -coordinate is measured horizontally along the longitudinal axis of the channel from the landward end of the estuary and h is the distance to the instantaneous position of the water surface from a horizontal

reference datum. If, as shown in Figure 1, the cross-section has both deep and very shallow portions, the channel may be divided into conveyance and storage regions. In this case the tidal flow is assumed to be confined to the conveyance channel area, defined by width B . The shallow portion, defined by width B_s , contributes to storage only. The cross-sectional area A is defined as the area of the conveyancy channel. Hence, the average velocity $U = Q/A$, where Q is the longitudinal discharge. Any embayment along the channel is included in the storage region.

After integration over the cross-sectional area, the one-dimensional form of the continuity equation may be written as:

$$\frac{\partial A}{\partial t} + \frac{\partial Q}{\partial x} - q = 0 \quad (7)$$

where q is the lateral inflow per unit length of the channel. The change in the surface width of the conveyancy portion with respect to time can usually be neglected and the conveyancy portion of the channel treated as a rectangular channel of constant width. Thus

$$A(x,t) = B(x) \cdot h(x,t)$$

Thus, the instantaneous position of the water surface, h , may be defined as

$$h(x,t) = z_b(x) + d(x) + \eta(x,t) \quad (8)$$

where z_b is the distance from a horizontal reference level to the channel bottom to some reference water level (e.g., mean sea level), and η is the instantaneous surface elevation in reference to the chosen datum water level. Thus the one-dimensional continuity equation

can be written as

$$B \frac{\partial \eta}{\partial t} + \frac{\partial Q}{\partial x} - q = 0 \quad (9)$$

In a one-dimensional representation, water transport in the vertical and lateral directions is assumed to be negligible. Therefore, the momentum equation in the y-direction can be eliminated and the equation in the z-direction reduces to the equation for hydrostatic pressure distribution:

$$-\frac{1}{\rho} \frac{\partial P}{\partial z} - q = 0 \quad (10)$$

Integrating equation (10) with respect to z and differentiating the result with respect to x yields an equation for the longitudinal pressure gradient:

$$\frac{\partial P}{\partial x} = \rho g \frac{\partial h}{\partial x} + g (h-z) \frac{\partial \rho}{\partial x} - \frac{\partial P_a}{\partial x} \quad (11)$$

Equation (11) states that the longitudinal pressure gradient is a result of three factors: the water surface slope, the density gradient and the atmospheric pressure gradient.

According to the Boussinesq hypothesis, the Reynolds stresses in the momentum equations can be related to mean velocity. For the x-directional momentum equation this would be:

$$-\overline{u'v'} = \epsilon_m \left(\frac{\partial u}{\partial y} + \frac{\partial v}{\partial x} \right) = \frac{\tau_{xy}}{\rho} \quad (12)$$

$$-\overline{u'w'} = \epsilon_m \left(\frac{\partial u}{\partial z} + \frac{\partial w}{\partial x} \right) = \frac{\tau_{xz}}{\rho} \quad (13)$$

where ϵ_m is turbulent eddy viscosity and τ_{xy} and τ_{xz} are components of the stress tensor.

The longitudinal eddy diffusion of momentum is negligible with respect to advection, so the longitudinal eddy diffusion term $(\frac{\partial}{\partial x} \overline{u'^2})$ in equation (2) can be neglected. Also, molecular viscosity is usually much less than the eddy viscosity so the molecular diffusion term $(\nu \nabla^2 u)$ can be neglected.

Substituting equations (11), (12) and (13) into equation (2), neglecting molecular diffusion and longitudinal eddy diffusion, and integrating over the cross-sectional area yields:

$$\frac{\partial U}{\partial t} + \frac{\partial U^2}{\partial x} = -g \frac{\partial h}{\partial x} - \frac{gk}{1+kS} d_c \frac{\partial S}{\partial x} - \frac{1}{\rho} \frac{\partial p_a}{\partial x} - \frac{\tau_B}{\rho} \frac{P_w}{A} + \frac{\tau_s}{\rho} \frac{B}{A} + \frac{M}{A} \quad (14)$$

where d_c is the distance between the water surface and the centroid of the cross-section, τ_B is the average stress by the boundary, P_w is the wetted perimeter of the cross-section, τ_s is the average stress on the water surface and M is the momentum flux of the lateral inflow.

The two terms on the left side of equation (14) are the local and convective acceleration terms. The terms on the right hand side of the equation represent the surface slope, the density gradient, the atmospheric pressure gradient, the boundary roughness effect, the local wind effect and the effect of lateral flow, respectively.

In the open channel, the average frictional shear stress on the boundary can be expressed as

$$\tau_B = \rho_g R S_E \quad (15)$$

where $R = A/P_w$ is the hydraulic radius and S_E is the slope of the energy gradient. S_E is evaluated from the Manning equation in which

$$S_E = n^2 \frac{Q|Q|}{A^2 R^{4/3}} \quad (16)$$

where n is the Manning roughness coefficient in m-sec units. Thus, the boundary roughness effect in equation (14) can be written

$$-\frac{\tau_B}{\rho} \frac{P_w}{A} = -g n^2 \frac{Q|Q|}{A^2 R^{4/3}} \quad (17)$$

The possibility of a change in the longitudinal momentum flux due to flow entering or leaving the main channel from the storage area and due to lateral inflow (g) has been discussed by various investigators (e.g., Dronkers, 1964). It is generally agreed that the effect on the momentum equation is small, hence, in this development it will be assumed that the lateral flows enter or leave the main channel at right angles to the longitudinal axis and that there is no contribution to the longitudinal momentum flux ($M = 0$).

Also, in this development it will be assumed that any atmospheric pressure gradient that may exist over the small streams considered here will be negligible. Thus, equation (14) reduces to

$$\frac{\partial U}{\partial t} + \frac{\partial U^2}{\partial x} = -g \frac{\partial h}{\partial x} - \frac{gk}{1+ks} d_c \frac{\partial S}{\partial x} - g n^2 \frac{Q|Q|}{A^2 R^{4/3}} + \frac{\tau_s}{\rho} \frac{B}{A} \quad (18)$$

Using equation (8) and the identity $Q = UA$, equation (18) can be rearranged to give

$$\begin{aligned} \frac{\partial Q}{\partial t} + \frac{\partial}{\partial x} \left(\frac{Q^2}{A} \right) &= -gA \frac{\partial \eta}{\partial x} - \frac{gk}{1+ks} Ad_c \frac{\partial S}{\partial x} - g n^2 \frac{Q|Q|}{A R^{4/3}} \\ &\quad + \frac{\tau_s}{\rho} B \end{aligned} \quad (19)$$

This equation can be simplified further under the condition that no longitudinal density gradient exists, i.e., in the freshwater region of a tidal system. In modeling such a region the second term on the right-hand side of equation (19) is always equal to zero.

From the Boussinesq hypothesis, the turbulent transport is proportional to the gradient of the mean concentration. The relation can be written as:

$$-\overline{u's'} = e_x \frac{\partial s}{\partial x}, \quad -\overline{v's'} = e_y \frac{\partial s}{\partial y} \text{ and } -\overline{w's'} = e_z \frac{\partial s}{\partial z} \quad (20)$$

where e_x , e_y and e_z are diffusion coefficients in the x, y and z directions, respectively. The three-dimensional mass-balance equation for turbulent flow, neglecting molecular diffusion, then becomes

$$\begin{aligned} \frac{\partial s}{\partial t} + u \frac{\partial s}{\partial x} + v \frac{\partial s}{\partial y} + w \frac{\partial s}{\partial z} = \frac{\partial}{\partial x} \left(e_x \frac{\partial s}{\partial x} \right) + \frac{\partial}{\partial y} \left(e_y \frac{\partial s}{\partial y} \right) \\ + \frac{\partial}{\partial z} \left(e_z \frac{\partial s}{\partial z} \right) \end{aligned} \quad (21)$$

The time average concentrations and velocity components can be defined as

$$\begin{aligned} s &= S + s'' \\ u &= U + u'' \\ v &= V + v'' \\ w &= W + w'' \end{aligned} \quad (22)$$

where the capital letters designate the cross-sectional mean and the double prime designates the deviation from the cross-sectional mean.

Note that

$$\iint_A u'' dA = 0$$

and that v'' and w'' are not zero even though the cross-sectional mean velocities V and W are zero in the one-dimensional flow. Equations (22) are introduced into the three-dimensional salt balance equation (21), the product of sums are expanded and each term is integrated over the cross-sectional area A (see Holley and Harleman, 1965). After simplification, the one-dimensional equation may be written as

$$\frac{\partial}{\partial t} (AS) + \frac{\partial}{\partial x} (AUS) = - \iint u''s'' + \frac{\partial}{\partial x} \left[A\bar{e}_x \frac{\partial S}{\partial x} \right] + q S_T \quad (23)$$

where the term qS_T is flux of salt through the lateral boundaries and S_T is the concentration of lateral flow.

For steady, uniform flow, Taylor (1954) and Aris (1956) have shown that the advective mass transport associated with the cross product of the spatial deviations u'' and s'' can be approximated with an analogous one-dimensional diffusive transport. To distinguish this process from turbulent diffusion, which is associated with the temporal deviations u' and s' , the transport due to spatial deviations is called longitudinal dispersion. On this basis a dispersion coefficient, E_x , is defined

$$\iint_A u''s'' dA = -AE_x \frac{\partial S}{\partial x}$$

The negative sign indicates mass transport in the direction of decreasing concentration. Taylor (1954) has shown that the turbulent diffusion coefficient, \bar{e}_x , is usually much smaller than the dispersion coefficient. Therefore, the two coefficients are usually added together (Harleman, 1971) and the sum referred to as the longitudinal dispersion coefficient, E , where

$$E = E_x + \bar{e}_x \quad (24)$$

Thus, the one-dimensional mass transfer equation for salt becomes

$$\frac{\partial}{\partial t} (AS) + \frac{\partial}{\partial x} (QS) = \frac{\partial}{\partial x} \left(EA \frac{\partial S}{\partial x} \right) + q S_T \quad (25)$$

In freshwater tidal systems some other essentially conservative substance (e.g., dye) may be described by the same equation and modeled as an aid in calibrating the hydrodynamics of the system.

B. Water Quality Submodel

The water quality submodel used for this study is a one-dimensional, intra-tidal model which simulates the longitudinal distribution of cross-sectional average concentrations of water quality measures, including the temporal variation of these concentration fields in response to tidal oscillation. Much of the following water quality submodel is based on previous work by Hyer et al. (1977) and Cerco and Kuo (1981). The water quality measures simulated in the model include dissolved oxygen, carbonaceous oxygen demand, organic nitrogen, ammonia nitrogen, nitrite-nitrate nitrogen, organic phosphorus, inorganic (ortho) phosphorus and phytoplankton (quantified as chlorophyll 'a'). Temperature, turbidity, and light intensity are important parameters for the biochemical interactions taking place, but are not modeled directly. Instead the values for these parameters are specified as inputs to the model. Their influence on the biochemical reaction is taken into account mathematically, as indicated below.

The submodel is based on the one-dimensional equation describing the mass-balance of a dissolved or suspended substance in a water body.

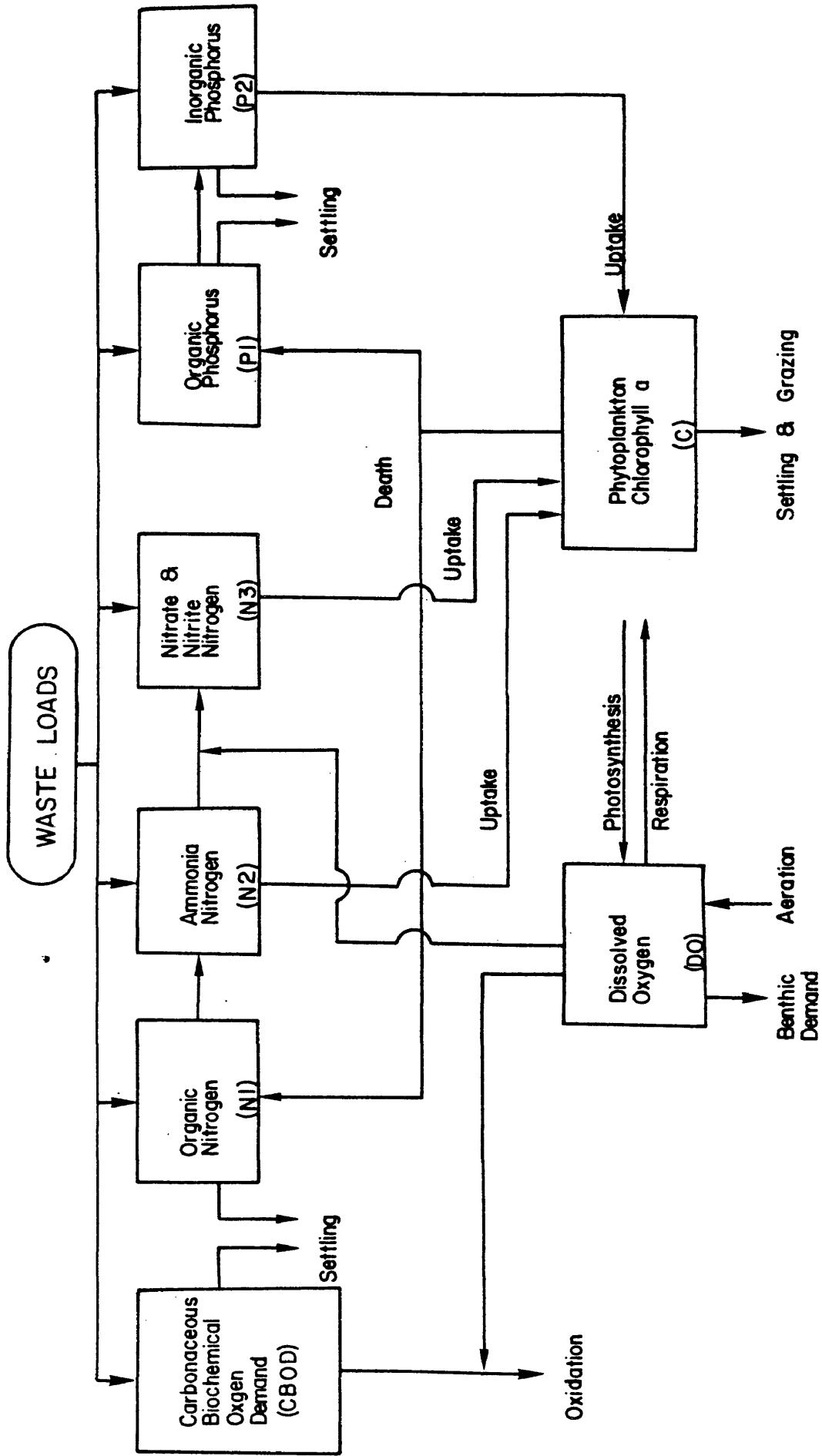


Figure 2. Schematic of Ecosystem Model

$$\frac{\partial}{\partial t} (AC) + \frac{\partial}{\partial x} (QC) = \frac{\partial}{\partial x} \left(EA \frac{\partial C}{\partial x} \right) + A \cdot S_e + A \cdot S_i \quad (26)$$

where

C = the concentration of dissolved or suspended substance,

S_e = the time rate of external addition (or withdrawal) of mass across the boundaries, i.e. free surface, bottom, and lateral boundary,

S_i = the time rate of increase or decrease of mass of a particular substance by biochemical reaction process.

The advection transport term, the second term on the left hand side of the equation, represents advection of mass by water movement; the dispersive transport term, the first term on the right hand side, represents dispersion of mass by turbulence and shearing flow. These two terms represent the physical transport processes in the flow field and are identical for all dissolved and suspended substances in the water. They will be treated in the same manner as those in the mass-balance equation of a conservative substance, equation (25). The last two terms of the equation represent the external additions and internal biochemical reactions and differ for different substances.

The model treats nitrogen, phosphorus, oxygen demanding material and dissolved oxygen through an interacting system of eight components as shown in the schematic diagram, Figure 2. Each rectangular box represents one component being simulated by the model. The arrows between components represent the biochemical transformation of one substance to the other. An arrow with one end unattached represents an external source (or sink) or an internal source (or sink) due to some biochemical reaction. The mathematical expressions for the terms S_e and S_i for each of the eight components are presented in the following:

1. Phytoplankton Population, CH - The phytoplankton population, quantified as the concentration of chlorophyll 'a', occupies a central role in the schematic ecosystem of Figure 2 and influences, to a greater or lesser extent, all of the remaining non-conservative dissolved constituents. The mathematical representation describing internal biochemical interaction and external sources (or sinks) are

$$S_i = CH \cdot (G-R-P) \quad (27)$$

and

$$S_e = -CH \cdot K_{sch}/h_t \quad (28)$$

where

CH = chlorophyll 'a' concentration (ug/l)

G = growth rate of phytoplankton (1/day)

R = respiration rate of phytoplankton (1/day)

P = predation rate of phytoplankton by zooplankton (1/day)

K_{sch} = settling rate of phytoplankton (m/day)

h_t = average local depth (m) below mean water level, including storage

Phytoplankton growth is dependent upon nutrient availability, ambient light and temperature. The functional relationships used in the model generally follow the forms of DiToro et al. (1971) and are as follows:

$$k_{gr} \cdot T \cdot I (I_a, I_s, k_e, CH, h) \cdot N (N_2, N_3, P_2) \quad (29)$$

Temp. effect	Light effect	Nutrient effect
-----------------	-----------------	--------------------

where

k_{gr} = optimum growth rate (1/day/ $^{\circ}$ C)

T = temperature ($^{\circ}$ C)

I = attenuation of growth due to suboptimal lighting

N = effect on growth of nutrient availability

$$I = \frac{2.718}{k_e h} (e^{-\alpha_1} - e^{-\alpha_0}) \quad (30)$$

$$k_e = k_e' + 0.0088 \cdot CH + 0.054 \cdot CH^{0.66} \quad (31)$$

$$\alpha_1 = \frac{I_t}{I_s} e^{-k_e h} \quad (32)$$

$$\alpha_0 = \frac{I_t}{I_s} \quad (33)$$

$$I_t = I_a \cdot \frac{24}{t_d - t_u} \cdot \frac{\pi}{2} \sin \left(\frac{t - t_u}{t_d - t_u} \right) \quad \text{if } t_u < t < t_d \quad (34)$$

where

k_e' = light extinction coefficient at zero chlorophyll concentration (1/meter)

k_e = light extinction coefficient corrected for self-shading of plankton (1/meter)

h = local channel depth (m)

I_s = optimum solar radiation rate (langley/day)

I_t = solar radiation at time t

I_a = total daily solar radiation (langley/day)

t_u = time of sunrise, in hours

t_d = time of sunset, in hours

t = time of day in hours

The nutrient effect, N, is based on the minimum limiting nutrient concept.

$$N = \text{minimum} \left\{ \begin{array}{l} \frac{N2 + N3}{K_{mn} + N2 + N3} \\ \frac{P2}{K_{mp} + P2} \end{array} \right. \quad (35)$$

where

N2 = ammonia nitrogen concentration (mg/l)

N3 = nitrite-nitrate nitrogen concentration (mg/l)

P2 = inorganic (ortho) phosphorus concentration (mg/l)

K_{mn} = half-saturation concentration for inorganic nitrogen (mg/l)

K_{mp} = half-saturation concentration for inorganic phosphorus (mg/l)

The respiration rate, R, is a linear function of temperature.

$$R = aT \quad (36)$$

where

a = temperature dependence of respiration rate (1/day/°C)

Predation rate, P, should be dependent on the time variable herbivore population which is in turn dependent upon the phytoplankton population. To avoid adding an additional trophic level to the model, however, a uniform rate of predation is assumed.

2. Organic Nitrogen, N1

$$S_i = -\frac{K_{n12} \cdot T \cdot N1}{K_{h12} + N1} + a_n \cdot (R + a_r \cdot P) \cdot CH \quad (37)$$

$$S_e = -N1 \cdot K_{n11} / h_t + PN1 + NPN1 + BENN1/h \quad (38)$$

where

K_{n12} = hydrolysis rate of organic nitrogen to ammonia (mg/l/day/°C)

K_{h12} = half-saturation concentration for hydrolysis (mg/l)

a_n = ratio of organic nitrogen to chlorophyll in phytoplankton (mg N/ug Chl)

a_r = proportion of consumed phytoplankton recycled by zooplankton (0.4 assumed)

K_{n11} = settling rate of organic nitrogen (m/day)

PN1 = point source wasteloading of organic nitrogen

NPN1 = nonpoint source wasteloading of organic nitrogen

BENN1 = benthic flux of organic nitrogen ($\text{g/m}^2/\text{day}$)

3. Ammonia Nitrogen, N2

$$S_i = -\frac{K_{n23} \cdot T \cdot N2}{K_{n23} + N2} + \frac{K_{n12} \cdot T \cdot N1}{K_{h12} + N1} - a_n \cdot G \cdot PR \cdot CH \quad (39)$$

$$S_e = PN2 + NPN2 + BENN2/h \quad (40)$$

where

K_{n23} = nitrification rate of ammonia to nitrate nitrogen ($\text{mg/l/day}/^\circ\text{C}$)

K_{h23} = half-saturation concentration for nitrification (mg/l)

PN2 = point source wasteloading of ammonia nitrogen

NPN2 = nonpoint source wasteloading of ammonia nitrogen

BENN2 = benthic flux of ammonia nitrogen ($\text{g/m}^2/\text{day}$)

PR = ammonia preference by phytoplankton given by

$$PR = \frac{N2 \cdot N3}{(K_{mn} + N2)(K_{mn} + N3)} + \frac{N2 \cdot K_{mn}}{(N2 + N3)(K_{mn} + N3)}$$

K_{mn} is the Michaelis constant.

4. Nitrite-Nitrate Nitrogen, N3

$$S_i = \frac{K_{n23} \cdot T \cdot N2}{K_{h23} + N2} - a_n \cdot G \cdot (1-PR) \cdot CH \quad (41)$$

$$S_e = -N3 \cdot K_{n33}/h_t + PN3 + NPN3 + BENN3/h \quad (42)$$

where

K_{n33} = escaping rate of nitrite-nitrate nitrogen (mg/l)

PN3 = point source wasteloading of nitrite-nitrate nitrogen

NPN3 = nonpoint source wasteloading of nitrite-nitrate nitrogen

BENN3 = benthic flux of nitrite-nitrate nitrogen ($\text{g}/\text{m}^2/\text{day}$)

5. Organic Phosphorus, P1

$$S_i = -K_{p12} \cdot T \cdot P1 + a_p \cdot (R + a_r P) \cdot CH \quad (43)$$

$$S_e = -P1 \cdot K_{p11} / h_t + PP1 + NPP1 + BENP1/h \quad (44)$$

where

K_{p12} = first order hydrolysis rate of organic to inorganic phosphorus ($1/\text{day}/^\circ\text{C}$)

a_p = ratio of organic phosphorus to chlorophyll in phytoplankton (mg P/ug Chl)

K_{p11} = settling rate of organic phosphorus (m/day)

PP1 = point source wasteloading of organic phosphorus

NPP1 = nonpoint source wasteloading of organic phosphorus

BENP1 = benthic flux of organic phosphorus ($\text{g}/\text{m}^2/\text{day}$)

6. Inorganic (Ortho) Phosphorus, P2

$$S_i = K_{p12} \cdot T \cdot P1 - a_p \cdot G \cdot CH \quad (45)$$

$$S_e = -P2 \cdot K_{p22} / h_t + PP2 + NPP2 + BENP2/h \quad (46)$$

where

K_{p22} = settling rate of inorganic phosphorus (m/day)

PP2 = point source wasteloading of inorganic phosphorus

NPP2 = nonpoint source wasteloading of inorganic phosphorus

BENP2 = benthic flux of inorganic phosphorus ($\text{g/m}^2/\text{day}$)

7. Carbonaceous Biochemical Oxygen Demand, CBOD

$$S_i = -K_c \cdot \text{CBOD} + a_c \cdot a_{co} \cdot (a_r \cdot P) \cdot \text{CH} \quad (47)$$

$$S_e = -\text{CBOD} \cdot K_{sc} / h_t + \text{PCBOD} + \text{NPCBOD} \quad (48)$$

where

K_c = first order decay rate of CBOD (1/day)

a_c = ratio of carbon to chlorophyll in phytoplankton
(mg C/ug Chl)

a_{co} = ratio of oxygen demand to organic carbon recycled = 2.67

K_{sc} = settling rate of CBOD (m/day)

PCBOD = point source wasteloading of CBOD

NPCBOD = nonpoint source wasteloading of CBOD

The effect of temperature on K_c is given as

$$K_c = K_{c(20)} \cdot 1.047^{(T-20)}$$

where

$K_{c(20)}$ = decay rate of CBOD at 20°C.

8. Dissolved Oxygen, DO

$$S_i = -K_c \cdot \text{CBOD} - a_{no} \cdot \frac{K_{n23} \cdot T \cdot N2}{K_{h23} + N2} + a_{co} \cdot a_c \cdot \text{PQ} \cdot \text{G} \cdot \text{CH} \\ - a_{co} \cdot a_c / \text{RQ} \cdot \text{R} \cdot \text{CH} \quad (50)$$

$$S_e = K_r \cdot (DO_s - DO) - \text{BENDO}/h + \text{PDO} + \text{NPDO} \quad (51)$$

where

a_{no} = ratio of oxygen consumed per unit of ammonia nitrified = 4.57

PQ = photosynthesis quotient (moles O_2 /mole C)

RQ = respiration quotient (moles CO_2 /mole O_2)

K_r = reaeration rate (1/day)

DO = saturation concentration of DO (mg/l)

BENDO = sediment oxygen demand ($g/m^2/day$)

PDO = point source wasteloading of DO

NPOD = nonpoint source wasteloading of DO

The reaeration rate, K_r , is further defined (O'Connor and Dobbins, 1958)

$$K_{r(20)} = K_{ro} u^{1/2} h^{-3/2} \quad (52)$$

where

$K_{r(20)}$ = reaeration rate at $20^\circ C$

K_{ro} = 3.93

u = mean cross-sectional velocity (m/sec)

The effect of temperature on the reaeration rate is evaluated (Elmer and West, 1961)

$$K_r = K_{r(20)} \cdot 1.024^{(T-20)} \quad (53)$$

Saturation dissolved oxygen concentration, DO, is calculated as a function of water temperature from a polynomial fitted to the tables of Carritt and Green (1967).

$$DO_s = 14.6244 - 0.367134 \cdot T + 0.004497 \cdot T^2 \quad (54)$$

The effect of temperature on sediment oxygen demand is evaluated by the equation (Thomann, 1972)

$$BENDO = BENDO_{(20)} \cdot 1.065^{(T-20)} \quad (55)$$

III. Mathematics of Solution

A. Method of Schematization

To facilitate the solution of differential equations by finite difference method, the length of the tidal creek is divided into a number of reaches (or elements) bounded by transects at two ends. The top view of the longitudinal schematization is shown below in Figure 3,

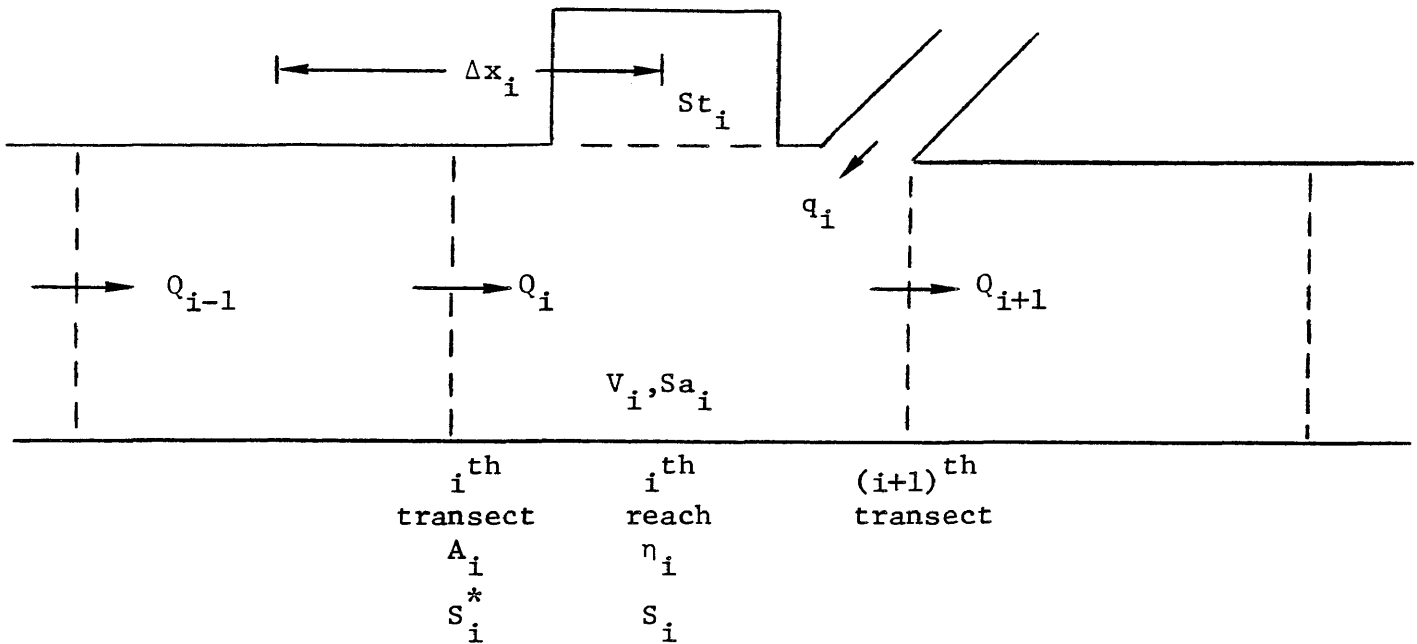


Figure 3. Schematization of a tidal creek.

in which the parameters given are

Δx_i = the distance between the centers of two reaches adjoining the i th transect,

- Q_i = the flow rate through the i th transect,
 A_i = the cross-sectional area of the i th transect,
 η_i = the water surface elevation, relative to mean sea level, of the i th reach,
 V_i = the volume of the i th reach,
 Sa_i = the surface area of the i th reach,
 St_i = the surface area of the storage embayment in the i th reach,
 q_i = the rate of total lateral inflow in the i th reach,
 S_i = concentration of dissolved substance in the i th reach,
 S_i^* = concentration of dissolved substance of the water flowing through the i th transect.

B. Finite Difference Equations

To write equation (9) into finite difference form it is first integrated with respect to x from the i th to the $(i+1)$ th transect and time differentiation substituted with finite time difference,

$$(\eta'_i - \eta_i)(Sa_i + St_i)/\Delta t = \beta(Q'_i - Q'_{i+1}) + \beta_c(Q_i - Q_{i+1}) + q_i \quad (56)$$

where Δt is the time increment. The primed variables designate the quantities evaluated at time $t + \Delta t$ and the unprimed variables designate those at time t . β and β_c are weighting factors which satisfy

$$\beta + \beta_c = 1$$

The momentum equation, equation (19), may be written in finite difference form at the i th transect as

$$\begin{aligned}
& \frac{1}{\Delta t} (Q'_i - Q_i) + \frac{1}{\Delta x_i} \left[\frac{Q_i + Q_{i+1}}{2} \cdot \frac{1}{2} \left(\frac{Q_i}{A_i} + \frac{Q_{i+1}}{A_{i+1}} \right) \right. \\
& \quad \left. - \frac{Q_{i-1} + Q_i}{2} \cdot \frac{1}{2} \left(\frac{Q_{i-1}}{A_{i-1}} + \frac{Q_i}{A_i} \right) \right] \\
& = - \frac{gA_i}{\Delta x_i} \left[\alpha (\eta'_i - \eta'_{i-1}) + \alpha_c (\eta_i - \eta_{i-1}) \right] \\
& \quad - \frac{gk d_{ci} A_i}{1+k(S_{i-1} + S_i)/2} \cdot \left(\frac{S_i - S_{i-1}}{\Delta x_i} \right) \\
& \quad - gn_i^2 \frac{Q_i}{A_i} |Q_i| R_i^{-4/3} + \frac{\tau_s}{\rho_i} B_i
\end{aligned} \tag{57}$$

where α and α_c are weighting factors which satisfy

$$\alpha + \alpha_c = 1$$

Similar to the continuity equation, the mass-balance equation for a conservative substance, equation (25), is first integrated with respect to x and, then, written as

$$\begin{aligned}
\frac{\partial}{\partial t} (V_i S_i) &= Q_i S_i^* - Q_{i+1} S_{i+1}^* + \left(EA \frac{\partial S}{\partial x} \right)_{i+1} \\
&\quad - \left(EA \frac{\partial S}{\partial x} \right)_i + S o_i
\end{aligned} \tag{58}$$

or, in terms of finite difference in time,

$$\begin{aligned}
\frac{V'_i S'_i - V_i S_i}{\Delta t} &= Q'_i S'^*_i - Q'_{i+1} S'^*_{i+1} + \left(EA \frac{\partial S}{\partial x} \right)_{i+1} \\
&\quad - \left(EA \frac{\partial S}{\partial x} \right)_i + S o_i
\end{aligned} \tag{59}$$

where S_i^* and S_{i+1}^* are concentrations in the water flowing through the i th and $(i+1)$ th transects, respectively, and $S o_i$ represents the effect

of change in storage volume. S_i^* may be expressed as a function of concentrations in the two adjacent reaches, i.e.,

$$S_i^* = \gamma_i S_{i-1} + \delta_i S_i$$

where

$$\gamma_i + \delta_i = 1$$

and

$$\begin{aligned} 0.5 \leq \gamma_i \leq 1.0 & \quad \text{if } Q_i \geq 0 \\ \gamma_i < 0.5 & \quad \text{if } Q_i < 0 \end{aligned}$$

C. Method of Solution

(a) Continuity and Momentum Equations

Equations (56) and (57) are a coupled system of algebraic equations, which needs to be solved simultaneously for η_i' and Q_i' for all i . The system is solved by substitution and elimination processes. Equation (57) may be written as

$$Q_i' = \alpha g A_i \frac{\Delta t}{\Delta x_i} (\eta_{i-1}' - \eta_i') + (CQ)_i \quad (60)$$

where

$$\begin{aligned} (CQ)_i = & Q_i + \frac{1}{4} \frac{\Delta t}{\Delta x_i} \left[(Q_{i-1} + Q_i) \left(\frac{Q_{i-1}}{A_{i-1}} + \frac{Q_i}{A_i} \right) \right. \\ & \left. - (Q_i + Q_{i+1}) \left(\frac{Q_i}{A_i} + \frac{Q_{i+1}}{A_{i+1}} \right) \right] \\ & - g n_i^2 \frac{Q_i}{A_i} |Q_i| R_i^{-4/3} \Delta t \\ & - \frac{g k d_{ci} A_i}{1 + k(S_{i-1} + S_i)/2} \cdot \frac{S_i - S_{i-1}}{\Delta x_i} \Delta t \\ & + \frac{\tau_s}{\rho_i} B_i \Delta t + \alpha_c g \frac{\Delta t}{\Delta x_i} A_i (\eta_{i-1}' - \eta_i') \end{aligned} \quad (60a)$$

Substituting equation (60) into equation (56), it is obtained

that

$$\begin{aligned}
 (\eta'_i - \eta_i)(S_{a_i} + S_{t_i})/\Delta t = & \beta \left[\alpha g A_i \frac{\Delta t}{\Delta x_i} (\eta'_{i-1} - \eta'_i) + (CQ)_i \right. \\
 & - \alpha g A_{i+1} \frac{\Delta t}{\Delta x_{i+1}} (\eta'_i - \eta'_{i+1}) \\
 & \left. - (CQ)_{i+1} \right] + \beta_c (Q_i - Q_{i+1}) + q_i
 \end{aligned}$$

or

$$\eta'_i = a_i \eta'_{i+1} + b_i \eta'_{i-1} + c_i \quad (61)$$

where

$$a_i = \alpha \beta g A_{i+1} \frac{\Delta t}{\Delta x_{i+1}} / \text{D1V}$$

$$b_i = \alpha \beta g A_i \frac{\Delta t}{\Delta x_i} / \text{D1V}$$

$$\begin{aligned}
 c_i = & \left[(S_{a_i} + S_{t_i}) / \Delta t \cdot \eta_i + \beta \left[(CQ)_i - (CQ)_{i+1} \right] \right. \\
 & \left. + \beta_c (Q_i - Q_{i+1}) + q_i \right] / \text{D1V}
 \end{aligned} \quad (61a)$$

$$\text{D1V} = (S_{a_i} + S_{t_i}) / \Delta t + \alpha \beta g \left[A_i \frac{\Delta t}{\Delta x_i} + \frac{A_{i+1} \Delta t}{\Delta x_{i+1}} \right]$$

To calculate the coefficients a_i , b_i and c_i at the most upstream reach, say $i=m_1$, some upstream boundary condition is required. The most common boundary condition for a tidal creek is the upstream nontidal discharge, specified as Q_{m_1} for all time. With Q'_{m_1} given, substitution of equation (60) with $i=m_1+1$ into equation (56) with $i=m_1$ yields

$$\begin{aligned}
 (\eta'_{m_1} - \eta_{m_1})(S_{a_{m_1}} + S_{t_{m_1}}) / \Delta t = & \beta Q'_{m_1} - \beta \left[\alpha g A_{m_1+1} \frac{\Delta t}{\Delta x_{m_1+1}} \cdot (\eta'_{m_1} - \eta'_{m_1+1}) \right. \\
 & \left. + (CQ)_{m_1+1} \right] + \beta_c (Q_{m_1} - Q_{m_1+1}) + q_{m_1}
 \end{aligned}$$

or

$$\eta'_{m1} = a_{m1} \eta'_{m1+1} + C_{m1} \quad (62)$$

where

$$a_{m1} = \alpha \beta g A_{m1+1} \frac{\Delta t}{\Delta x_{m1+1}} \Big/ \text{DIV}$$

$$C_{m1} = \left[\beta Q'_{m1} - \beta (CQ)_{m1+1} + \beta_c (Q_{m1} - Q_{m1+1}) + q_{m1} \right. \\ \left. + (S a_{m1} + S t_{m1}) \Big/ \Delta t \cdot \eta_{m1} \right] \Big/ \text{DIV}$$

$$\text{DIV} = (S a_{m1} + S t_{m1}) \Big/ \Delta t + \alpha \beta g A_{m1+1} \frac{\partial t}{\partial x_{m1+1}}$$

Equation (61) may be solved by an elimination process if the downstream boundary condition η'_i is given at the most downstream reach, say $i=\mu$. Let

$$\eta'_i = P_i \eta'_{i+1} + O_i \quad (63)$$

where P_i and O_i are recursion coefficients yet to be determined.

Substituting

$$\eta'_{i-1} = P_{i-1} \eta'_i + O_{i-1}$$

into equation (61) it becomes

$$\eta'_i = a_i \eta'_{i+1} + b_i (P_{i-1} \eta'_i + O_{i-1}) + C_i$$

or

$$\eta'_i = \frac{a_i}{1 - b_i P_{i-1}} \eta'_{i+1} + \frac{b_i O_{i-1} + C_i}{1 - b_i P_{i-1}} \quad (64)$$

Comparing equation (64) with equation (63), the recursion equations obtained are

$$P_i = \frac{a_i}{1 - b_i P_{i-1}} \quad (65)$$

$$O_i = \frac{b_i O_{i-1} + C_i}{1 - b_i P_{i-1}}$$

Equation (62) gives

$$P_{m1} = a_{m1} \quad (66)$$

$$O_{m1} = C_{m1}$$

In summary, the numerical calculation will proceed as follows:

- (1) Calculate $(CQ)_i$ for $m1+1 \leq i \leq \mu$, equation (60a).
- (2) Calculate a_i, b_i, c_i for $m1 \leq i \leq \mu-1$, eqn. (61a) or (62a).
- (3) Calculate P_i and O_i for $m1 \leq i \leq \mu-1$, eqn. (65) or (66).
- (4) Calculate η' for $m1 \leq i \leq \mu-1$, equation (63).
- (5) Calculate Q'_i for $m1+1 \leq i \leq \mu$, equation (60).

(b) Mass-Balance Equation

Equation (59) represents a system of algebraic equations, which may be solved by elimination process. Substituting $S_i^{*'}$ and $S_{i+1}^{*'}$, and rearranging the terms, equation (59) becomes

$$\begin{aligned} S'_i = & \frac{\Delta t}{V_i'} Q'_i (\gamma_i S'_{i-1} + \delta_i S'_i) - \frac{\Delta t}{V_i'} Q'_{i+1} (\gamma_{i+1} S'_i + \delta_{i+1} S'_{i+1}) \\ & + \frac{V_i}{V_i'} S_i + \frac{\Delta t}{V_i'} \left[EA \frac{\partial S}{\partial x} \right]_{i+1} - \frac{\Delta t}{V_i'} \left[EA \frac{\partial S}{\partial x} \right]_i + \frac{\Delta t}{V_i'} S_{o_i} \end{aligned} \quad (67)$$

The dispersive transport terms may be written as

$$\begin{aligned} \left[EA \frac{\partial S}{\partial x} \right]_i &= E_i A_i \frac{S_i - S_{i-1}}{\Delta x_i} \\ \left[EA \frac{\partial S}{\partial x} \right]_{i+1} &= E_{i+1} A_{i+1} \frac{S_{i+1} - S_i}{\Delta x_{i+1}} \end{aligned}$$

After substitution, equation (67) becomes

$$S'_i = a_i S'_{i+1} + b_i S'_{i-1} + C_i \quad (68)$$

where

$$a_i = -\frac{\Delta t}{V_i'} \delta_{i+1} Q'_{i+1} / \text{D1V}$$

$$b_i = \frac{\Delta t}{V_i'} \gamma_i Q'_i / \text{D1V}$$

$$C_i = \left[\frac{V_i}{V_i'} S_i + \frac{\Delta t}{V_i'} E_{i+1} A_{i+1} \frac{S_{i+1} - S_i}{\Delta x_{i+1}} \right. \\ \left. - \frac{\Delta t}{V_i'} E_i A_i \frac{S_i - S_{i-1}}{\Delta x_i} + \frac{\Delta t}{V_i'} S_{o_i} \right] / \text{D1V} \quad (68a)$$

$$\text{D1V} = 1 + \frac{\Delta t}{V_i'} (\gamma_{i+1} Q'_{i+1} - \delta_i Q'_i)$$

Given the upstream boundary conditions S'_{m1} , S'_{m1+1} may be expressed in terms of S'_{m1+2} through equation (68) with $i = m1+1$, i.e.

$$S'_{m1+1} = a_{m1+1} S'_{m1+2} + b_{m1+1} S'_{m1} + C_{m1+1} \quad (69)$$

where the only unknown on the right hand side of the equation is S'_{m1+2} . Equation (69) may in turn be substituted back into equation (68) with $i = m1+2$, and thus one arrives at an expression for S'_{m1+2} in terms of S'_{m1+3} . In general, there exists the following relation

$$S'_i = P_i S'_{i+1} + O_i \quad (70)$$

where the recursion coefficients P_i and O_i may be calculated from the upstream boundary condition S'_{m1} .

Equation (70) is similar to equation (63) and, therefore, the recursion equations are the same as equation (65), i.e.

$$P_i = \frac{a_i}{1 - b_i P_{i-1}}$$

$$O_i = \frac{b_i O_{i-1} + C_i}{1 - b_i P_{i-1}}$$
(71)

Since S'_{m1} is a known quantity, the comparison between equations (69) and (70) with $i = m1+1$ gives

$$P_{m1+1} = a_{m1+1}$$

$$O_{m1+1} = b_{m1+1} S'_{m1} + C_{m1+1}$$

or, comparing with equation (71) for $i = m1+1$

$$P_{m1} = 0$$

$$O_{m1} = S'_{m1}$$
(71)

Then, the order of numerical computations is

- (1) Calculate a_i , b_i , c_i for $m1+1 \leq i \leq \mu-1$, equation (68a).
- (2) Calculate the recursion coefficients by applying equation (71) or (71a) repeatedly with $i = m1, m1+1, \dots, \mu-1$.
- (3) With S'_{μ} given as the downstream boundary condition, the concentration of the interior segments are calculated by applying equation (70) repeatedly with $i = \mu-1, \mu-2, \dots, m1+1$.

The term S_0 in equation (59) represents the effect of the change in storage volume with the change in tidal elevation. The storage in

each reach will act as a source to the main channel when the tide is falling and act as a sink on the rising tide. The source term can be written as

$$S_{o_i} = - (V_{s_i}' - V_{s_i}) \cdot S_{s_i} \quad \text{if } V_{s_i}' < V_{s_i}$$

where

V_{s_i} is storage volume of the i th reach at time t ,

V_{s_i}' is storage volume of the i th reach at time $t + \Delta t$,

S_{s_i} is concentration of dissolved substance in the storage portion of the i th reach,

or

$$S_{o_i} = - (V_{s_i}' - V_{s_i}) \cdot S_i \quad \text{if } V_{s_i}' > V_{s_i}$$

Equation (26) in the water quality submodel is approximated with a finite difference scheme and solved for the time varying concentration field in the same way as the mass-balance equation for a conservative substance, equation (25) in the hydrodynamic submodel. In instances where the equation of one constituent involves other constituents, the concentrations of the other constituents are expressed in terms of known values, i.e., the values of time t . Therefore, the biochemical interaction terms in the coupled ecosystem do not introduce additional unknowns for the finite difference equation of each individual constituent over that of a conservative substance.

D. Boundary Conditions

The upstream boundary conditions are the freshwater discharge and the concentrations of dissolved substances in the discharge. The most upstream reach is usually set at the limit of tidal influence, allowing upstream salinity boundary conditions to be set to zero.

Appropriate upstream boundary conditions for other dissolved substances must be determined from field data.

In this development, a 'no flux' condition is defined for the most upstream transect. That is, the discharge through the most upstream transect is set to zero. The upstream freshwater discharge is treated as lateral inflow.

The downstream boundary conditions are the tidal level fluctuation and the variation in the concentrations of dissolved substances entering the most downstream reach during the flood tide. When available, tide gauge data may be entered directly into the calculations. Another alternative is to analyze tide gauge or tide table data as a continuous function of time by harmonic analysis (Dronkers, 1964; Harleman and Lee, 1969).

Appropriate values for downstream boundary conditions for the dissolved constituents must be determined from field data. In this development, concentrations in the most downstream reach are stepped up or down to the downstream boundary condition during flood tide. During flood, the interval during which the concentrations in the most downstream approach downstream boundary concentrations is determined during model calibration. On the ebbing tide, concentrations in the most downstream reach are influenced only by advection from the adjacent upstream reach.

E. Computational Tests

Several computational tests were conducted to assure that the proper governing equations had been formulated correctly in the numerical program. The physical problem for the tests is the reflection of a tidal wave propagating into a closed-end channel of uniform rectangular cross-section. The following parameters were used in the tests:

length of channel = 96.3 km;
depth of channel = 10 m;
amplitude of incoming tidal wave = 10 cm;
period of tidal wave = 12.42 hours;
wave length = 442.6 km;
 $\Delta x = 5.5$ km;
 $\Delta t = 0.01$ tidal cycles.

All computations were started with initial conditions of velocity equal zero and tidal height equal zero throughout the channel. The salinity is set to zero so that salinity effects are not included in the tidal dynamics. The computation proceeds with the water surface elevation at the channel entrance varying in simple harmonic motion while the velocity at the closed end of the channel is kept constantly at zero.

The model was first run with a Manning friction coefficient of 0.015. A time step of 0.01 tidal cycles (approximately 7.5 minutes) was found to be optimal for the test run and it was used for all the computational tests. The model was run for a time equivalent to 12 tidal cycles to assure the establishment of a tidal regime. The resulting time-varying tidal height and current are shown in Figures 4, 5, and 6 for locations at the channel entrance, at the mid-point of the channel, and near the closed end. These figures show that all of the initial transients have been damped by the eighth tidal cycle. Figures 7 and 8 show the longitudinal variation of tidal amplitude and tidal current. Theoretical curves based on the linear frictionless model (Ippen, 1966) are presented in the figures for comparison.

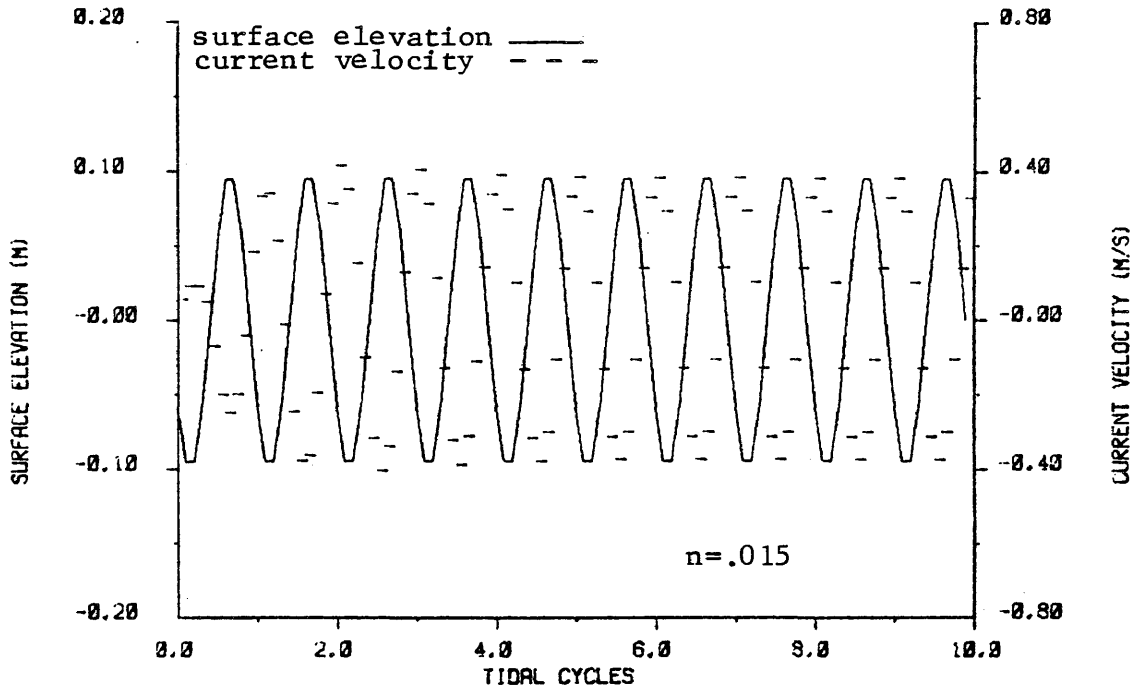


Figure 4. Time variations of tidal height and velocity at the channel entrance.

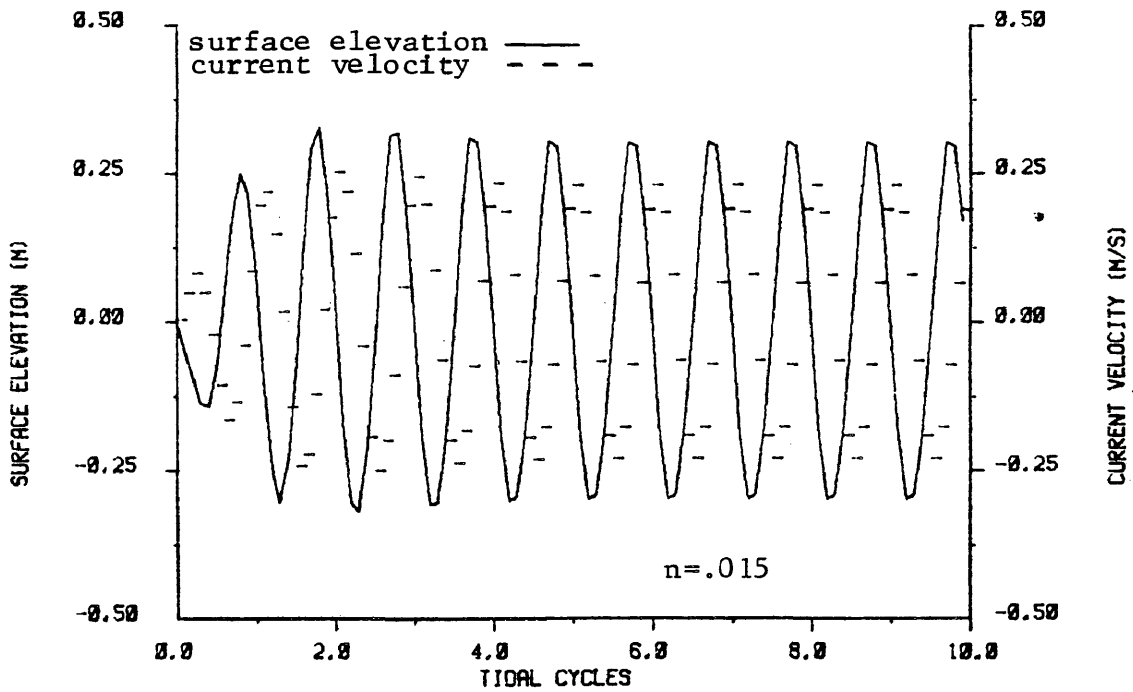


Figure 5. Time variations of tidal height and velocity at the midpoint of the channel.

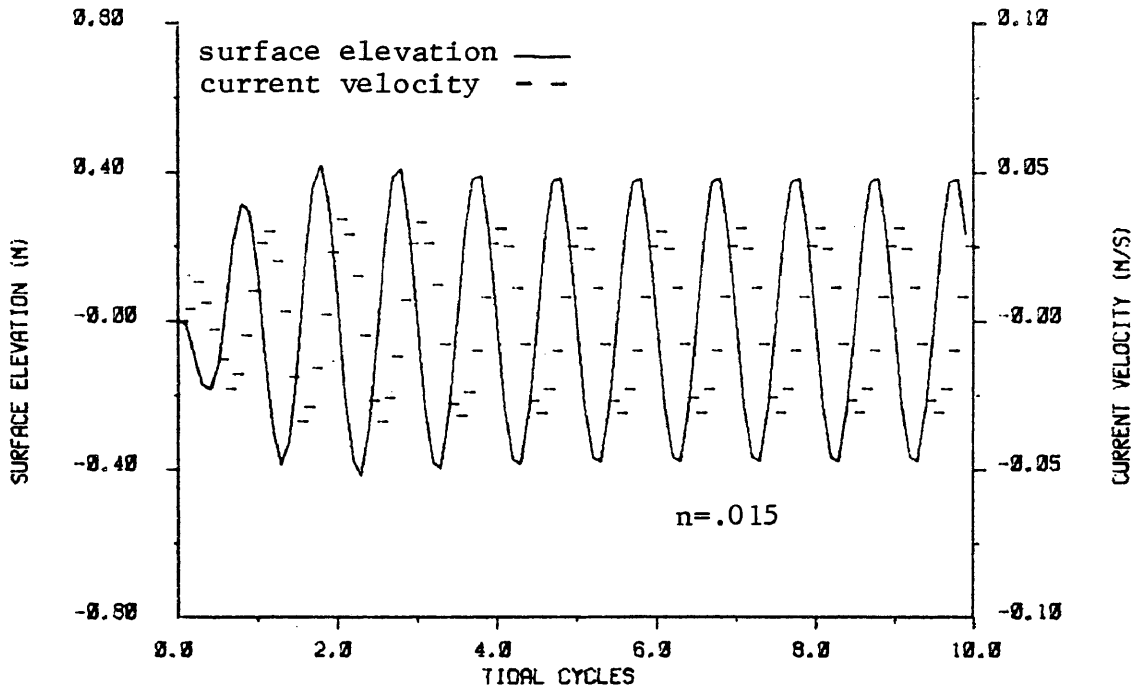


Figure 6. Time variations of tidal height and velocity near the closed-end of the channel.

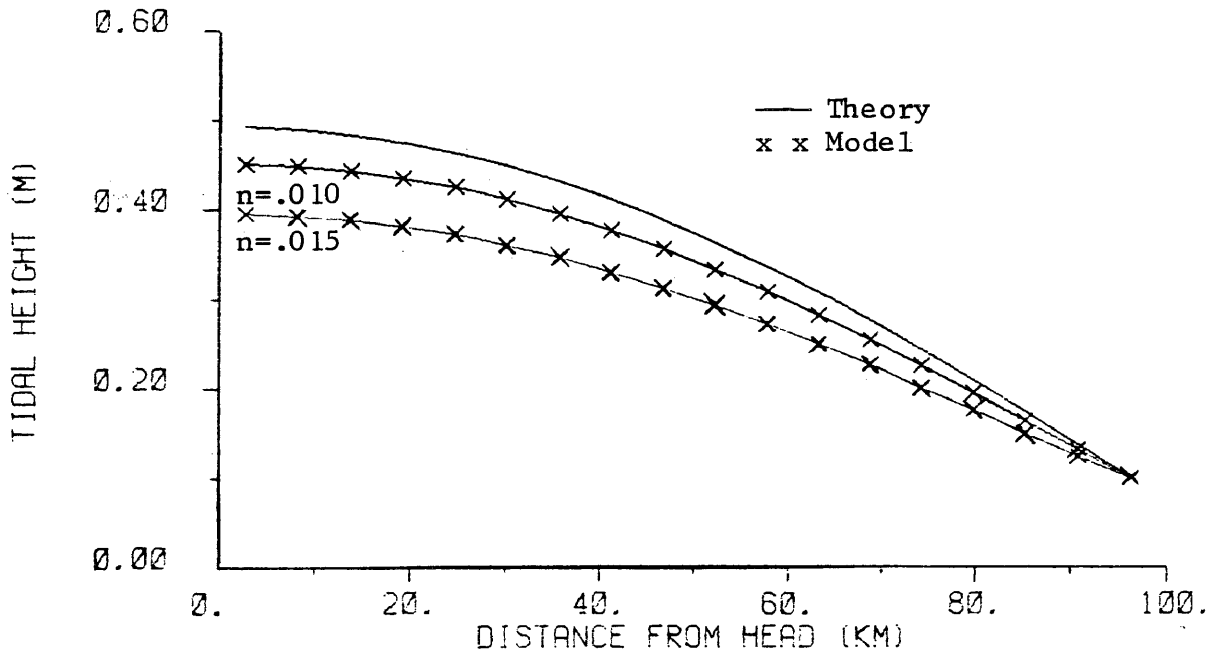


Figure 7. Longitudinal distribution of tidal amplitude along a closed-end channel.

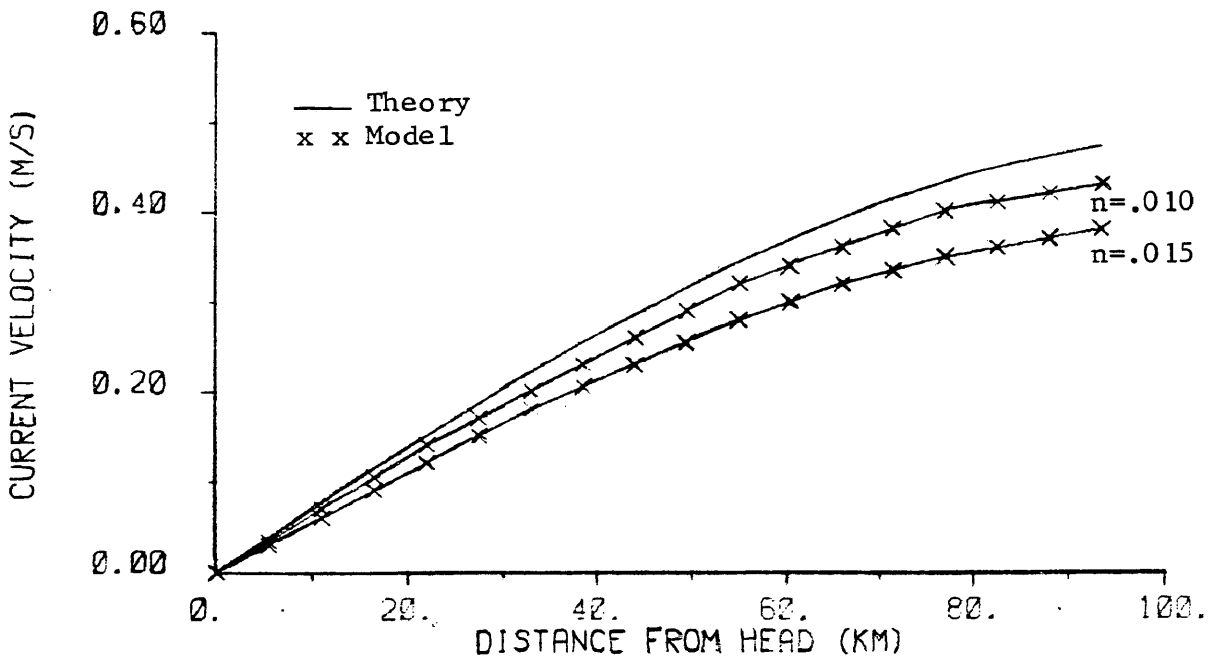


Figure 8. Longitudinal distribution of the amplitude of tidal current along a closed-end channel.

The model was also run with a Manning friction coefficient of 0.010, and the results for tidal amplitude and current are shown in Figures 7 and 8. The model agrees with the theory: the predicted tidal amplitudes and tidal current are smaller than the frictionless theory, and the model results approach the theoretical results when the friction coefficient is decreased. Since no analytical solution exists for the non-linear friction model, the numerical results cannot be tested quantitatively.

The model was also run with a Manning friction coefficient of 0.010, and the results for tidal amplitude and current are shown in Figures 7 and 8. The model agrees with the theory: the predicted tidal amplitudes and tidal current are smaller than the frictionless theory, and the model results approach the theoretical results when the friction coefficient is decreased. Since no analytical solution exists for the non-linear friction model, the numerical results cannot be tested quantitatively.

Model sensitivity test runs were made to determine the relative importance of the nonlinear term in the momentum equation, the second term on the right hand side of equation (60a). For this test, the hydrodynamic submodel was run using the geometry of a small tidal stream (see Chapter IV). Model results for two runs, one with and one without the nonlinear term, were compared. Omitting the nonlinear term led to an increase of approximately 1% in maximum current within a tidal cycle and a comparable decrease in maximum surface elevation within a cycle.

Although the nonlinear term had little effect on model results in this case, the computation time saved by omitting the term is very small. Since there may exist other systems where the model can be applied in which the nonlinear term is of more importance, it was decided to retain the term in the model.

IV. MODEL APPLICATION - A CASE STUDY

The case study presented in this chapter is made to illustrate the application of the model to a particular tidal creek, and to show the abilities of the model in reproducing and predicting prototype behavior under varying inputs. The model is applied to the Little Hunting Creek, a small stream located in the Mount Vernon area of Fairfax County, Virginia (Figure 9). The creek drains a 33 square kilometer urban-suburban basin and consists of two upland branches which drain into a tidal section approximately 3.5 kilometers in length. The tidal portion joins a small embayment on the upper Potomac River. This essentially freshwater region of the tidal Potomac is impacted by major municipal wastewater discharges (Champ et al., 1981). The Little Hunting Creek receives discharges within the tidal portion from a 6.6 mgd sewage treatment plant.

Excess algae is a recurring problem in the Little Hunting Creek as it is in other embayments along the Potomac. These large algal populations lead to undesirable pH levels and dissolved oxygen fluctuations. A predictive model developed here for the Little Hunting Creek could serve as a tool in the management of water quality in nearby embayments as well.

Application of the mathematical model requires the specification of three groups of parameters - physical parameters, input parameters, and calibration parameters. Physical parameters are measures such as

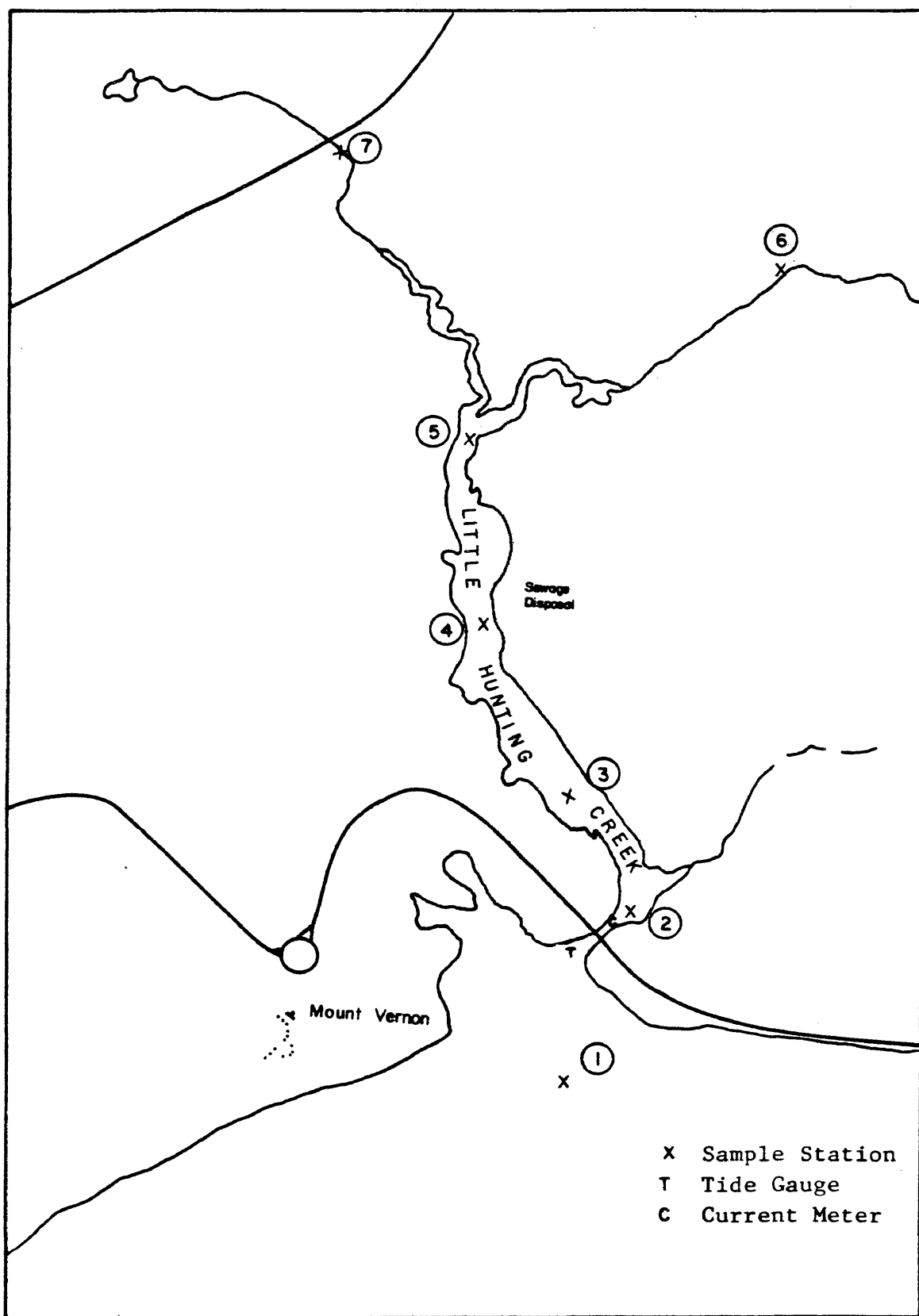


Figure 9. Little Hunting Creek sample stations.
(USGS Mt. Vernon quadrangle).

channel cross-sectional area and depth which define the physical characteristics of the water body. Input parameters are the variables upon which model predictions are based e.g. tidal forcing, temperature and wasteloadings. Calibration parameters are the coefficients or rate constants which cannot be measured directly but must be derived through repeated adjustments until the model can satisfactorily simulate the prototype behavior.

The field program in this study was developed to provide a comprehensive data base useful in assessing water quality conditions in the Little Hunting Creek and in calibrating and validating a predictive mathematical water quality model. To provide this data base a series of physical surveys and slackwater and intensive water quality surveys were conducted from May to September of 1980 by the Department of Physical Oceanography, Virginia Institute of Marine Science.

Physical surveys included a bathymetry survey, an aerial survey of high tide and low tide surface area, and the monitoring of tidal height and currents. Surveys of water quality were conducted approximately bi-weekly from May 21 to September 30, 1980. The surveys were conducted under varying conditions of freshwater flow, stream temperature and wasteloading. The locations of survey sampling stations, tide gauges, current meters and that of the STP outfall are shown in Figure 9. In-situ measures of dissolved oxygen, temperature, pH and secchi depth were taken at each station. Samples were withdrawn from mid-depth and analyzed for the other water quality parameters of interest. In addition, sediment oxygen demand was measured during the first slackwater survey. The intensive and diurnal surveys differed from the slackwater surveys in that sampling was conducted continuously

for two tidal cycles, providing data on the intra-tidal and the diurnal parameter fluctuations in the creek. The dispersion and flushing characteristics of the creek were investigated through a dye study conducted concurrently with the intensive water quality survey.

A. Hydrodynamic Submodel Calibration

1. Physical Parameters

To construct a mathematical model, the creek is divided longitudinally into a number of reaches bounded by transects. The transects were chosen to coincide when possible with the cross-sectional profiles measured in the field. Additional transects were placed at or near mid-distance between field transects. The characteristics of transects so chosen were interpolated from the adjacent measured transects with additional reference to aerial survey information and available topographic maps. The transects are placed away from the regions of sharp bends or narrow constrictions and are spaced on an average of approximately 200 meters apart. Model segmentation is presented in Figure 10.

Values for cross-sectional areas, depths, surface areas and volumes were determined from information gathered during the physical surveys of the creek. The values of the physical parameters used as input to the model are given in Table I.

2. Input Parameters

a. Upstream boundary condition - The discharge through the most upstream transect was set to zero and freshwater input into the most upstream model reach was treated as lateral inflow.

b. Lateral inflow - Daily values of runoff from the Little

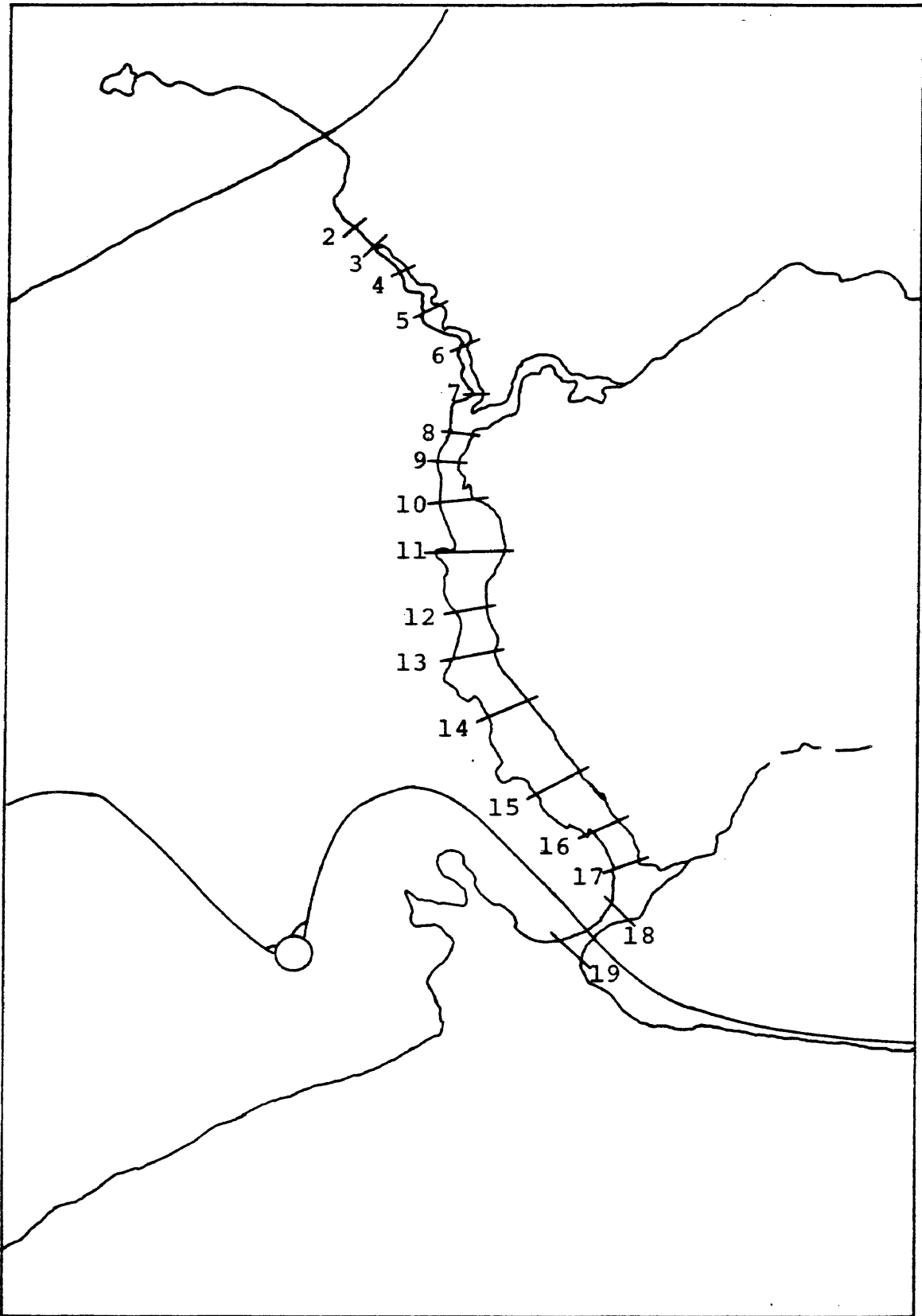


Figure 10. Model segmentation.

Table I. Physical Parameters

Transect	Distance from Mouth (km)	Conveyance Cross-sectional Area (m ²)	Total Cross-sectional Area (m ²)	Transect Depth (m)
2	3.64	1.0	1.0	0.8
3	3.46	1.7	2.0	0.8
4	3.34	2.6	3.0	0.8
5	3.10	3.4	5.0	0.8
6	2.87	4.0	7.2	0.8
7	2.72	5.0	8.0	0.8
8	2.50	42.0	47.0	1.10
9	2.37	42.0	57.0	1.10
10	2.19	41.0	51.0	1.20
11	2.01	38.0	45.0	1.30
12	1.79	36.0	64.0	1.20
13	1.56	32.0	50.0	1.20
14	1.24	26.0	35.0	1.60
15	0.94	39.0	66.0	1.20
16	0.69	30.0	44.0	1.30
17	0.52	37.0	52.0	1.40
18	0.38	44.0	51.0	1.50
19	0.07	44.0	51.0	1.50

Table I. (Cont'd)

Reach	Reach Depth (m)	Conveyancy Surface Area (10^3 m^2)	Storage Surface Area Low Tide (10^3 m^2)	Change in Surface Area (10^3 m^2)	Storage Volume Low Tide (10^3 m^3)
2	0.8	0.5	.00	.00	.00
3	0.8	0.85	.00	1.00	.00
4	0.8	1.0	.00	2.70	.00
5	0.8	1.2	.00	4.30	.00
6	0.8	1.6	.00	4.90	.00
7	0.95	4.0	10.00*	25.00*	3.00*
8	1.10	3.0	0.00	6.00	0.00
9	1.15	1.5	.00	13.40	.00
10	1.25	6.0	.00	21.80	.00
11	1.25	5.6	.00	26.90	.00
12	1.20	8.5	1.00	23.20	.30
13	1.40	6.5	6.00	39.00	1.01
14	1.40	8.1	5.80	36.20	.71
15	1.25	8.0	7.80	26.90	.90
16	1.35	5.0	8.00	7.50	1.50
17	1.45	3.0	4.00	18.50	.70
18	1.50	5.0	3.50	16.00	.40

* includes tributary

Hunting Creek drainage basin were supplied by the Northern Virginia Planning District Commission. Based on the distribution of drainage area along the creek, runoff was divided into two lateral inflows: three-fourths of the total going into the most upstream reach and one-fourth going into the reach associated with the tributary. Values for these lateral inflows are read into the model once for each day of simulation. Discharge from the STP outfall averaged 0.22 cubic meters per second and was included as a constant lateral inflow to the model.

c. Downstream boundary condition - At each iteration of time step a value for downstream surface elevation is read into the hydrodynamic submodel. Surface elevation values so used were prepared from the tide gauge record measured near the mouth of the creek.

d. Initial conditions - As the hydrodynamic submodel was to be started at a point of time corresponding to that of the first sample taken during the August intensive survey, it was necessary to determine appropriate initial conditions for surface elevation, discharge and dye concentration for input to the submodel. Initial conditions for surface elevation and discharge were arrived at by running the submodel from two tidal cycles before the time corresponding to that of the first sample. Output for the appropriate time from this run was used as initial conditions in calibration runs made later.

Dye concentrations in the creek could not be adequately determined from field measurements made at the beginning of the intensive survey. Not until hour 4 (1900) was the concentration curve for dye sufficiently defined by field data. For this reason it was decided to set the initial dye concentrations for the model to the equivalent of background readings (0.2 ppb) and then, at a point in the

simulation corresponding to hour 4 of the intensive survey, to redefine the dye concentrations for all model reaches to approximate the concentration curve measured in the field at that time.

3. Calibration Parameters

a. Friction coefficient - Model runs were made with the value of Manning's friction coefficient (n) varied from zero to a maximum of 0.04. A value of 0.02 was chosen and assigned uniformly throughout the creek.

b. Weighting factors - Implicit weighting factors for surface and velocity gradients affect the numerical stability and dispersion of the finite difference scheme. A compromise between the two needs to be reached. Test runs indicated that a value of 0.75 would result in a stable numerical scheme without introducing excessive numerical dispersion.

c. Dispersion coefficient - The dispersion coefficient (E) in the mass-balance equation (Equation 25) is determined by the relationship

$$E = 63.2 n R^{5/6} |U| + E_0$$

where

n = Manning's friction coefficient,

R = the hydraulic radius, in meters, assumed equal to mean depth plus surface elevation above mean tide level,

U = the current velocity, in m/sec, and is equal to discharge divided by channel cross-sectional area,

E_0 = a constant to be determined.

The calibration constant, E_o , was adjusted until dye dispersion in the model satisfactorily reproduced that measured in the field. In this manner, a value for E_o of 1.0 square meters per second was determined.

4. Simulation Results

The hydrodynamic submodel was run for eleven tidal cycles, simulating a period corresponding to the beginning of the August 20-21 intensive field survey and ending with the last slackwater dye survey taken on August 26, 1980. Tidal height and current velocity for the first two tidal cycles of simulation were compared to tide staff readings and current meter records for the period of the intensive survey.

The model results for tidal heights at the most upstream tidal station (station 5) after calibration are presented in Figure 11 which shows that the model simulation at this point is quite good.

The simulation of current velocities at two locations are compared to current meter records in Figure 12. Model results compare satisfactorily to field measurements in most instances. The notable exception occurs at the location near the mouth of the creek (station 2). As can be seen from Figure 9, on the flooding tide flow at this location would be entering an area of rapid expansion. The current meter record indicates a great amount of turbulence due to this rapid expansion. This condition cannot be replicated by the one-dimensional equations employed in the hydrodynamic submodel. However, when the reverse flow on the ebb enters the narrow constriction at the bridge the current record shows little turbulence. During the ebb flow model

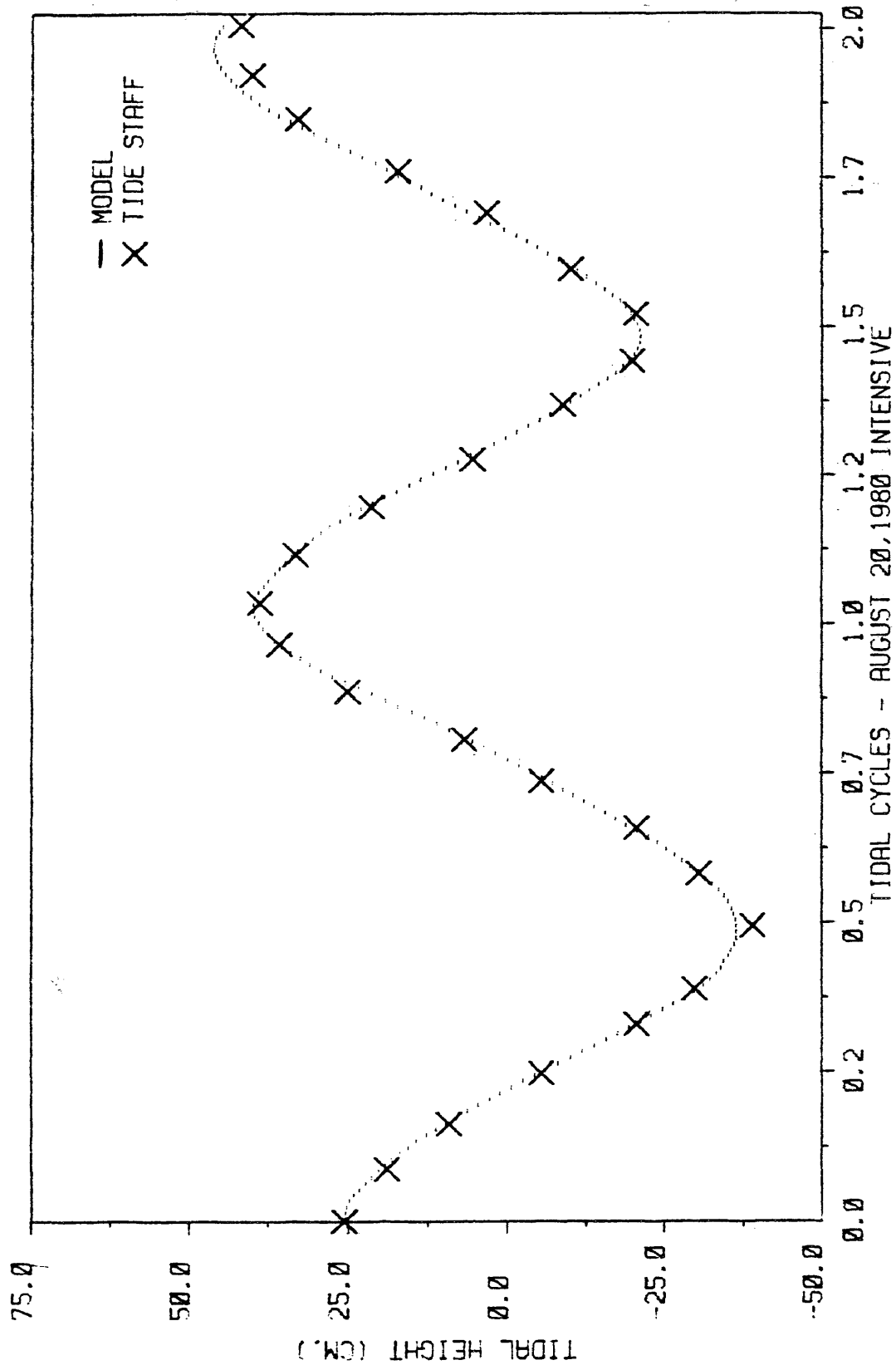
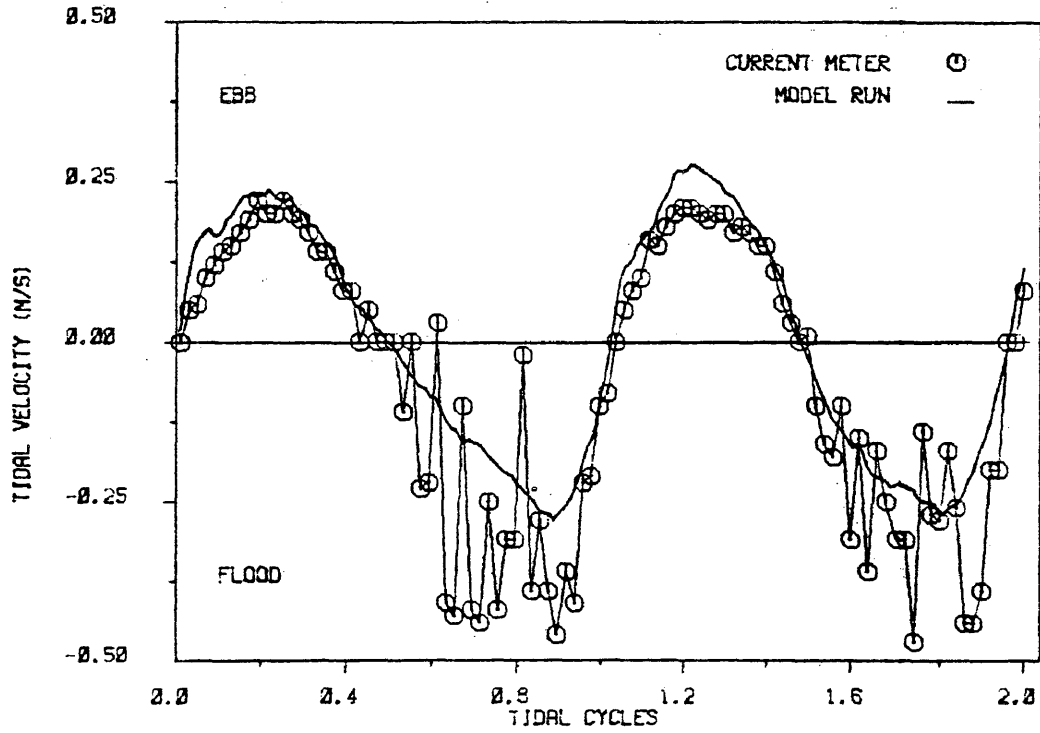
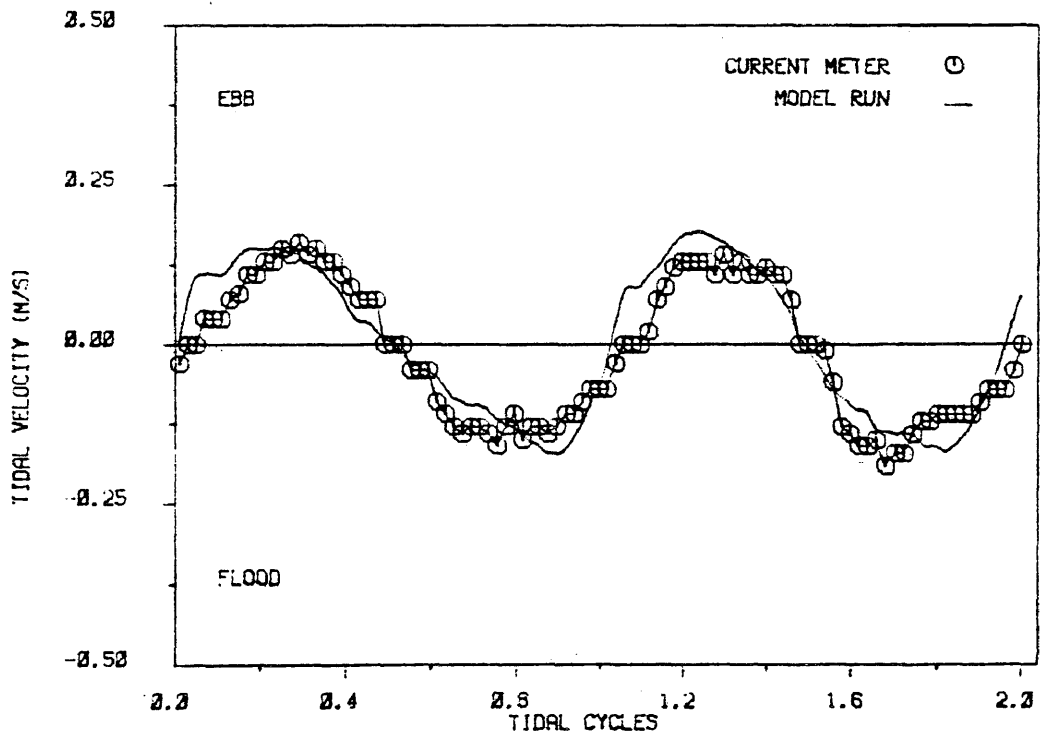


Figure 11. Tidal simulation - station 5 (2.5 km).



station 2 (0.23 km)



station 1 (1.5 km)

Figure 12. Current velocity simulation.

results compare well with field records for station 2.

Model simulation of dye dispersion in the creek are compared graphically to some hourly field measurements in Figures 13 through 18. In Figures 19 through 22, model results are compared to dye concentrations measured at 3.5, 4, 6, and 8 tidal cycles after the beginning of the intensive survey. As mentioned previously, concentrations measured in the creek at 1900 hours on August 20 were used to define the initial dye concentrations and are read into the model at the point in the simulation corresponding to hour 4. For a period equivalent to about four hours after concentrations in the model are redefined in the above manner, the model fails to recreate the concentrations measured in the field for the downstream stations (stations 2 and 3). By hour 8, however, the model results compare well with the field measurements for all four stations in the creek. The assumption of total cross-sectional homogeneity is an approximation which cannot describe adequately the concentration field during the initial mixing period after dye injection. Therefore, one-dimensional dispersion theory always fails to apply during the initial mixing period and it is not surprising that the model results and field measurements do not agree between hour 4 and hour 8.

B. Water Quality Submodel Calibration

1. Input Parameters

a. Parameters calculated by hydrodynamic submodel - To provide input parameters to the water quality submodel, new initial conditions of surface elevation were determined from tide gauge records and the hydrodynamic submodel was used to simulate a 14 tidal cycle period

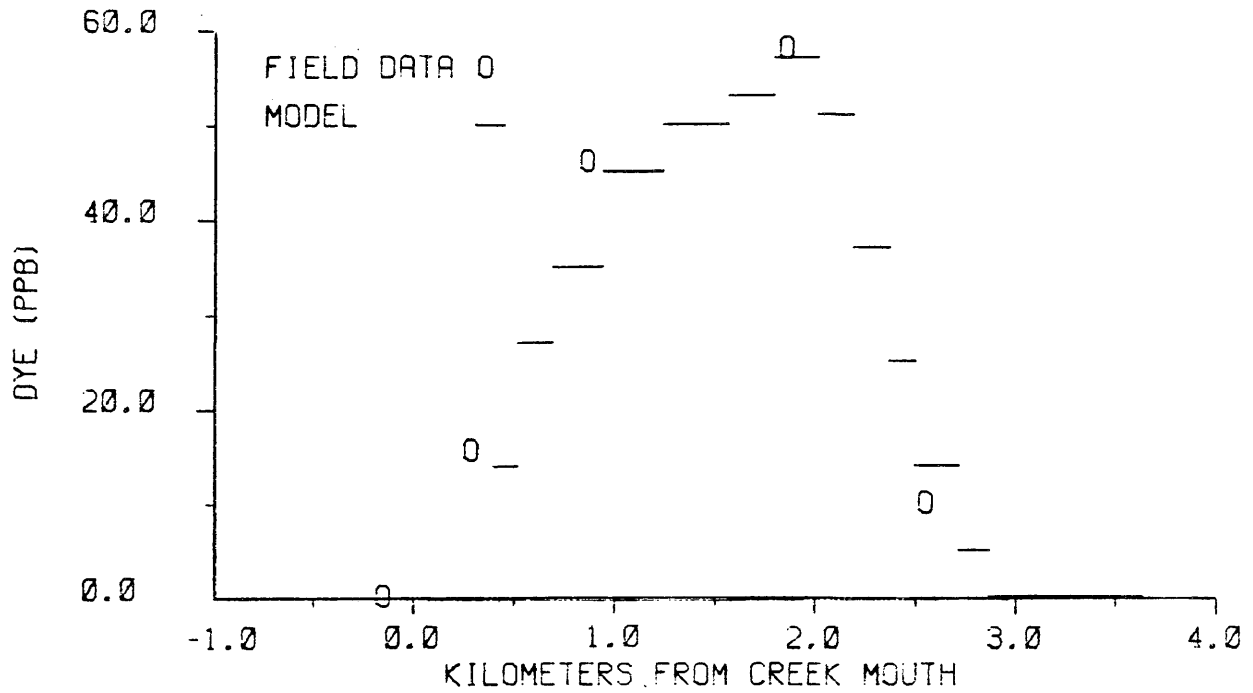


Figure 13. Hour 4 (1900) of dye dispersion simulation.

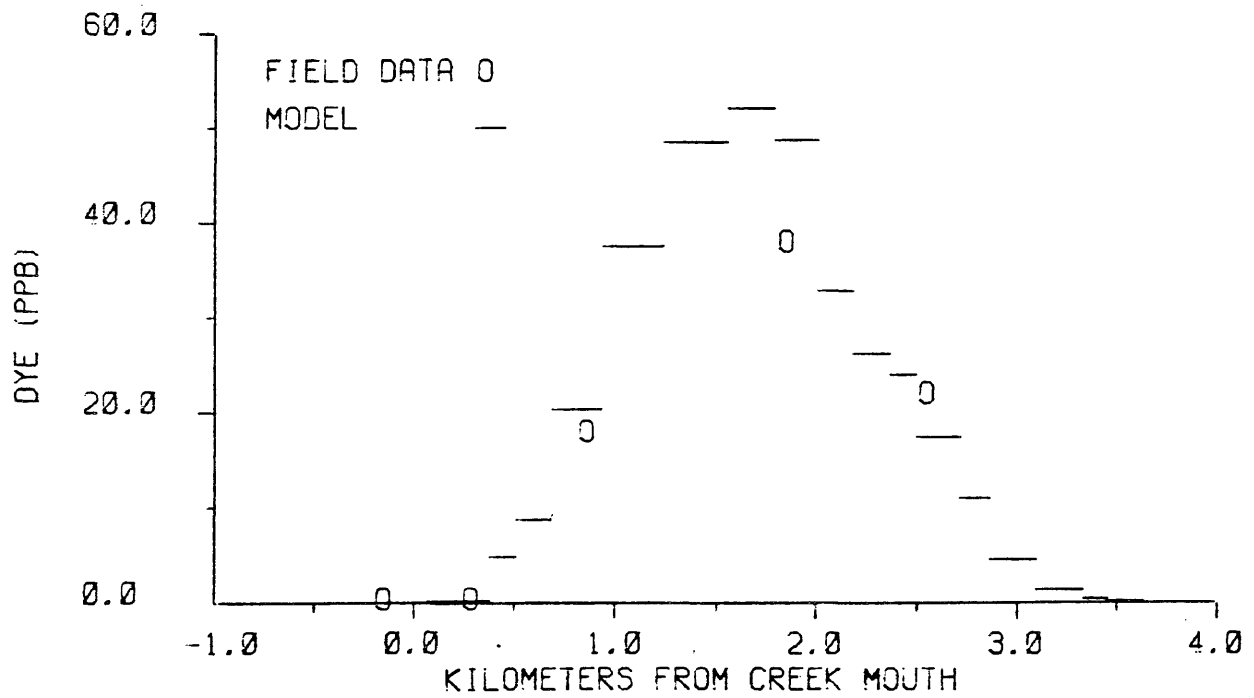


Figure 14. Hour 8 (2300) of dye dispersion simulation.

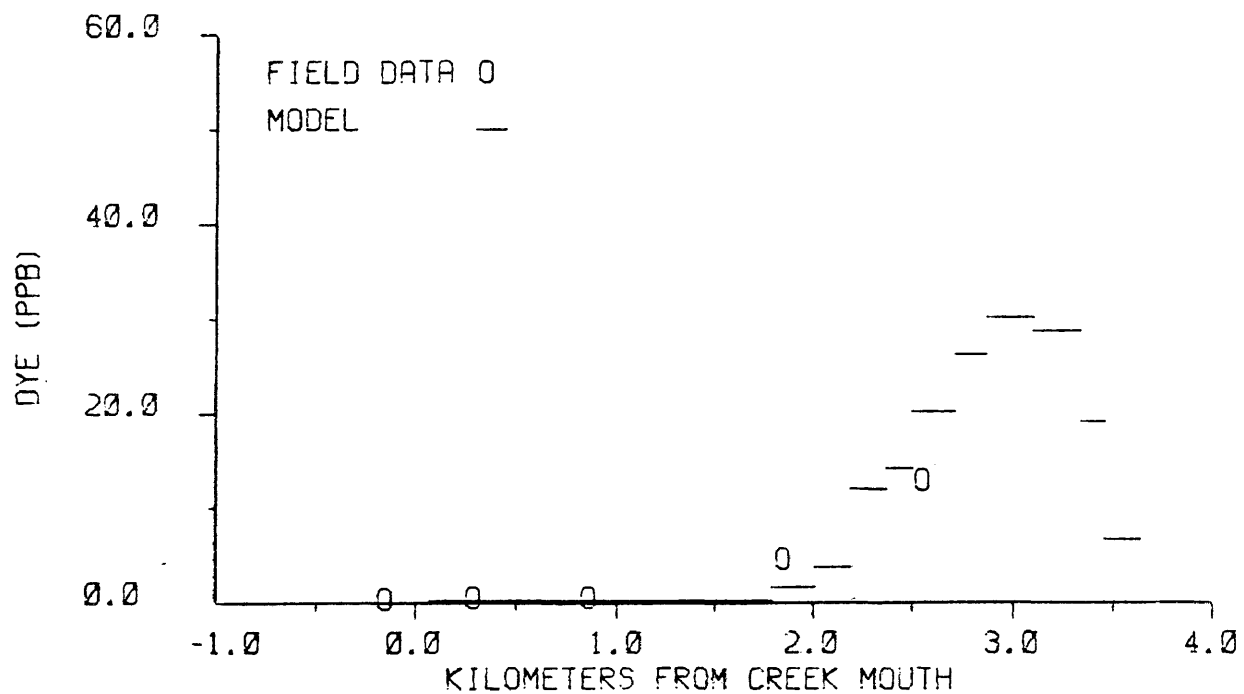


Figure 15. Hour 12 (0300) of dye dispersion simulation.

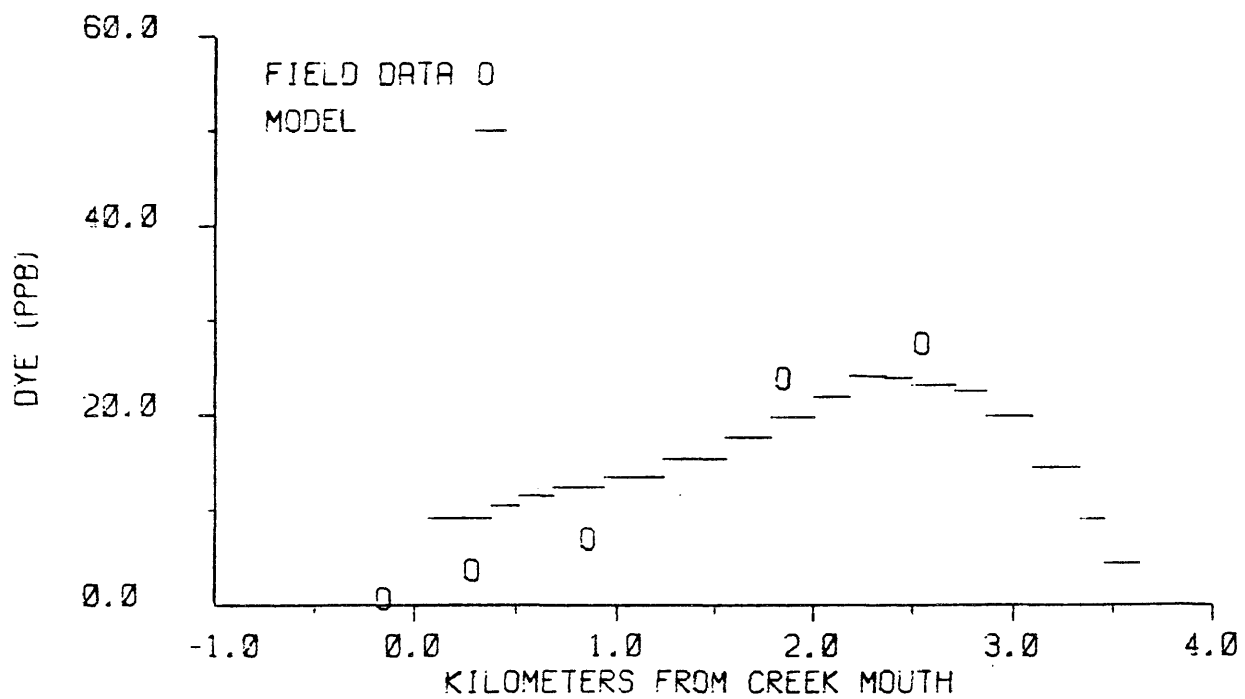


Figure 16. Hour 16 (0700) of dye dispersion simulation.

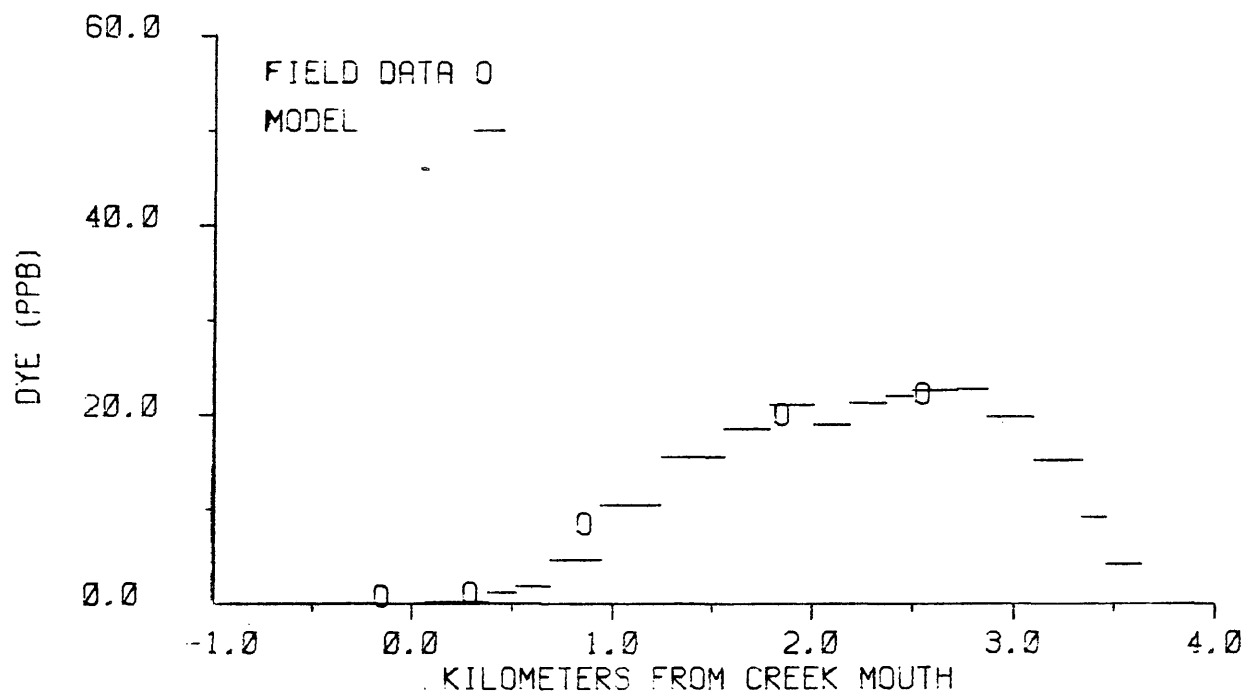


Figure 17. Hour 20 (1100) of dye dispersion simulation.

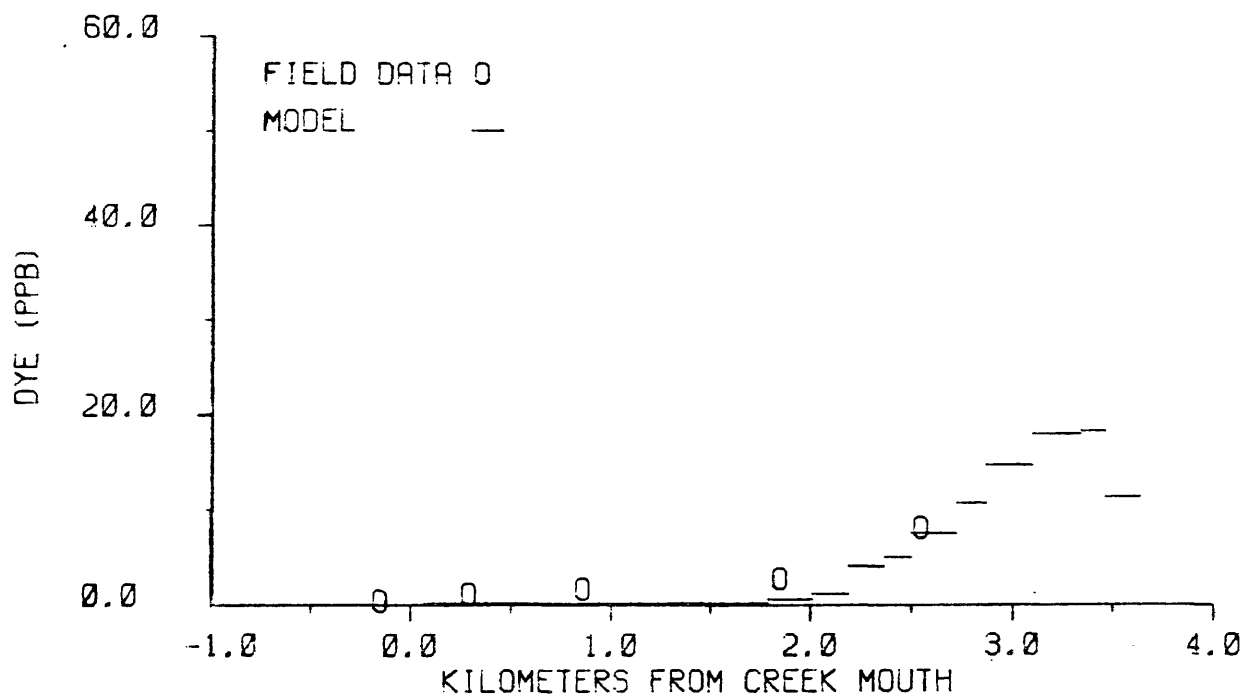


Figure 18. Hour 24 (1500) of dye dispersion simulation.

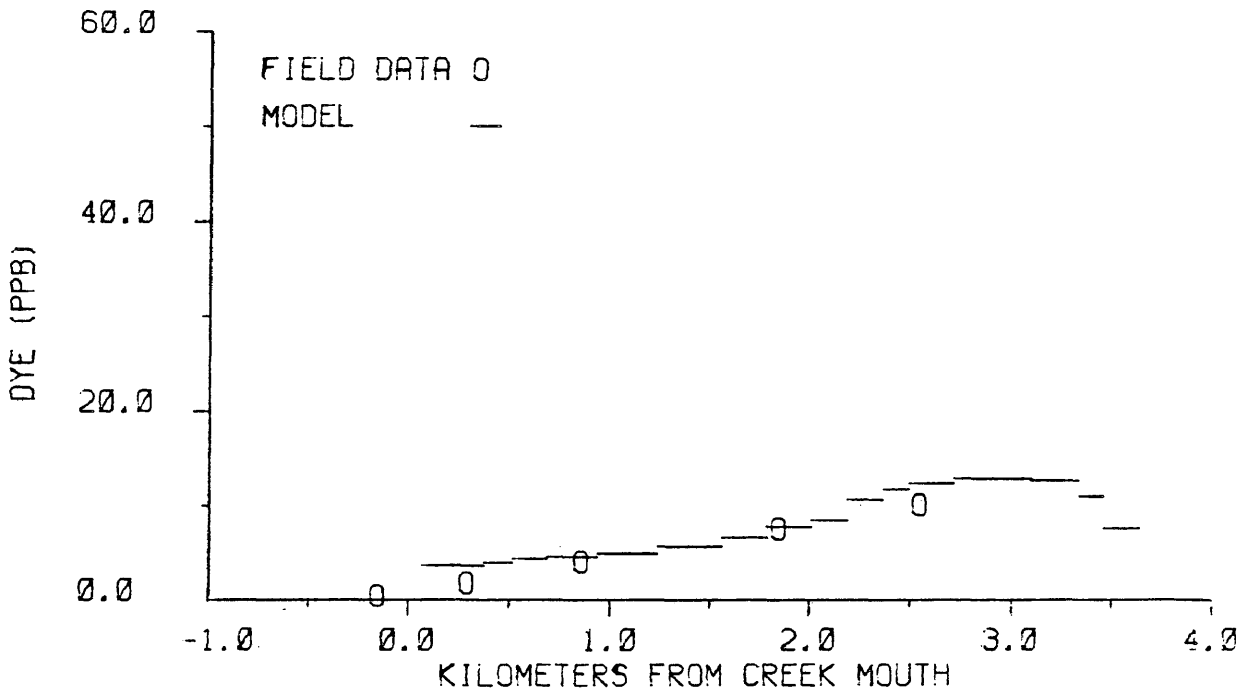


Figure 19. Cycle 3.5 (low slack) - dye dispersion simulation.

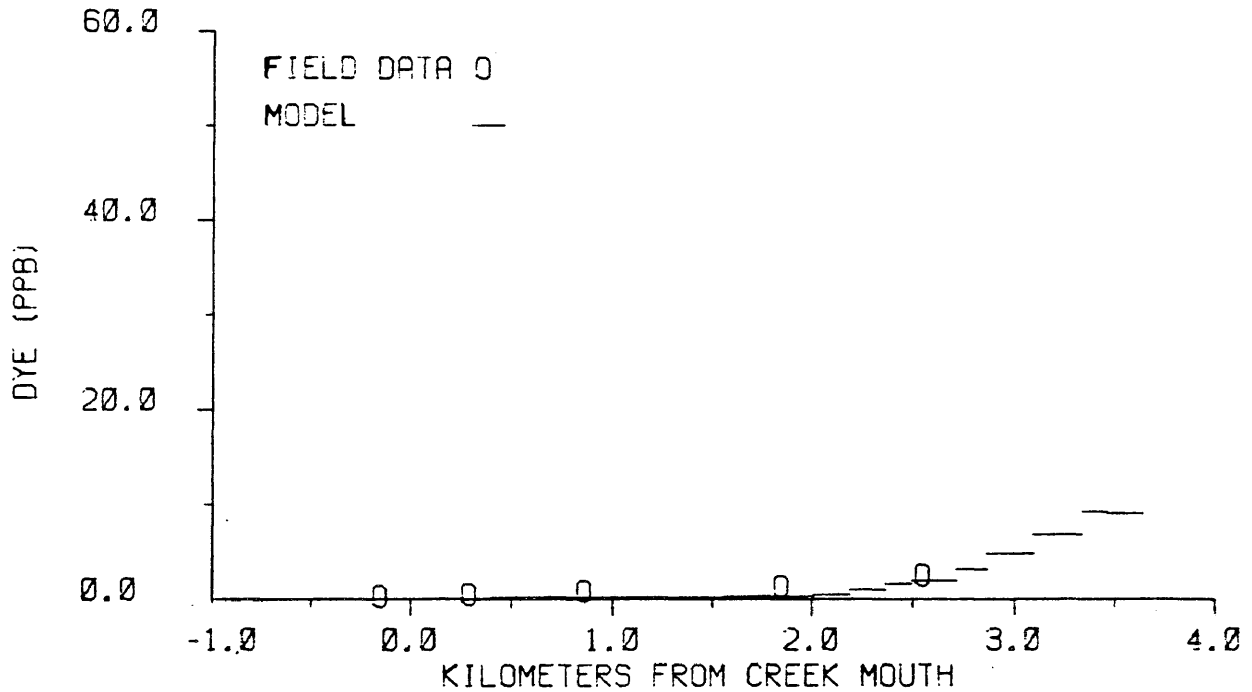


Figure 20. Cycle 4.0 (high slack) - dye dispersion simulation.

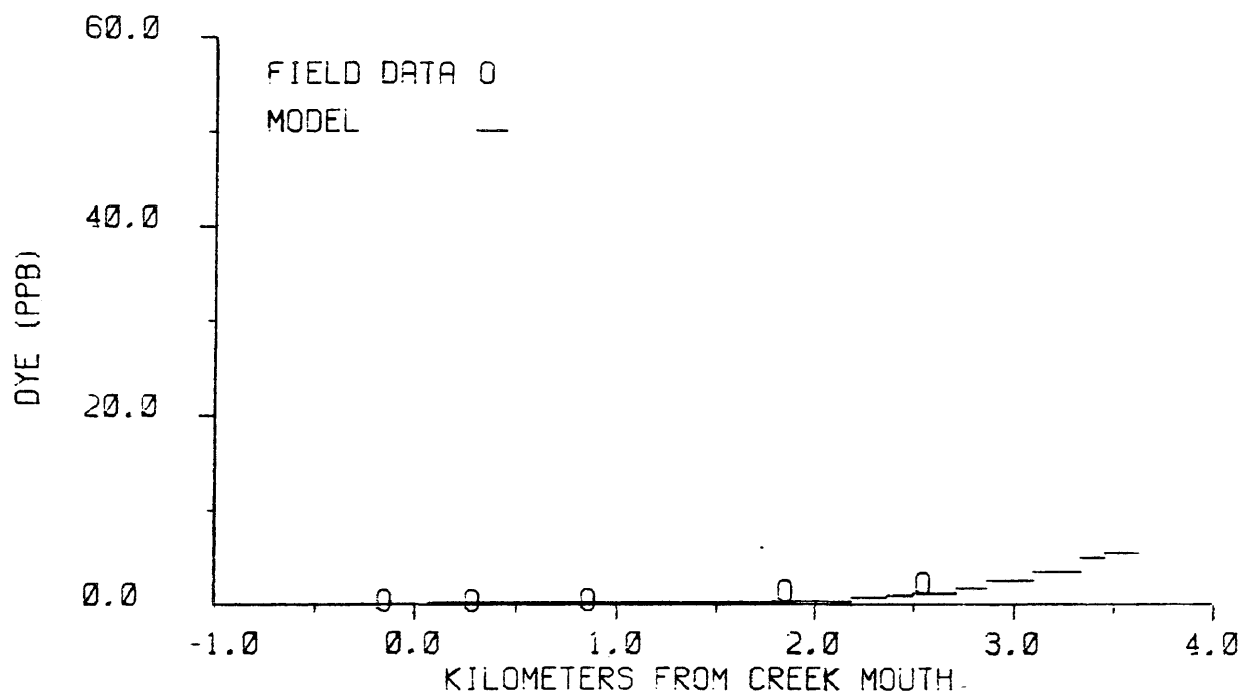


Figure 21. Cycle 6.0 (high slack) - dye dispersion simulation.

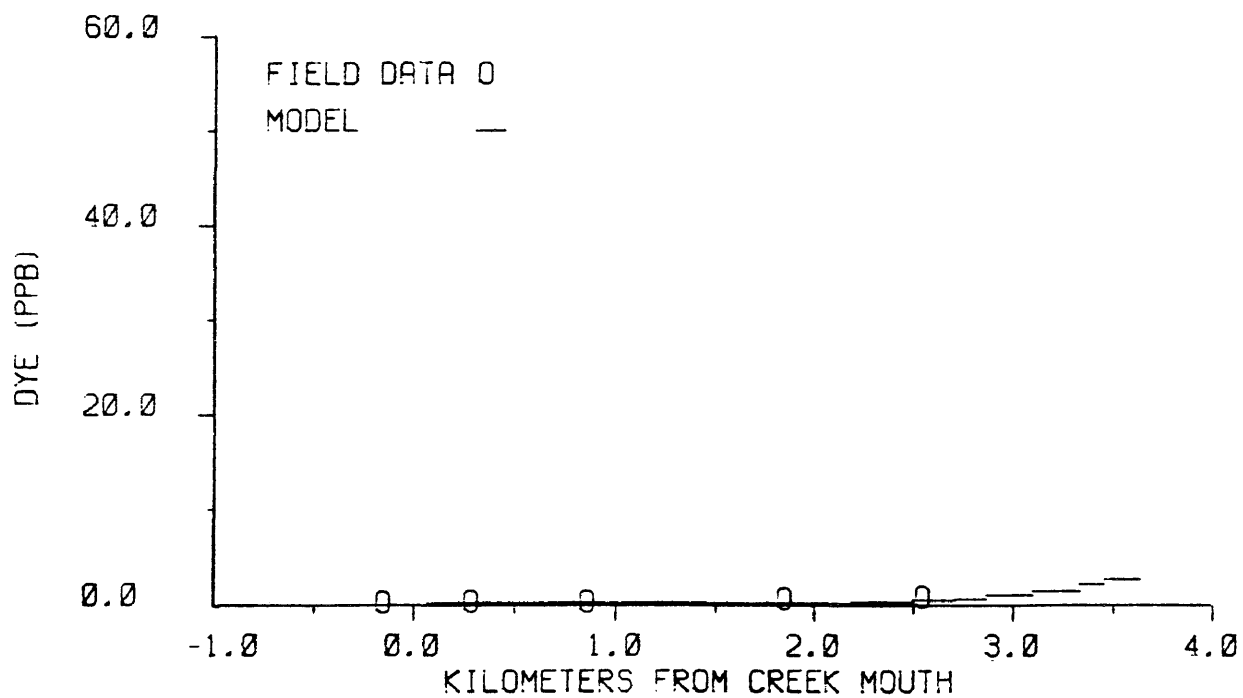


Figure 22. Cycle 8.0 (high slack) - dye dispersion simulation.

corresponding to the 7 days from the August 14 high slackwater survey through the August 20-21 intensive survey. At each time step, for all reaches, instantaneous values of channel cross-sectional area, current velocity, surface elevation, dispersion coefficient, channel volume and storage volume were stored for use in the water quality submodel.

b. Point source loading - For each water quality parameter (except chlorophyll 'a') an average of the concentrations from four 12 hour composite samples taken at the STP outfall during the intensive survey was used to determine point source input to the model. The average concentrations in milligrams per liter were converted to kilograms per day by using the average flow (4.45 mgd) measured at the STP outfall during the intensive survey. The formulas for determining organic nitrogen and organic phosphorus gave zero or negative values for two samples. For the purpose of averaging, negative values were set to zero. The value for point source flow rate used in the model is the average of the value measured during the August 14 slackwater survey and the values from the intensive survey.

Values for the parameters measured at the STP outfall are given in Table II together with the values used and held constant throughout the model simulation.

c. Nonpoint source loading - A daily time series of nonpoint source input to the creek for the period May 1 - October 31, 1980 was provided by the Northern Virginia Planning District Commission (NVPDC). Runoff volume, mass fluxes of organic nitrogen, ammonia nitrogen, nitrite + nitrate nitrogen, organic phosphorus, ortho-phosphorus, and CBOD and dissolved oxygen concentrations were provided. Table III gives the portion of this time series from 8/14/80 to 8/21/80.

Table II. STP Field Measurements (12 hour composite samples) and Corresponding Model Point Source Inputs

Date	Time	Flow (m ³ /s)	Org N (kg/day)	NH ₄ -N (kg/day)	NO ₂ +NO ₃ -N (kg/day)	Org P (kg/day)	Ortho P (kg/day)	CBOD _u (kg/day)	D.O. (mg/l)	Temp. (°C)
8/20/80	0300	.20	60.6	236.	30.8	0.0	2.02	288.	9.0	22.0
8/20/80	1500	-	43.8	253.	37.7	0.0	1.68	281.	8.0	22.0
8/21/80	0300	.19	0.0	239.	34.0	2.36	1.01	286.	7.8	25.0
8/21/80	1500	-	0.0	296.	43.1	2.19	1.18	288.	7.5	25.0
Model Input		.22+	26.1	256.	36.4	1.15	1.48	286.	8.1	-

+ STP flow rate is an average of the value for 8/14/80 (.24) and 8/20-21/80 (.20)

Table III. Non-point Source Loadings

Date	Flow (m ³ /s)	Org N (kg/day)	NH ₄ -N (kg/day)	NO2+NO3-N (kg/day)	Org P (kg/day)	Ortho P (kg/day)	CBOD _u (kg/day)	D.O. (mg/l)
8/14/80	.045	1.1	0.4	2.9	0.2	0.1	9.5	10.
8/15/80	.037	1.0	0.3	2.5	0.2	0.1	8.2	10.
8/16/80	.051	16.4	2.1	6.7	2.2	0.7	97.3	10.
8/17/80	.028	0.7	0.2	1.8	0.1	0.1	5.9	10.
8/18/80	.722	300.5	35.8	91.3	39.6	12.8	1749.5	10.
8/19/80	.045	6.0	0.9	3.2	0.8	0.3	35.9	10.
8/20/80	.023	0.6	0.2	1.5	0.1	0.0	5.0	10.
8/21/80	.020	0.5	0.2	1.3	0.1	0.0	4.5	10.

The nonpoint loadings were obtained by the NVPDC through employment of the Commission's nonpoint source prediction models. Predictions were based on local rainfall data, land use data and other characteristics, and on calibration parameters determined in a study of the Occoquan Basin (Hydrocomp, Inc., 1977; NVPDC, 1979).

Based on the distribution of drainage area along the creek, nonpoint source loadings were divided into two parts: three-fourths of the total going to the most upstream reach, one-fourth going to the reach containing the tributary. Daily totals for nonpoint loadings are read into the model at the beginning of each day of simulation.

Table IV gives the NVPDC predictions, in mg/l, and the field measurements from station 7, the station on the Little Hunting Creek above the head of tide.

d. Solar radiation - A monthly average daily solar radiation of 450 langleys for the month of August (U.S. Dept. of Commerce Weather Bureau) was employed. Daily values for solar radiation were not yet available.

e. Sediment oxygen demand - Values for sediment oxygen demand were obtained from flux studies of the Little Hunting Creek undertaken in May, 1980. SOD was measured as 2.5 gram/m²/day at station 2 and 2.9 gram/m²/day at stations 3, 4 and 5. This same distribution was employed in the model. In the model reaches corresponding to the creek upstream of station 5 the SOD was tapered down to 2.5 gram/m²/day.

f. Boundary conditions - The downstream boundary condition for each parameter is the concentration measured at the station near the mouth of the creek (station 2), the location of which is approximately that of the most downstream transect of the model. The values employed

Table IV. Concentrations of Nonpoint Runoff as Predicted by NVPDC and Field Measurements at Station 7. Concentrations are in mg/l except chlorophyll which is in µg/l.

	Org-N	NH ₄ -N	NO ₂ +NO ₃	Org-P	Ortho-P	CBOD	D.O.	Chl.
5/21/80	NVPDC Sta.7	.68 .49	.10 0.1	.37 .55	.10 .04	4.1 7.7	10.0 8.0	0.0 1.4
6/3/80	NVPDC Sta.7	2.77 .72	.33 <0.1	.85 .25	.37 .15	16.2 10.3	10.0 6.3	0.0 56.8
6/24/80	NVPDC Sta.7	.21 .29	.08 <0.1	.56 .05	.04 <.08	1.9 2.4	10.0 6.3	0.0 2.7
7/8/80	NVPDC Sta.7	1.18 .48	.14 <0.1	.37 .64	.16 .06	6.8 20.6	10.0 4.5	0.0 3.3
7/22/80	NVPDC Sta.7	.67 .47,.38	.08 <0.1	.21 .40,.33	.09 <.07,<.08	3.9 14.7,16.8	10.0 4.2	0.0 6.4,5.5
7/23/80	NVPDC Sta.7	.80 .39,.18	.11 0.1,<0.1	.43 .50,.38	.11 <.05,<.06	4.8 6.0,8.5	10.0 5.3	0.0 2.4,3.7
8/14/80	NVPDC Sta.7	.29 .22	.09 <0.1	.74 .14	.06 .03	2.4 5.6	10.0 7.5	0.0 16.2
8/20/80	NVPDC Sta.7	.30 .57,.40	.09 0.1,0.8	.77 .18,.23	.07 .06,<.04	2.6 6.5,6.0	10.0 6.5,6.3	0.0 6.2,0.6
8/21/80	NVPDC Sta.7	.29 0.2,0.3	.11 0.3,0.6	.77 .22,.30	.05 .13,.11	2.7 4.0,4.0	10.0 6.9,6.9	0.0 -

in the model are given in Table V.

Table V. Downstream Boundary Conditions

Org N	NH ₄ -N	NO ₂ +NO ₃ -N	Org P	Ortho-P	CBOD	D.O.	Chl.'a'
(----- mg/l -----)							(ug/l)
0.7	0.3	.92	.12	.02	7.4	11.1	27.0

Since the upstream runoff is accounted for by the nonpoint source, a 'no flux' upstream boundary condition is specified.

g. Temperature - Temperature was read in every other day of simulation. Temperature varied from 28 degrees centigrade on the first day of simulation to 25.3 degrees centigrade on the last day.

h. Extinction coefficient - The average values of the extinction coefficient as measured during the intensive survey for stations 2 through 5 were 3.5, 3.8, 3.5 and 2.9 per meter, respectively. The value of 3.5 per meter was used in the model for the entire creek. This value compares closely to field measurements.

2. Calibration Parameters

Calibration of the water quality submodel was conducted in the following manner: A set of initial conditions for each water quality parameter based on data collected on the August 14 survey were provided to the model. Simulations of the period from that slackwater to the intensive survey were then conducted using the inputs specified in the preceding sections. The results of that part of the simulations corresponding to the intensive survey, in the form of maximum, average and minimum values for the last two tidal cycles for each parameter, were compared to corresponding values obtained from the intensive field survey. Successive model runs were conducted in which the rate

constants and calibration parameters were varied until a reasonable fit between field data and model results was achieved. The values of the calibration parameters so determined are presented in Table VI.

Initial calibration runs provided predictions of nitrite-nitrate nitrogen far in excess of the observed concentrations. In order for model predictions to match field measurements from the intensive survey it was necessary to introduce denitrification in the form of benthic flux of nitrite-nitrate nitrogen. A maximum value of $-1.6 \text{ gram/m}^2/\text{day}$ was assigned to the reaches corresponding to the creek from station 4 to station 5. This value was tapered to zero in the reaches below station 4 and tapered to -0.3 in the reaches above station 5. Although these values of the flux of nitrate are high they are not without precedent. Edwards and Rolley (1965) found denitrification rates varying from -0.1 to $-1.5 \text{ gram/m}^2/\text{day}$ in the sediment of an English river. Denitrification rates varying from -0.065 to $-1.1 \text{ gram/m}^2/\text{day}$ with an average nitrate removal rate of $-0.9 \text{ gram/m}^2/\text{day}$ were estimated by Van Kessel (1977) for an 800 meter stretch of a canal receiving sewage effluent.

As can be seen in Table IV, NVPDC predictions of nonpoint loadings of nitrite-nitrate are high for the calibration period when compared to field measurements of concentration. Also, unusually high values for point source loadings were recorded during the intensive survey. In light of this evidence, model runs were made to determine to what extent reducing the point source and eliminating the nonpoint source inputs would reduce the necessary benthic flux of nitrite-nitrate nitrogen. For these runs nonpoint inputs of nitrite-nitrate were reduced to zero while point source loadings of

Table VI. Calibration Parameters - Water Quality Sub-model

a. Phytoplankton Related Parameters									
k_{gr}	I_s	K_{mn}	K_{mp}	a	P	a_n	a_p		
1/day/C ^o	langleys/day	mg N/l	mg P/l	1/day/C ^o	1/day	mg N/ μ g Chl	mg P/ μ g Chl		
.13	340.	0.02	0.005	0.008	.00	.01	0.0014		
b. Nutrient Transfer and Decay Coefficient									
a_c	PQ								
mg C/ μ g Chl	moles O ₂ /mole C	moles CO ₂ /mole O ₂							
K_{n12}	K_{n23}	K_{p12}	$K_{c(20)}$	K_{h12}	K_{h23}				
1/day/C ^o	1/day/C ^o	1/day/C ^o	1/day	mg/l	mg/l				
0.005	.037	0.005	0.10	1.0	2.0				
c. Settling Coefficient									
K_{n11}	K_{n33}	K_{p11}	K_{p22}	K_{sch}	K_{sc}				
m/day	m/day	m/day	m/day	m/day	m/day				
0.12	.00	0.12	0.17	0.00	0.10				

nitrite-nitrate were computed based on the lowest concentration recorded at the STP outfall during the intensive. Point source loadings were thus reduced from 36.4 to 30.8 kg/day. Under these conditions the rate of flux of nitrite-nitrate to the sediments could be reduced to $-0.8 \text{ gram/m}^2/\text{day}$ at the point of greatest loss and the model results still compare well with field data. From these studies it can be inferred that some process was removing nitrite-nitrate nitrogen from the water column at a relatively high rate. One plausible candidate for this removal mechanism is denitrification in the extensive shallow areas of the creek.

3. Simulation Results

The results of the water quality submodel calibration are compared with data from the intensive survey in Figures 23 through 30 for organic nitrogen, ammonia nitrogen, nitrite-nitrate nitrogen, organic phosphorus, inorganic (ortho) phosphorus, CBOD, chlorophyll 'a' and dissolved oxygen, respectively. On the graphs are indicated the maximum, average and minimum over the two tidal cycles of the intensive survey. For comparison, the graphs also give the maximum, average and minimum concentrations for the appropriate tidal cycles of the model simulation corresponding to the survey. The results of the calibrated model generally agree well with the field data with the exception of inorganic phosphorus for which the concentrations are too high in the upper reaches of the model.

Some examples of the temporal variation in the model output during the last two tidal cycles of the final calibration run are presented in Figures 31 through 33. In these figures model output for ammonia, chlorophyll 'a' and dissolved oxygen are compared to field

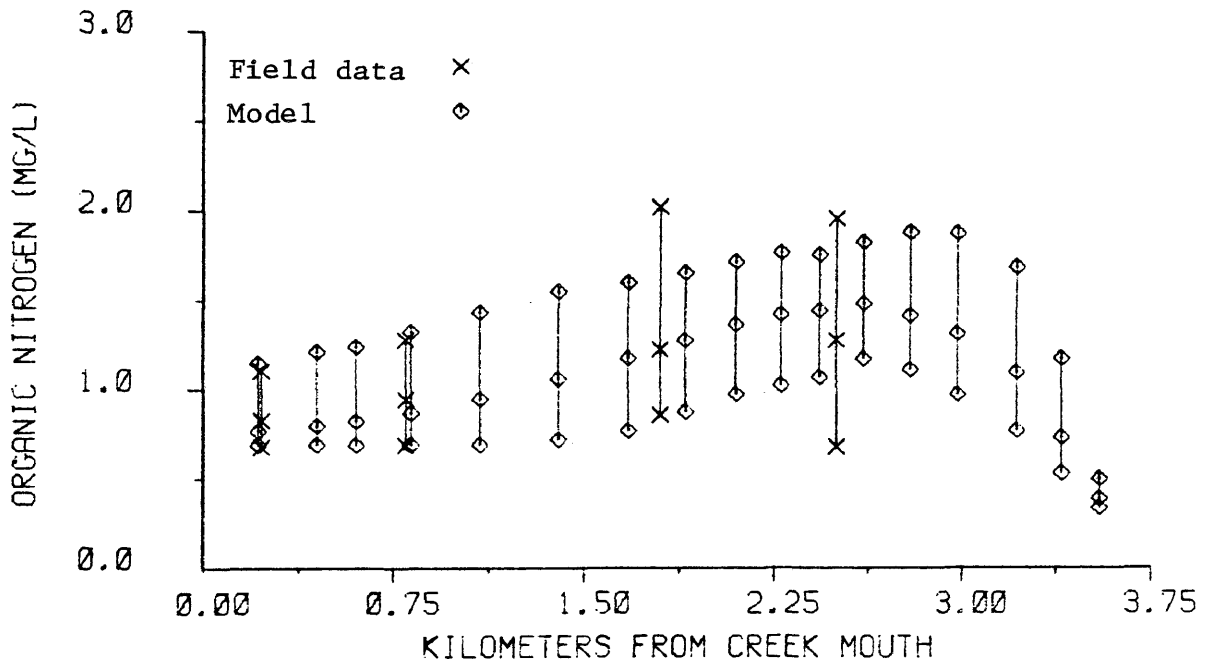


Figure 23. Calibration results - organic nitrogen.

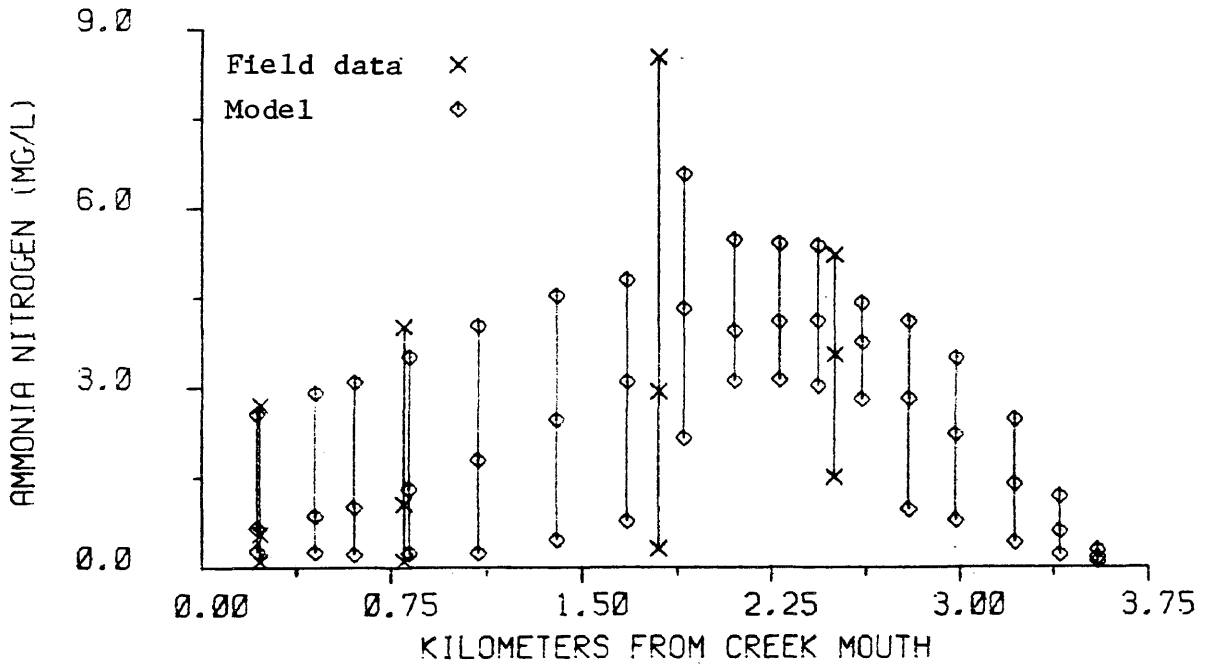


Figure 24. Calibration results - ammonia nitrogen.

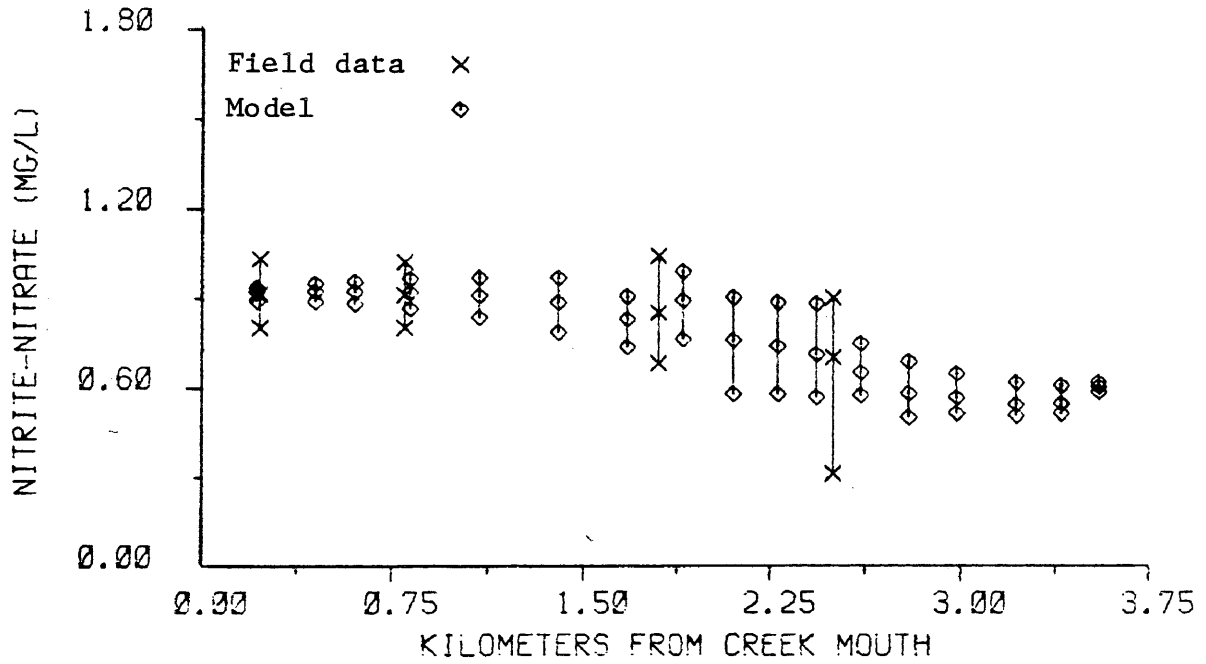


Figure 25. Calibration results - nitrite-nitrate nitrogen.

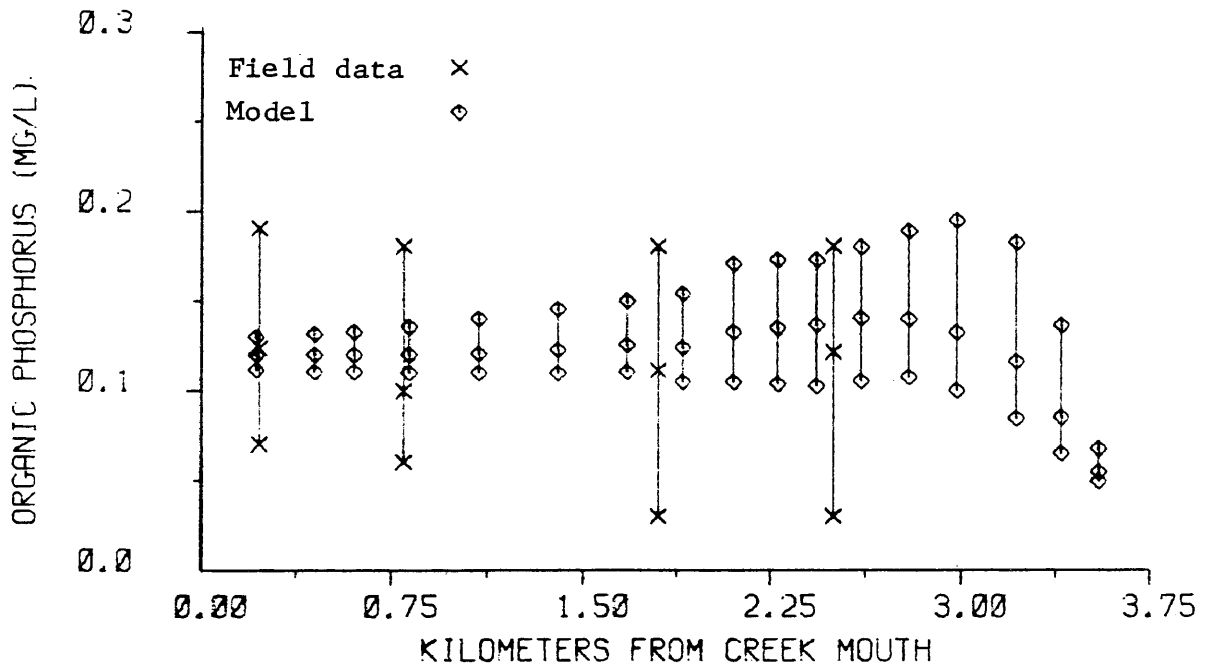


Figure 26. Calibration results - organic phosphorus.

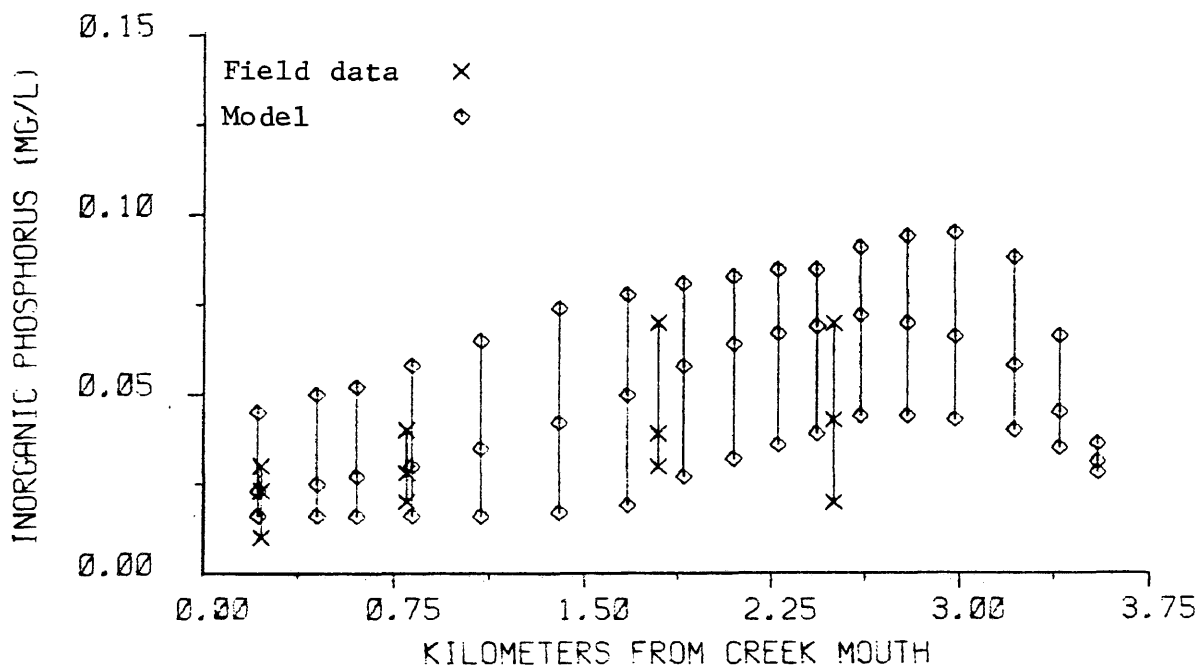


Figure 27. Calibration results - inorganic (ortho) phosphorus.

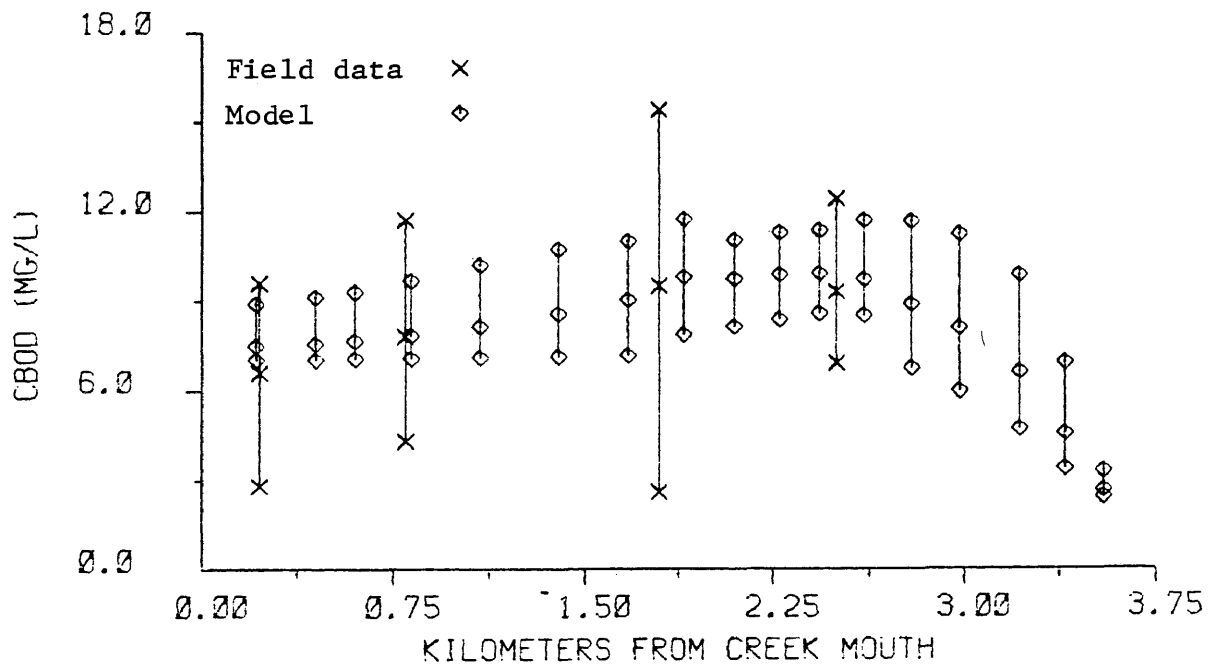
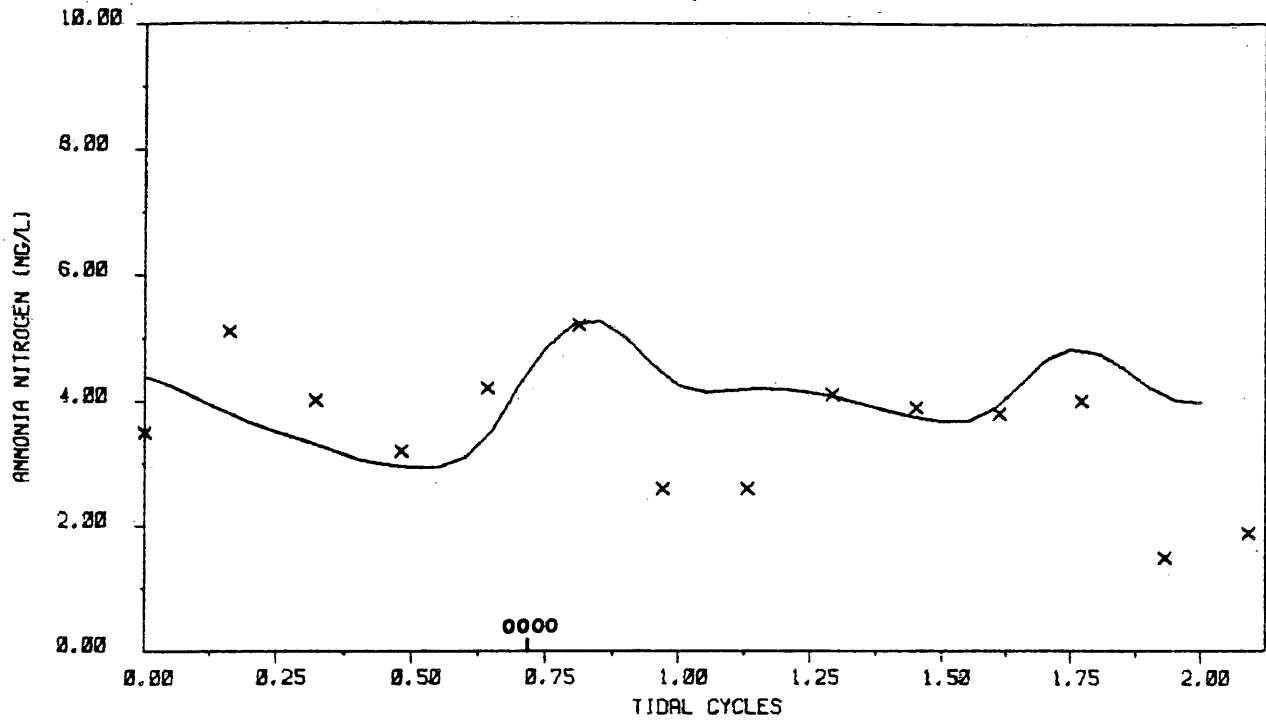
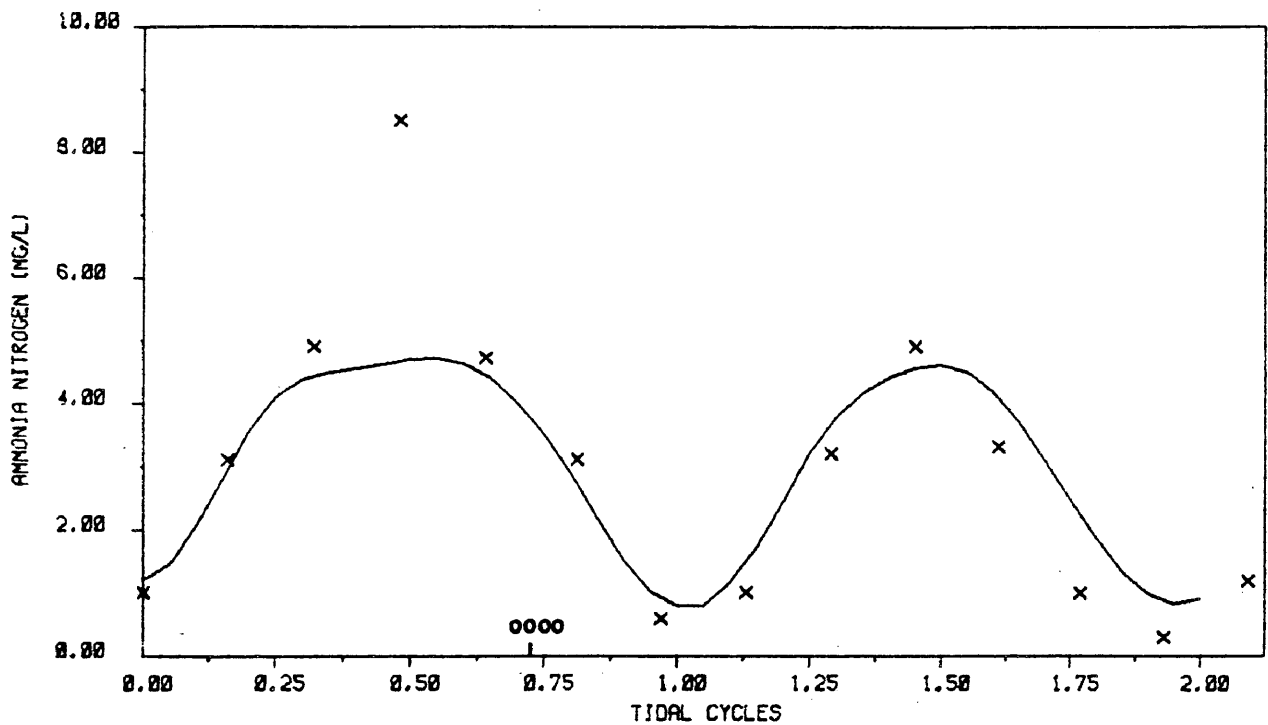


Figure 28. Calibration results - CBOD.

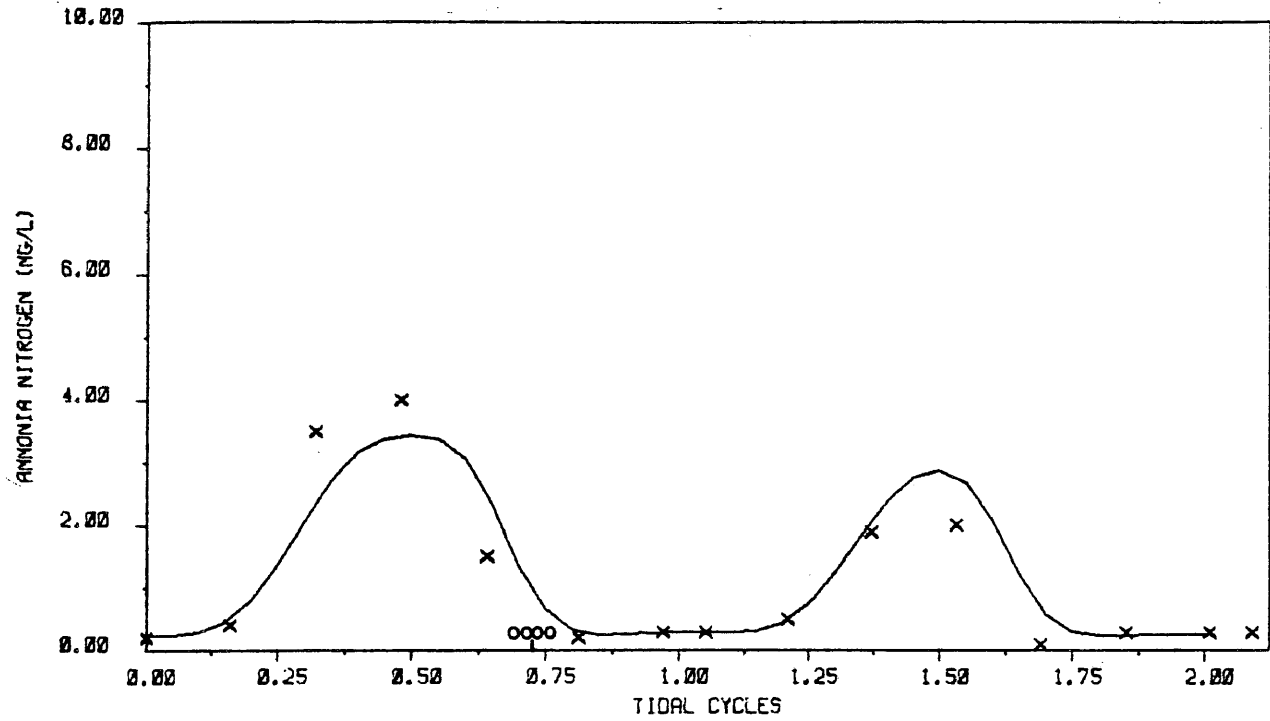


a. Field station 5 (x), model reach 8 (—).

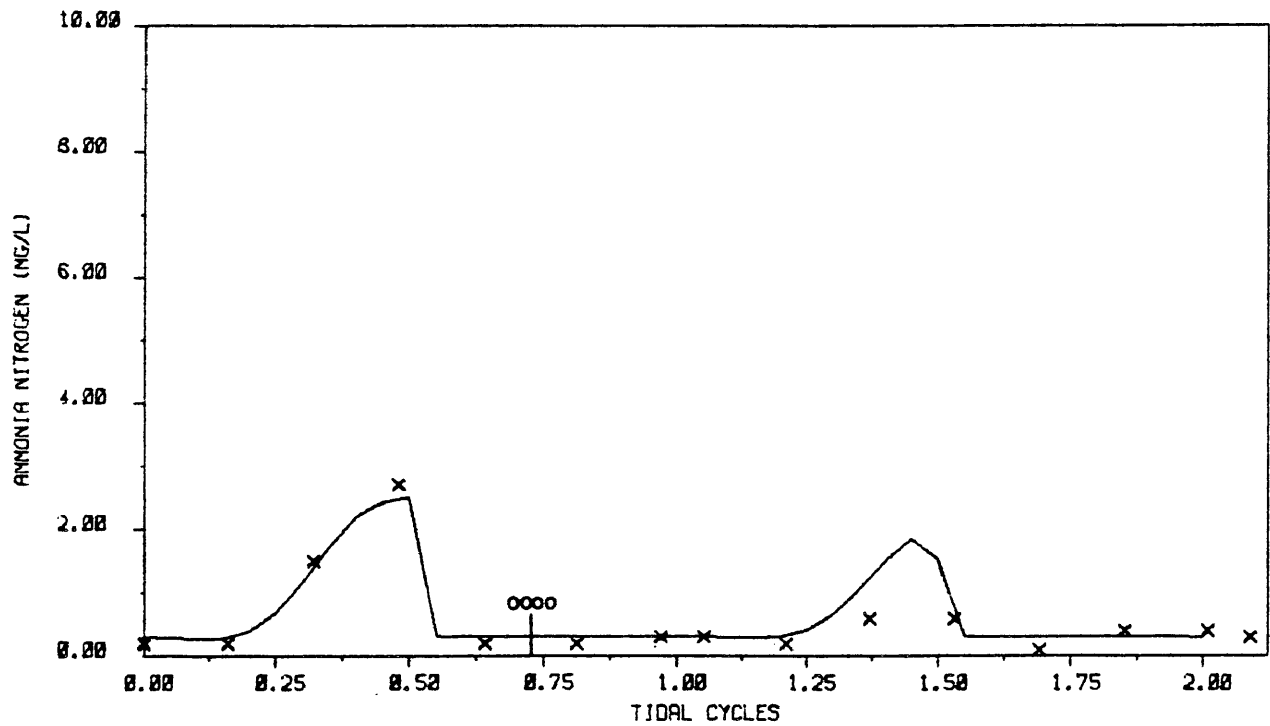


b. Field station 4 (x), model reach 12 (—).

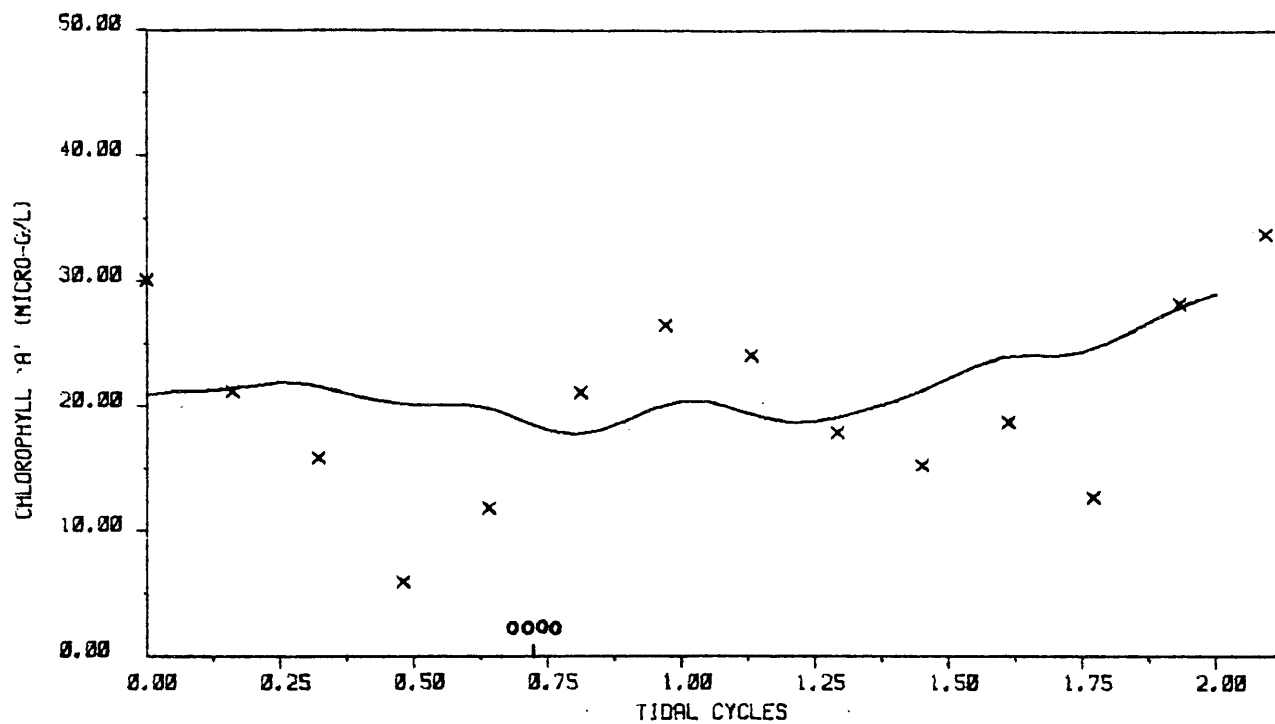
Figure 31. Ammonia - field data (August, 1980 intensive survey) versus model output.



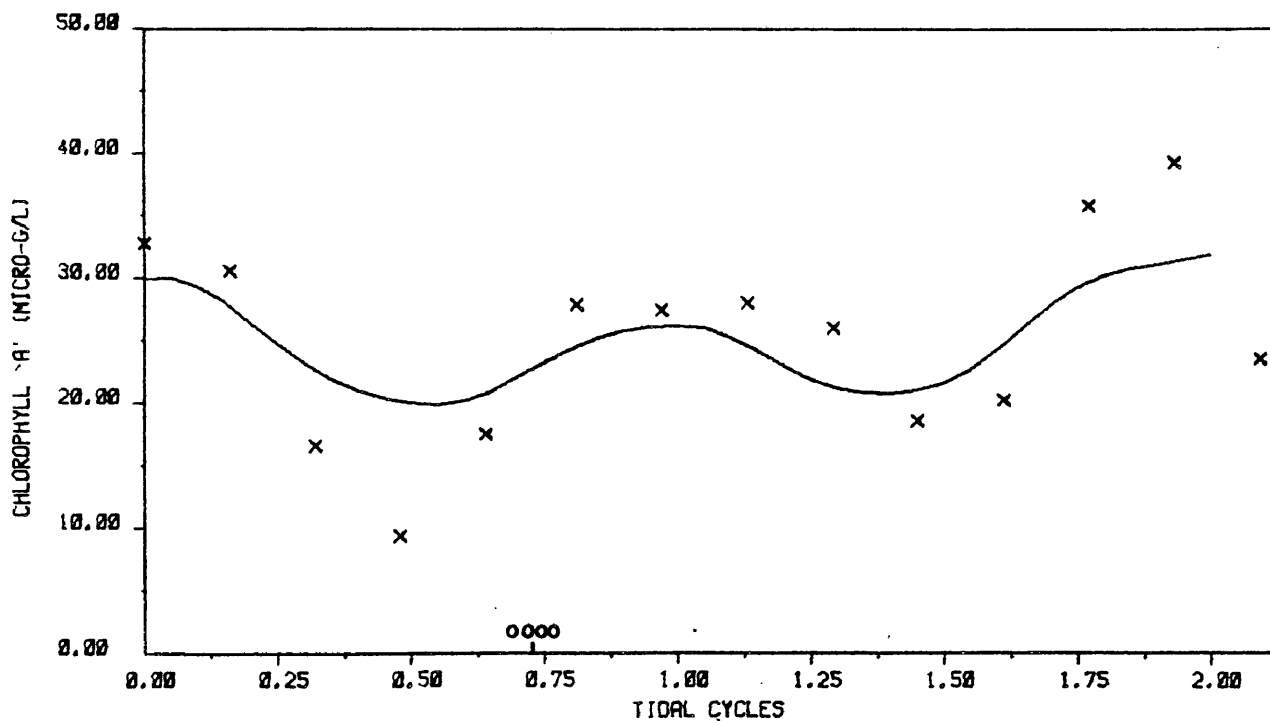
c. Field station 3 (x), model reach 15 (—).



d. Field station 2 (x), model reach 18 (—).

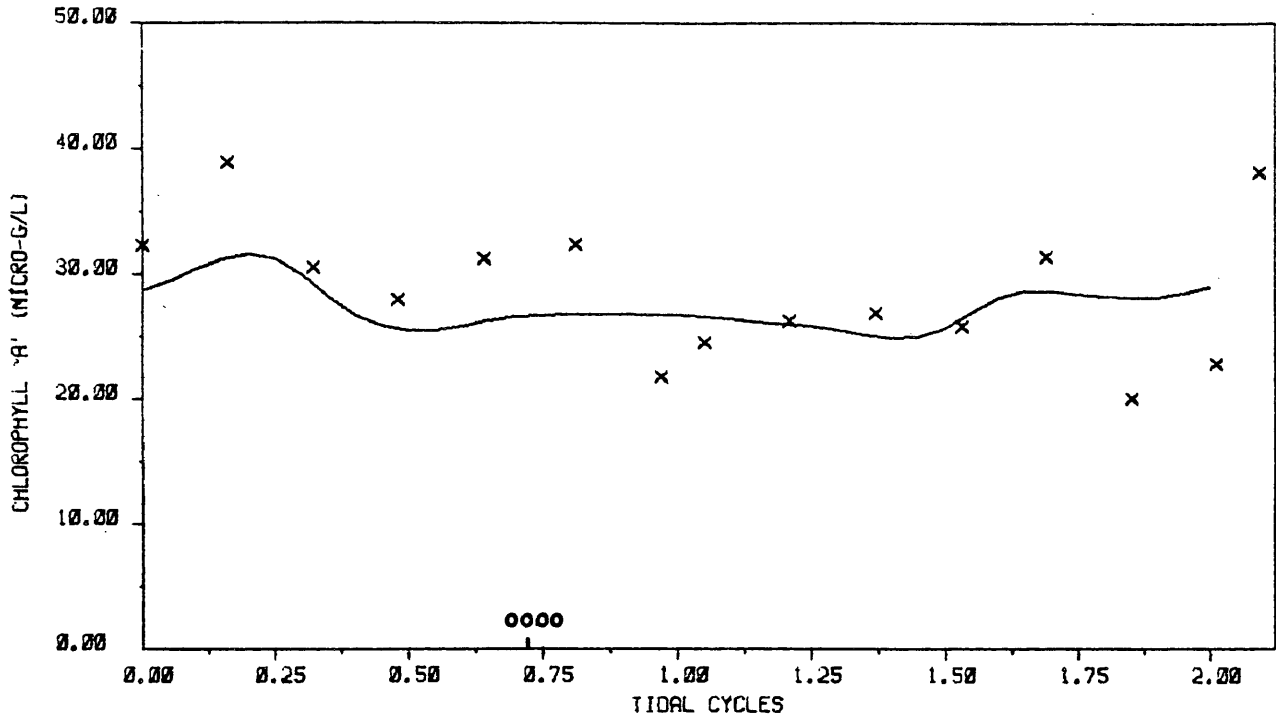


a. Field station 5 (x), model reach 8 (—).

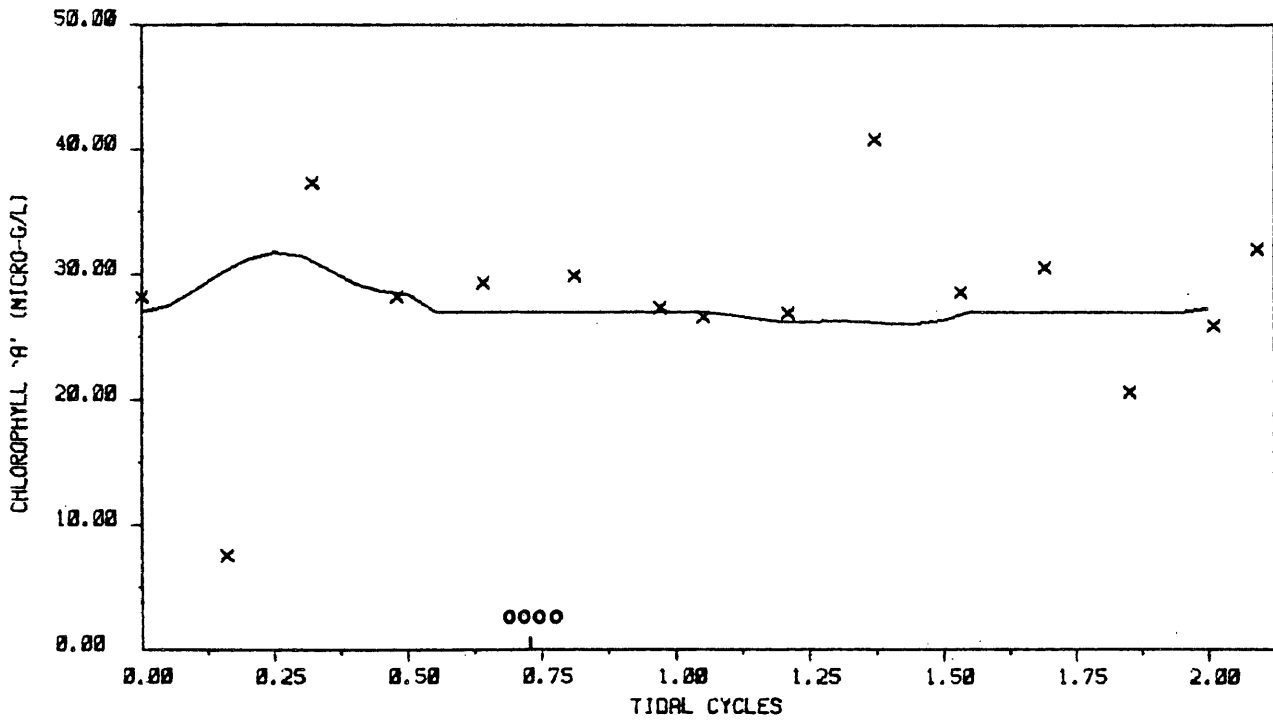


b. Field station 4 (x), model reach 12 (—).

Figure 32. Chlorophyll 'a' - field data (August, 1980 intensive survey) versus model output.

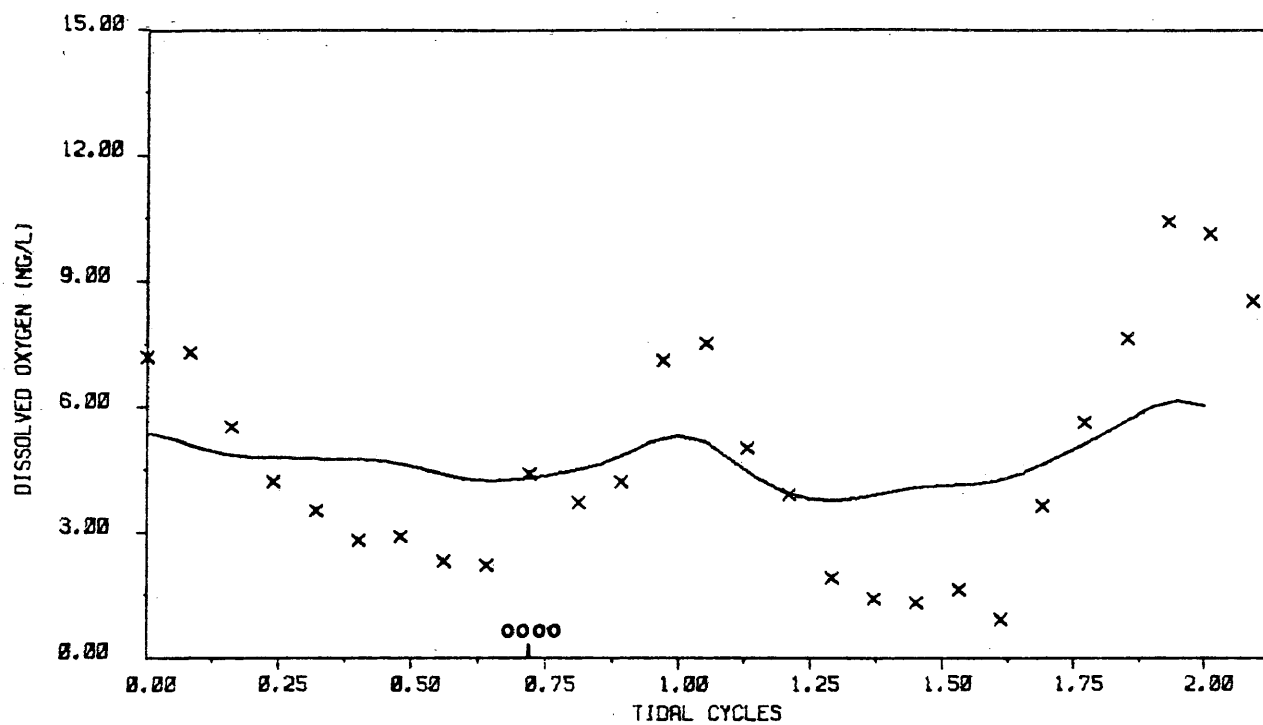


c. Field station 3 (x), model reach 15 (—).

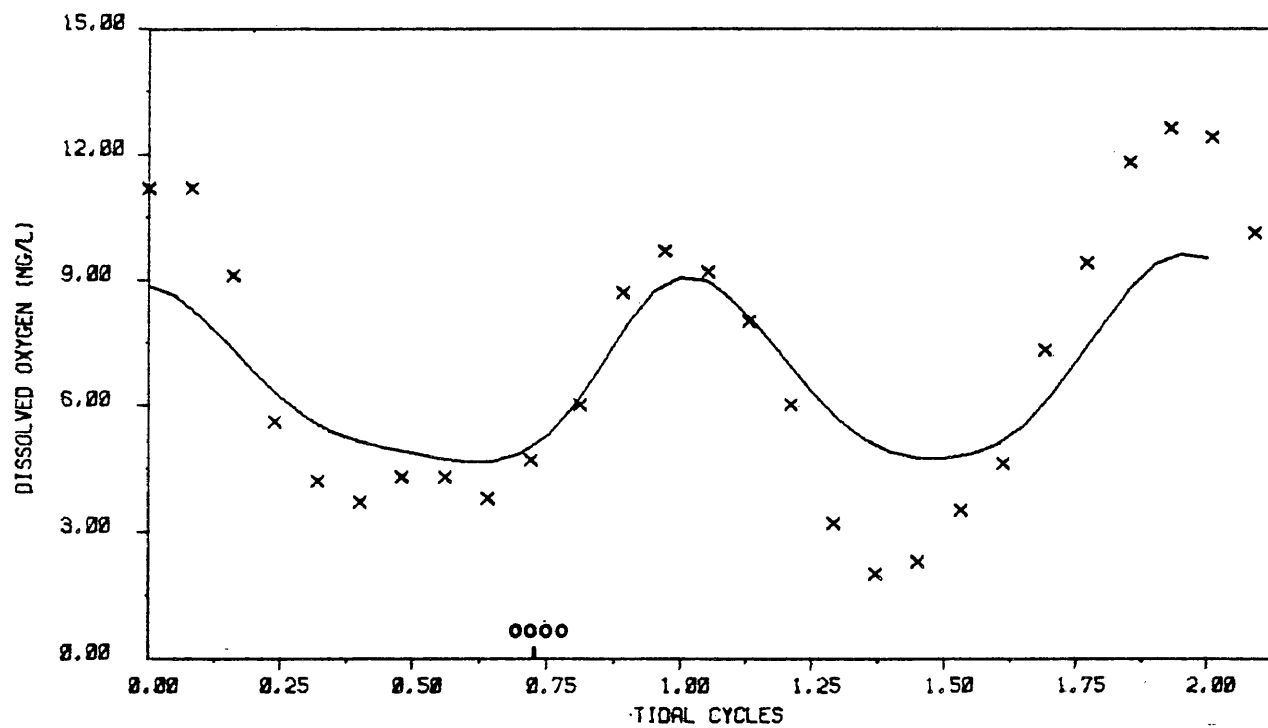


d. Field station 2 (x), model reach 18 (—).

Figure 32. (Cont'd).

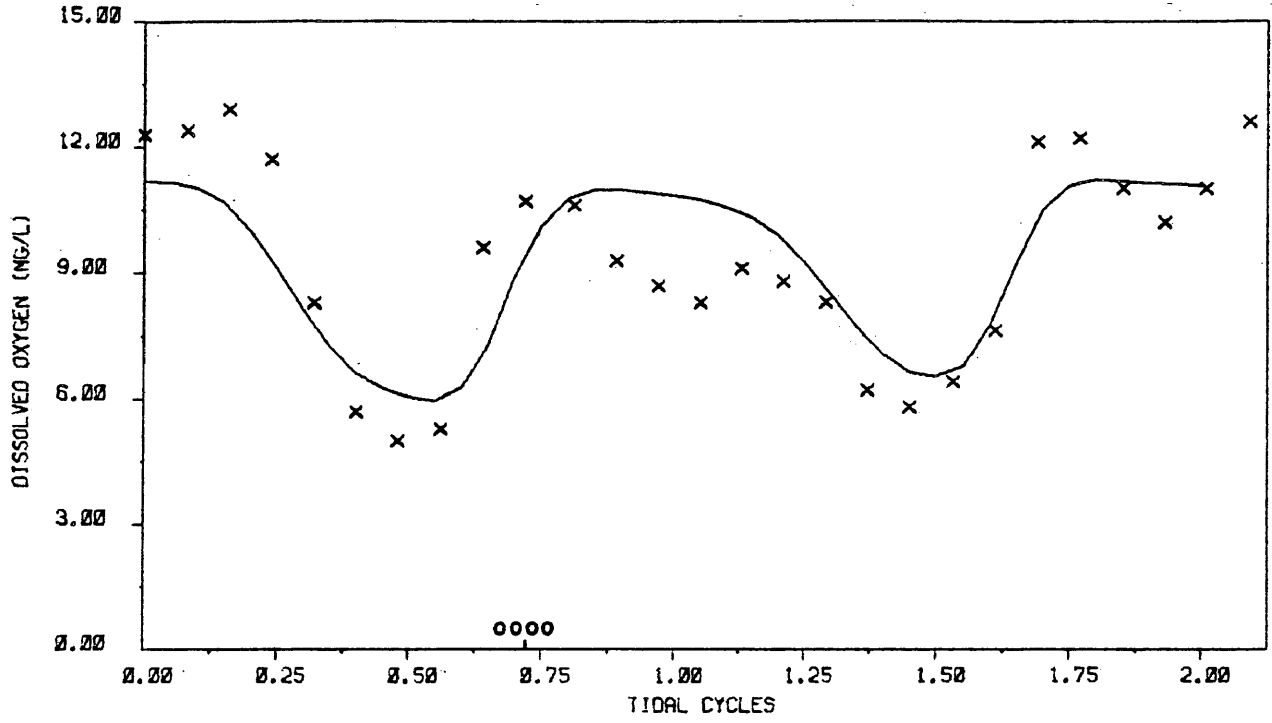


a. Field station 5 (x), model reach 8 (—).

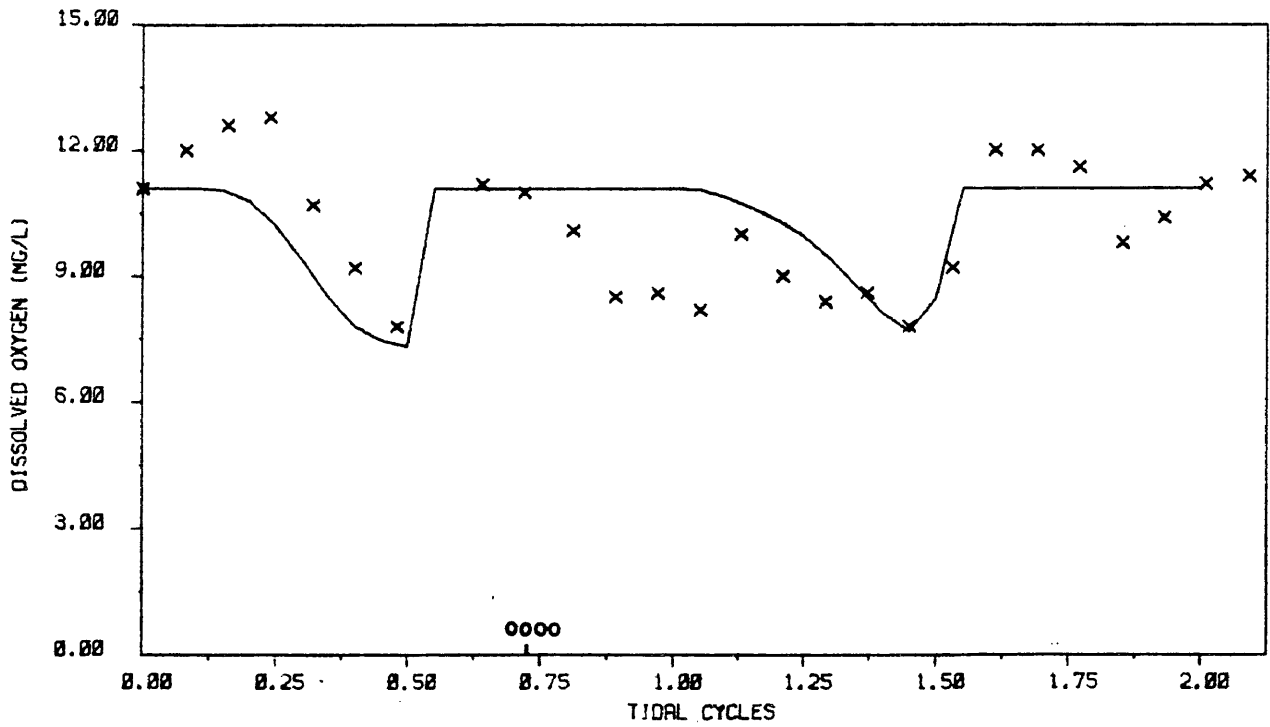


b. Field station 4 (x), model reach 12 (—).

Figure 33. Dissolved oxygen - field data (August, 1980 intensive survey) versus model output.



c. Field station 3 (x), model reach 15 (—).



d. Field station 2 (x), model reach 18 (—).

Figure 33. (Cont'd).

data from the intensive survey.

While semi-diurnal tidal fluctuations in concentrations can be seen in the figures, no diurnal fluctuations are apparent. As shown by these figures and by Figures 23 - 30, ranges of concentrations produced by the model are generally less than those measured in the field. Some of this difference can be ascribed to the necessity of comparing field samples taken at a point along the channel of the creek to model output which represent the average values over the total volume of a model segment.

C. Model Validation

The reason behind the validation process is to demonstrate the model's ability to simulate future conditions. For the purpose of validation, the model was run for 195 tidal cycles simulating the period from the slackwater survey of 5/21/80 to the end of the tide gauge record on 8/29/80. The data from the tide gauge record was compiled and used as the downstream boundary condition for the hydrodynamic submodel. Validation of the hydrodynamic submodel is provided by comparing the tide staff readings made at station 5 during July 22-23, 1980 to model output for the same period. The results are presented in Figure 34 and, as can be seen, upstream surface elevations as predicted by the model compare well to those measured in the field.

For this simulation point source loadings were assumed to be constant and were determined by averaging measurements made at the STP outfall during the slackwater and intensive surveys. The average values for point source loadings determined in this manner are presented in Table VII.

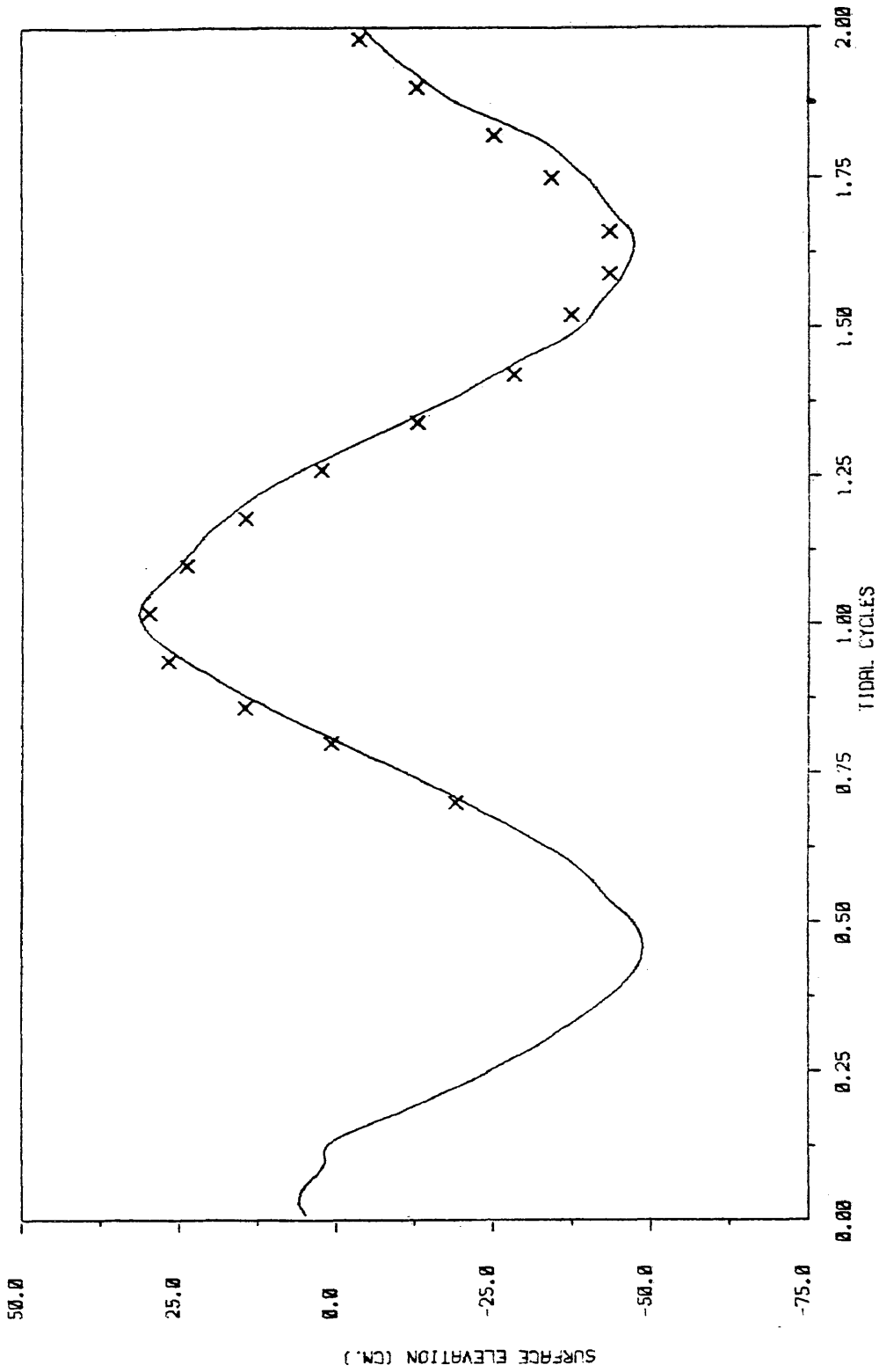


Figure 34. Results of hydrodynamics sub-model validation - Station 5 (2.5 km), tide staff readings (X) for July 22-23 intensive survey compared to model predictions for surface elevation (-) for the same period.

TABLE VII. Point Source Loadings for Model
Validation Run

Flow (m ³ /s)	Org.N (-----)	NH ₄ -N	NO ₂ +NO ₃ -N kg/day	Org.P (-----)	Ortho-P	CBOD	D.O. (mg/l)
.22	33.7	343.7	34.1	1.14	1.48	301.	8.0

As in the calibration runs, nonpoint source loadings were read in for every day of simulation. Initial concentrations in the creek were determined from measurements made during the first slackwater survey (5/21/80). Downstream boundary conditions were changed during the simulation at times corresponding to the dates of the field surveys (tidal cycles 25.0, 65.5, 92.5, 120.0, 164.0, 176.0). Boundary conditions were thus read into the model at roughly two week intervals of simulation. With two exceptions, boundary conditions were determined from high slackwater data collected at station 2. The two exceptions were the June 24 and the July 8 surveys which were conducted at or near low tide. For these two surveys data collected at station 1 in the Potomac River was used to define boundary conditions for the period of simulation following each survey. Water temperature was also varied according to field survey measurements. Temperature was read into the model on an average of about every ten tidal cycles, with values between field surveys arrived at by linear interpolation.

Results of this long-term simulation are presented graphically in the Appendix. Model results are compared to concentrations measured in the field during the slackwater surveys and to the average concentrations determined from the intensive and diurnal surveys. A maximum of eight values per station were obtained from the field surveys for comparison to model output. However, only for the most

downstream station in the creek, station 2, were all eight samplings made.

The model results for stations 2 and 3 exhibit a strong influence by the downstream boundary conditions. Although a change in the boundary condition can be detected at station 4, the effect is much less pronounced than at station 3. Any boundary condition effect at station 5 is usually lost in the variations in concentration and range due to changes in nonpoint inputs or to diurnal variations.

Rain events appear on the graphs at stations 4 and 5 as rapid increases or decreases in concentrations, depending on the parameter. The effect of rain events on concentrations at stations 2 and 3 is considerably damped.

The model simulation results for ammonia nitrogen compare well with field data for stations 2, 3 and 4 (Figures A1-A3). Predicted concentrations at station 5 run high in comparison to field data for the period from cycle 164 to cycle 177 (Figure A4). This corresponds to the calibration period and results here echo those of the final calibration run. The results for nitrite-nitrate nitrogen compare well with field results for all stations with the exceptions of stations 4 and 5 for the period of cycles 120-121 (Figures A5 and A6). During that period of high nonpoint runoff model predictions are lower than corresponding field data. Perhaps there exists some delay between the time of precipitation over the creek drainage basin and the entry of runoff into the tidal portion of the creek which has not been taken into account in the nonpoint source model.

Comparing graphs for stations 4 and 5 for ammonia nitrogen reveals a phase difference of about 180 degrees in the concentration

curves at those stations. Concentrations are lowest at high tide at station 4 and are highest at high tide at station 5. The STP outfall is located between stations 4 and 5 and such a phase difference would be expected for those parameters for which the point source inputs are dominant. Rain events are indicated in the graphs of ammonia and nitrite-nitrate nitrogen by rapid decreases in concentrations at the upstream stations. These effects are evidence for the dominance of point source inputs over nonpoint inputs for these two parameters.

Long-term model predictions for organic nitrogen (Figures A7 and A8) are generally in agreement with field data. With the exceptions of the low slackwater survey of 7/8/80 (cycle 92.5) the field data points generally fall within or just outside the range of predicted concentrations. Concentrations of organic nitrogen also exhibit the phase difference between stations 4 and 5 but only during periods of no major rain events. Rain events are revealed in the graphs of organic nitrogen by rapid increases in concentrations. This indicates that nonpoint loading is an important source of organic nitrogen and can become the dominant source during periods of heavy runoff.

In general, field data points fall within or near the concentrations predicted for inorganic (ortho) phosphorus (Figures A9 and A10). A notable exception is the concentrations measured during the 8/14/80 (cycle 164.0) high slackwater survey at stations 4 and 5. This survey is unique among the slackwater surveys, not only in the magnitude of its measurements of inorganic phosphorus, but also in that it is the only slackwater survey where high concentrations were recorded at all four stations along the creek.

Organic phosphorus concentrations predicted by the model for

stations 2 and 3 agree well with field data. At stations 4 and 5 (Figures A11 and A12) the model does not predict the low concentrations measured during the July 22-23, 1980 intensive survey (cycles 120-121). And, as with inorganic phosphorus, the field data for 8/14/80 (cycle 164.0) are much higher than model simulation results at stations 4 and 5.

In the graphs for organic and inorganic phosphorus rain events are indicated by a very rapid rise in predicted concentrations. The magnitude of these increases suggest that nonpoint source inputs dominate, at least for the upstream stations. A diurnal variation in inorganic phosphorus at all four stations is also indicated by the graphs.

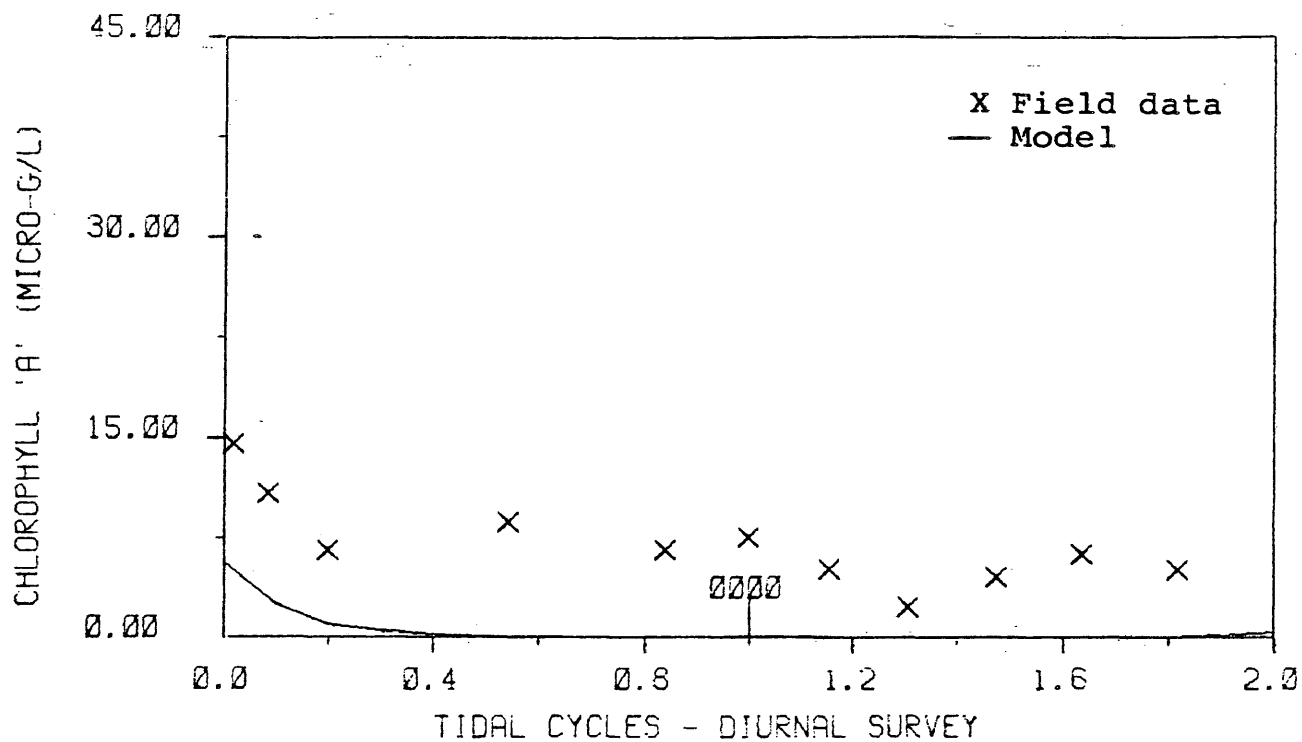
Long-term predictions for CBOD concentrations compare well in general for stations 2, 3 and 4. Figure A13 compares model predictions to field data from station 4. Predictions for station 5 compare well with field data with the exception of the measurement during the 8/14/80 survey which is well above predicted values (Figure A14).

In most instances model predictions of chlorophyll 'a' concentrations at all stations compare well with field data (Figures A15-A18). However, predictions for stations 4 and 5 for the period corresponding to the 6/24/80 slackwater survey (cycle 65.5) are well above field measurements. The average values obtained from the diurnal and intensive surveys fall within or near the model predictions. This, taken with the calibration results for chlorophyll, indicates that while the model does not reproduce the range of chlorophyll in a diurnal cycle, it appears to adequately predict the average concentrations for the cycle.

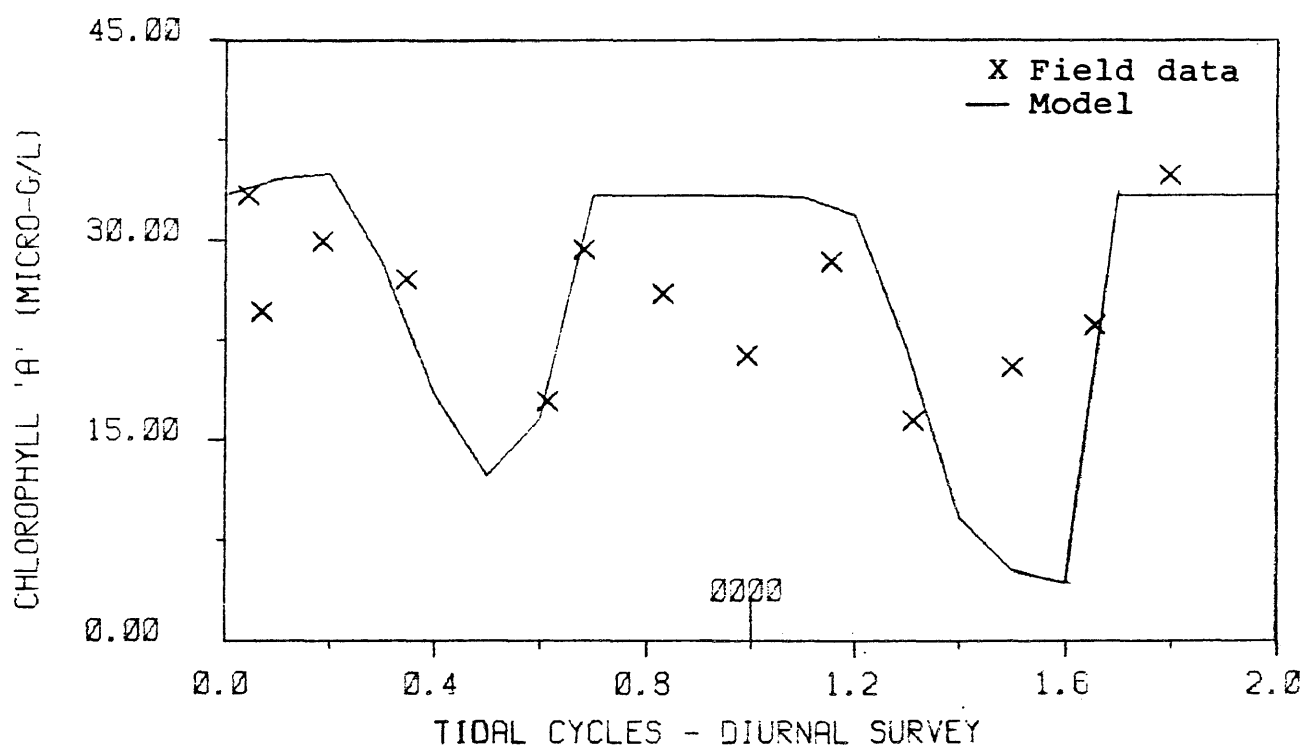
Rain events are discernable in the graphs of chlorophyll as rapid decreases in concentrations at stations 4 and 5 (Figures A17 and A18). During periods of high runoff concentrations drop to near zero at these upstream stations. This is a result of setting nonpoint inputs for chlorophyll to zero. Field measurements at the nontidal station 7 yielded highly varied concentrations between surveys (Table IV) and no discernable pattern. Although it is not possible to determine a reasonable average concentration for nonpoint chlorophyll concentration from station 7 data, it appears that the value of zero supplied by the NVPDC does not reflect true input to the creek. This could explain some of the discrepancy between model predictions and field measurements made during rainy days - e.g., the June 3 diurnal survey (cycles 25-26) and the July 22-23 intensive survey (cycles 120-121). A more detailed view of model predictions versus field measurements of chlorophyll from the 6/3/80 diurnal survey is given in Figure 35.

The effect of the large change in downstream boundary condition for chlorophyll beginning at approximately cycle 92 is noticeable even at station 5, although this effect is considerably damped and the picture confused by a series of rain events. A strong diurnal effect is exhibited in the model results for chlorophyll at all four stations.

The model adequately predicts dissolved oxygen concentrations in most instances (Figures A19 and A20). The greatest difference between field measurements and model predictions occur at station 5. Rain events appear in the DO graph for station 5 as increases in concentrations, the result of the NVPDC prediction of a constant 10.0 mg/l concentration for nonpoint dissolved oxygen. As can be seen in



a. Station 5

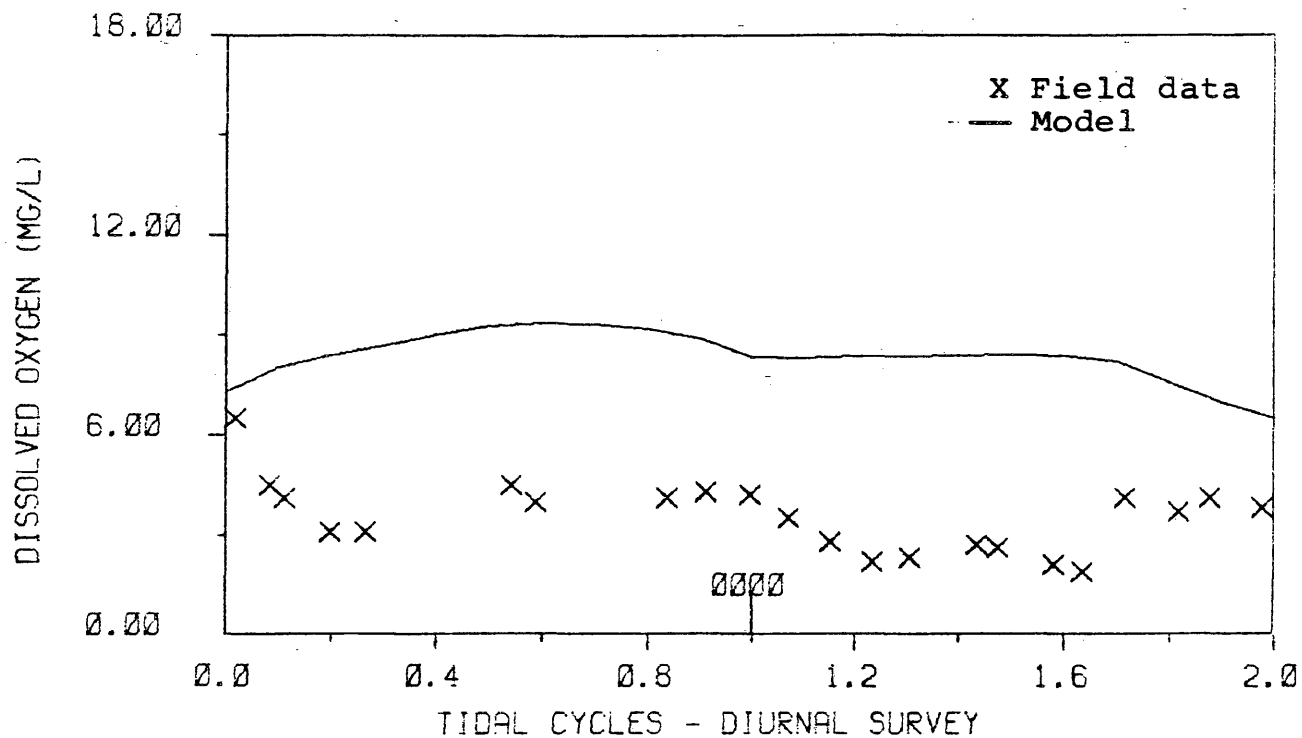


b. Station 2

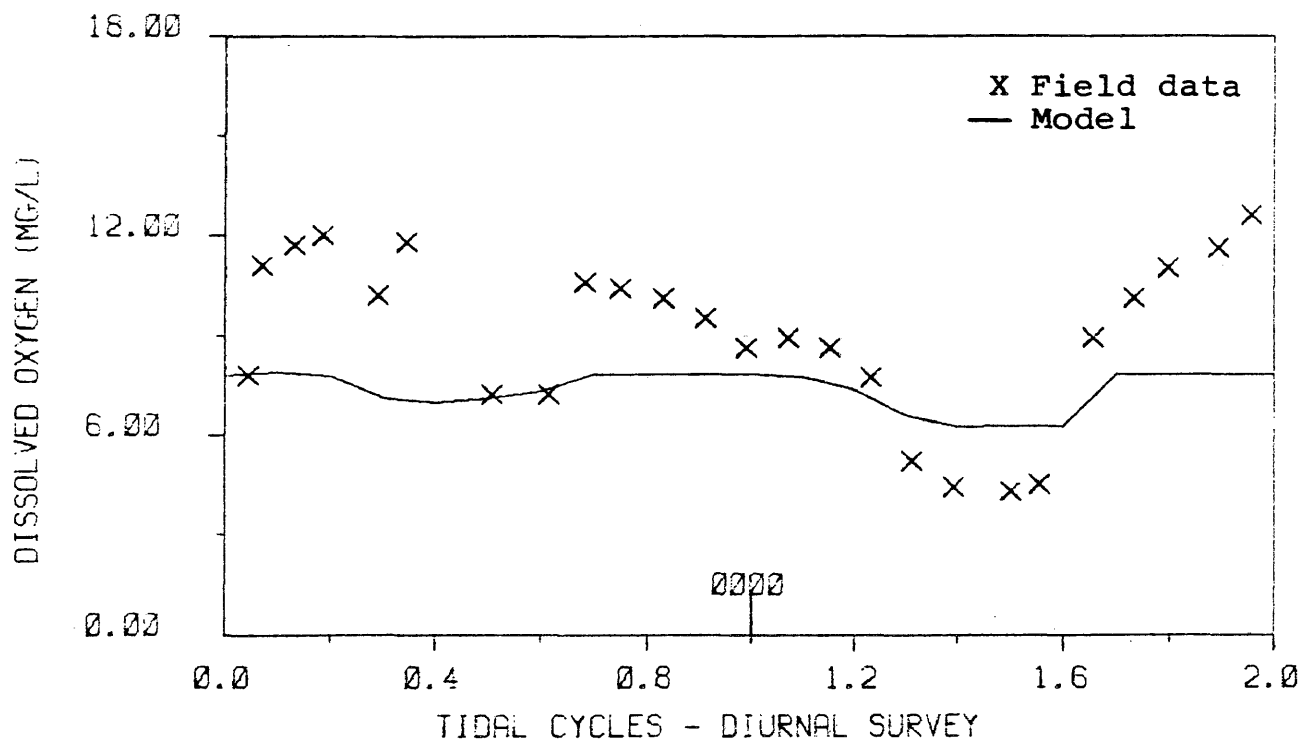
Figure 35. Model predictions versus field measurements of chlorophyll 'a' from the June 3, 1980 diurnal survey.

Table IV, field measurements at the nontidal station (station 7) never approach the value predicted by the NVPDC. Of particular interest are the low values recorded during the 6/3, 7/8 and the 7/22-23 surveys. In these surveys, each made during a rain period, DO concentrations of 6.3, 4.5 and 4.2 mg/l were recorded, respectively. In light of these field measurements a second long-term simulation was undertaken in which nonpoint DO concentrations were set to 4.2 mg/l for all time. The results are given in Figures A21 and A22. In these figures it can be seen that under this new condition DO predictions for the periods corresponding to the June diurnal survey (cycles 25-26) and the July intensive survey (cycles 120-121) are much closer to the average values from field data. Predictions for periods of low runoff are little affected by this change in nonpoint DO. Figures 36 and 37 present a more detailed look at field data versus model predictions for the period of the diurnal survey. In Figure 36 nonpoint DO concentrations were set to 10 mg/l. In Figure 37 concentrations were set to 4.2 mg/l.

In general, the model succeeds in simulating the water quality conditions of the creek even though the results of the long-term simulation fails to match some of the data points. In comparing slackwater survey data with model simulation results, it should be born in mind that each data point is from a single grab sample and that data scattering is inevitable. The model not only adequately simulates the impact of point source loadings on the water quality, but also the water quality response to the time varying nonpoint source loadings. Both the seasonal time scale and intra-tidal time scale of water quality variations can be simulated with the model in a single model run. This is possible because of the efficient numerical scheme

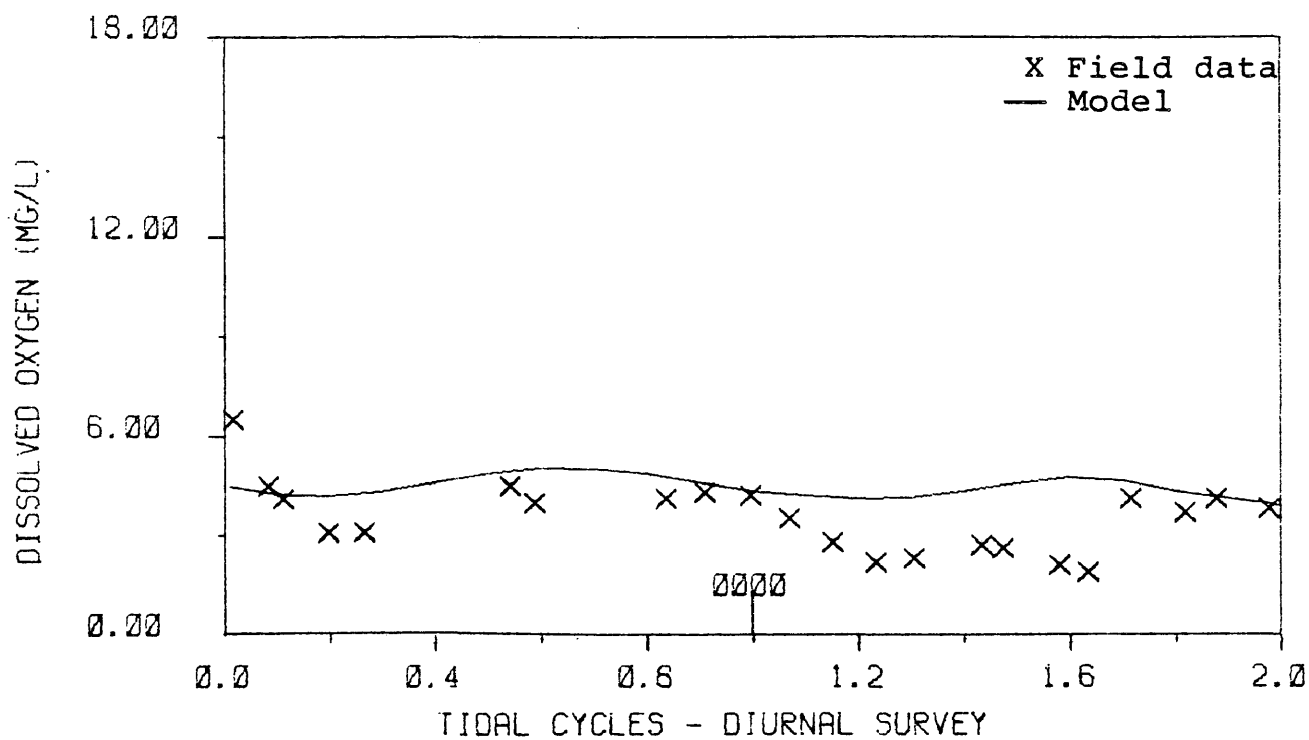


a. Station 5

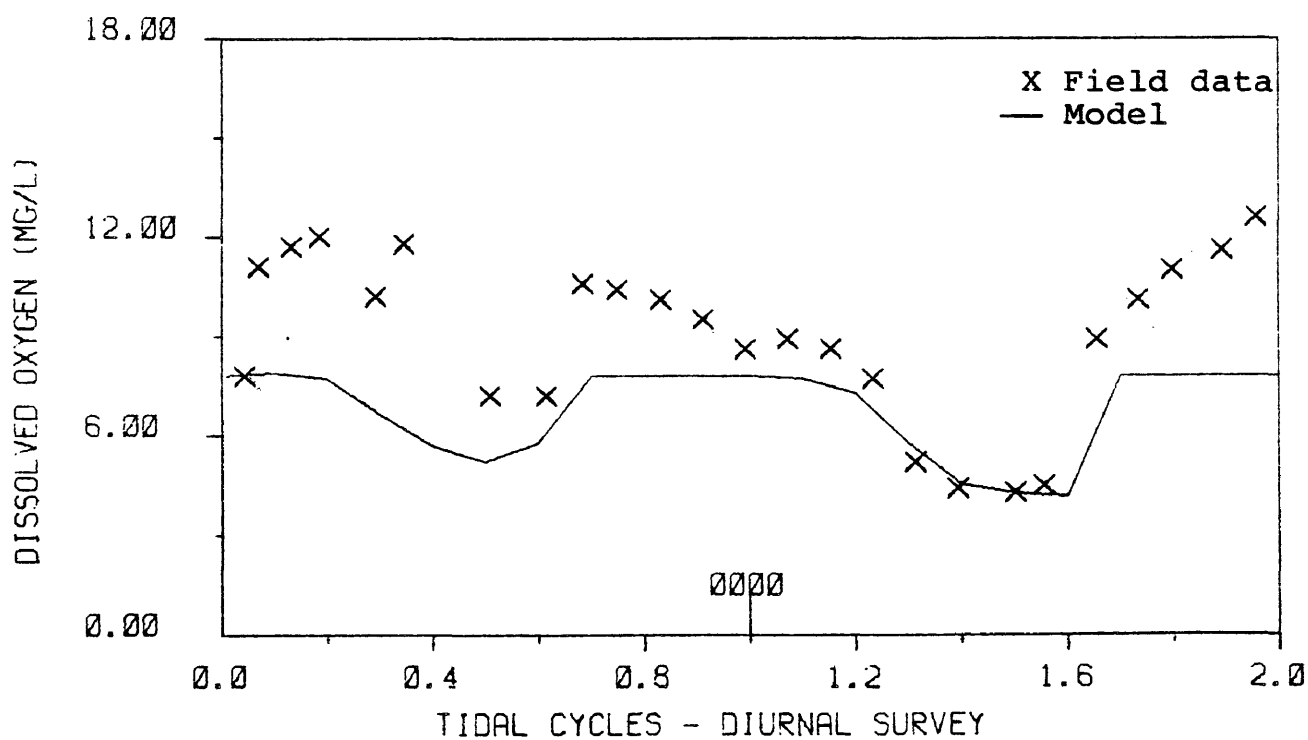


b. Station 2

Figure 36. Model predictions versus field measurements from June 3, 1980 diurnal survey - nonpoint DO concentrations set to 10.0 mg/l.



a. Station 5



b. Station 2

Figure 37. Model predictions versus field measurements from June 3, 1980 diurnal survey - nonpoint DO concentrations set to 4.2 mg/l.

employed in the model and the smallness of the creek.

D. Diagnostic Capabilities of the Model

After a model has been calibrated and validated it can then be used to investigate the cause-and-effect relationships operative in the system, and to evaluate future water quality conditions under potential changes in the system. The various scenarios may include changes in point source or nonpoint source loadings, or proposed changes in system geometry. The results of such analyses can then be useful to decision makers in developing alternative water quality management plans.

A series of model runs was made to determine the impact of point source and nonpoint source loadings on the water quality of the Little Hunting Creek. The input data employed in model calibrations were used as the base of this analysis. A model run was made with point source loadings for the nitrogen parameters, the phosphorus parameters and CBOD set to zero. For this run STP discharge was held at 0.22 cubic meters per second with a DO concentration of 8.1 mg/l. A separate run was made with all nonpoint loadings of CBOD, nitrogen and phosphorus set to zero. For this run, as with the calibration runs, nonpoint inflow varied with each day of simulation and nonpoint DO was a constant 10.0 mg/l.

The elimination of nonpoint loadings made little difference in concentrations of ammonia nitrogen. Setting point source inputs to zero led to drastic reductions in ammonia throughout the creek (Figure 38). Reducing nonpoint source inputs to zero had a significant effect on the upstream concentrations of nitrite-nitrate nitrogen, however, the elimination of the point source had a greater effect in all reaches

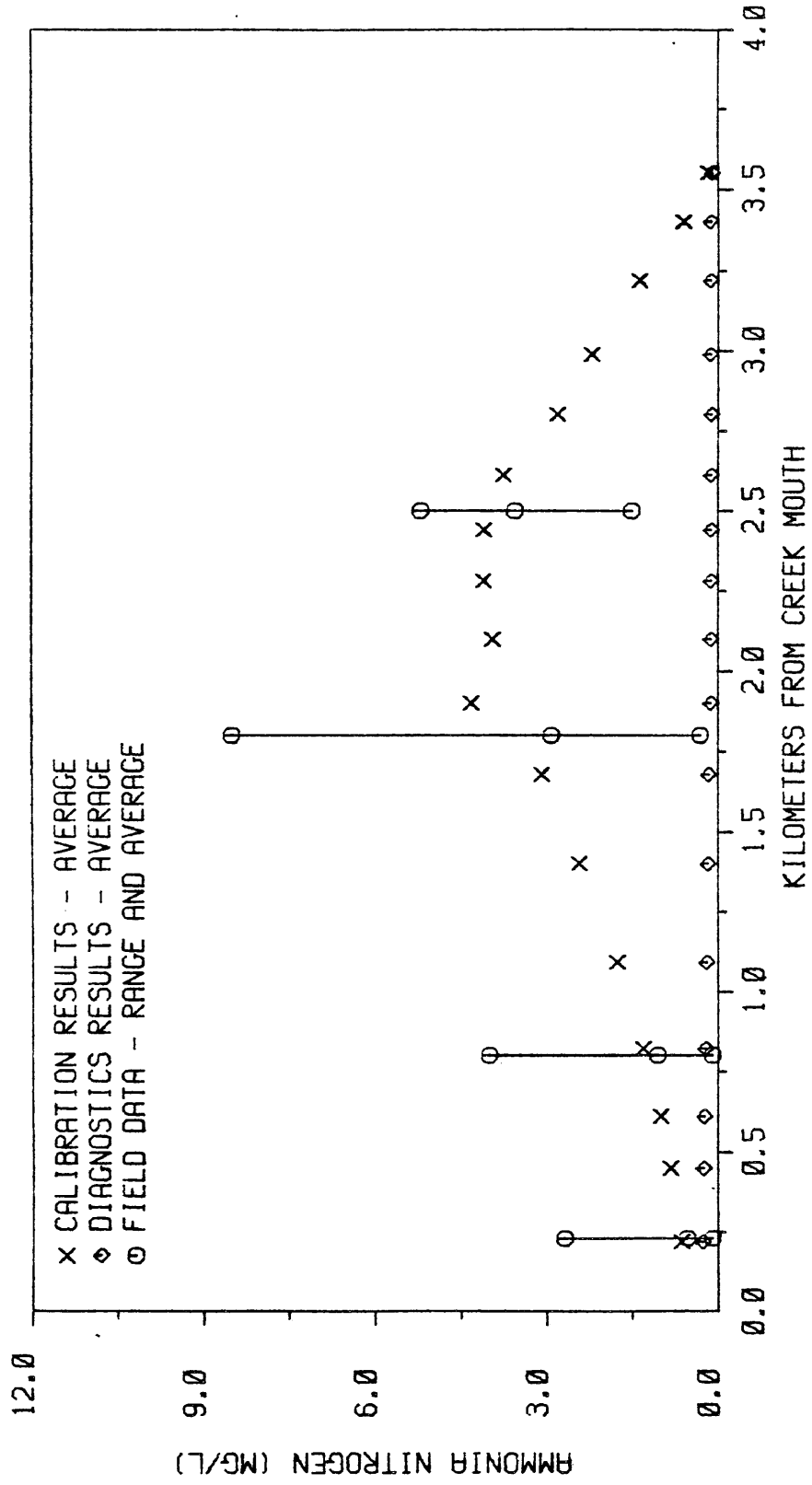


Figure 38. Results for ammonia nitrogen - point source inputs set to zero.

below reach 5 (Figure 39). Organic nitrogen showed a moderate decrease when point source loadings were eliminated, but reducing the nonpoint source to zero had a greater effect. These results suggest that the nitrite-nitrate nitrogen and the ammonia nitrogen in the creek are primarily contributed by the point source, while organic nitrogen is primarily contributed by nonpoint runoff.

Elimination of the point source had little effect on either organic or ortho-phosphorus concentrations. However, the elimination of nonpoint inputs had a significant effect on concentrations of both forms of phosphorus (Figures 40 and 41). These results suggest that nonpoint runoff is the major contributor of phosphorus in the creek.

Both the point source and the nonpoint source are significant to CBOD concentrations in the creek. The elimination of the nonpoint source had a greater effect on reaches upstream of reach 10 while the elimination of point source inputs had a slightly greater effect downstream of that reach.

While the elimination of the point source had some effect in reducing phytoplankton growth (Figure 42), the elimination of nonpoint loadings resulted in a larger decrease in the phytoplankton population (Figure 43). Comparing these results to those of nitrogen and phosphorus suggests that when point sources were eliminated phytoplankton growth was nitrogen limited, while when nonpoint inputs were eliminated growth was phosphorus limited.

The elimination of the point source affected the distribution curve for average dissolved oxygen in two ways. The point of minimum DO moved upstream a distance of 0.4 kilometers and the DO at this point was 1 mg/l higher than the old minimum (Figure 44). The improvement in

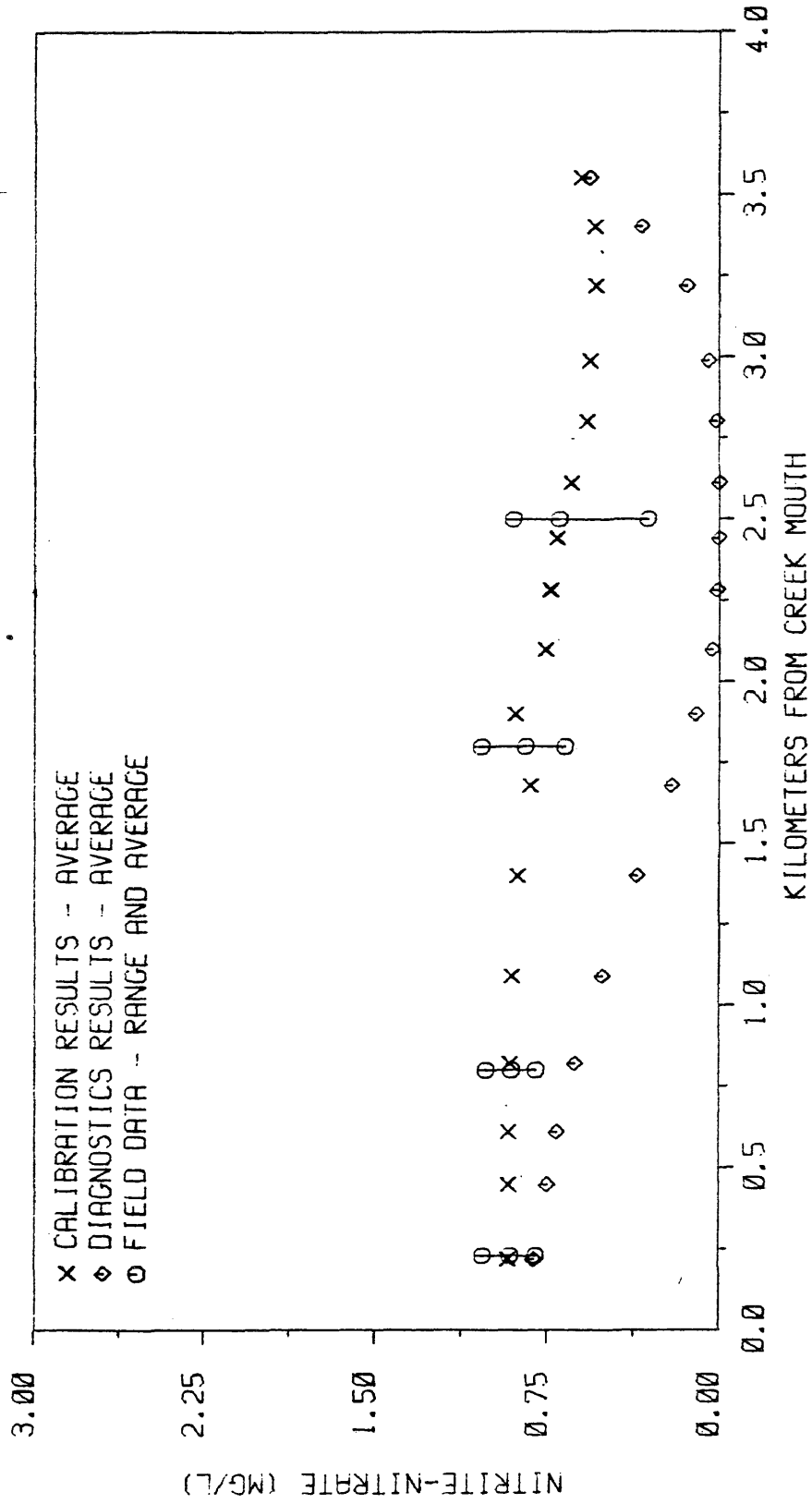


Figure 39. Results for nitrite-nitrate nitrogen - point source inputs set to zero.

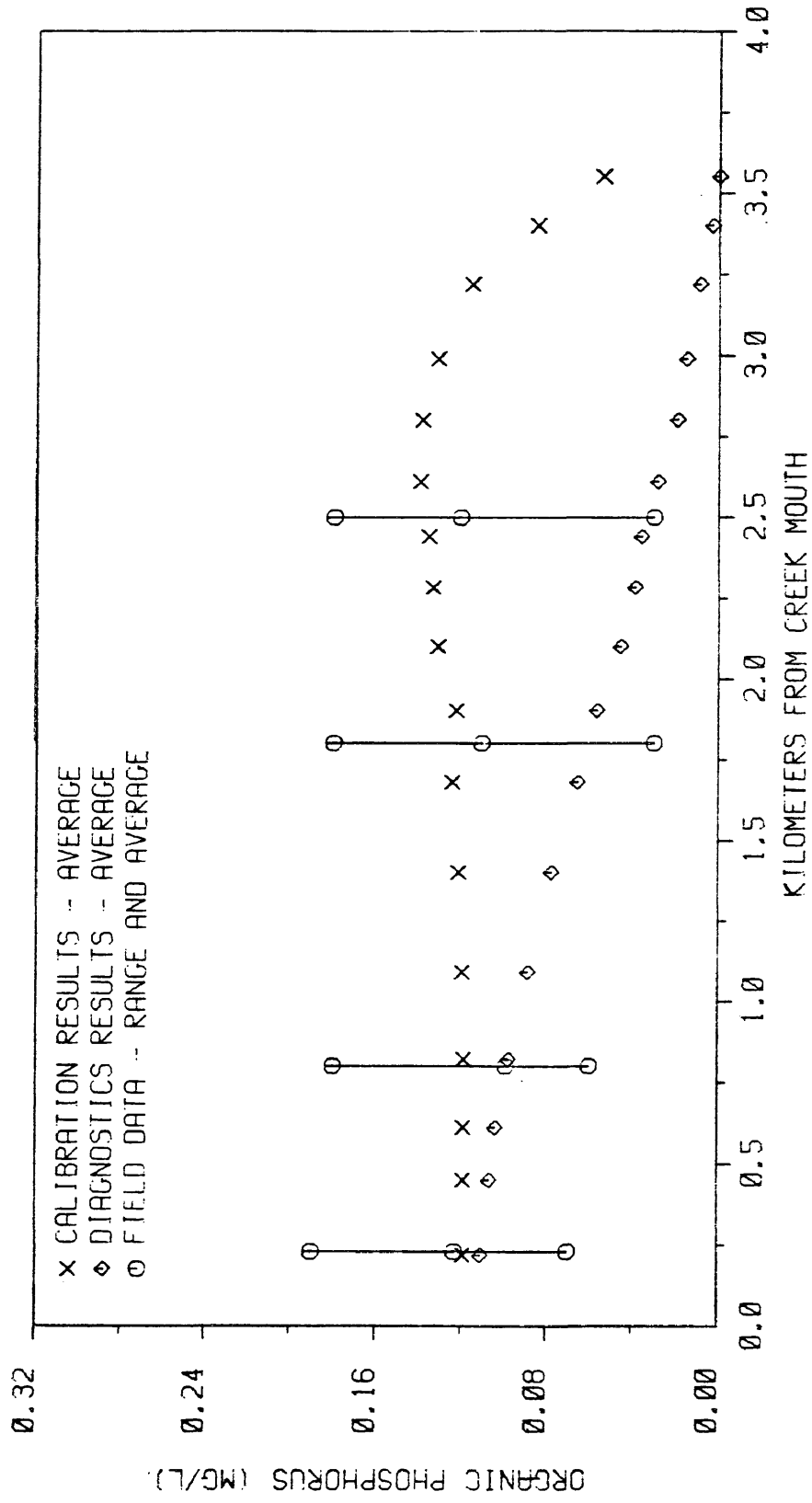


Figure 40. Results for organic phosphorus - nonpoint source inputs set to zero.

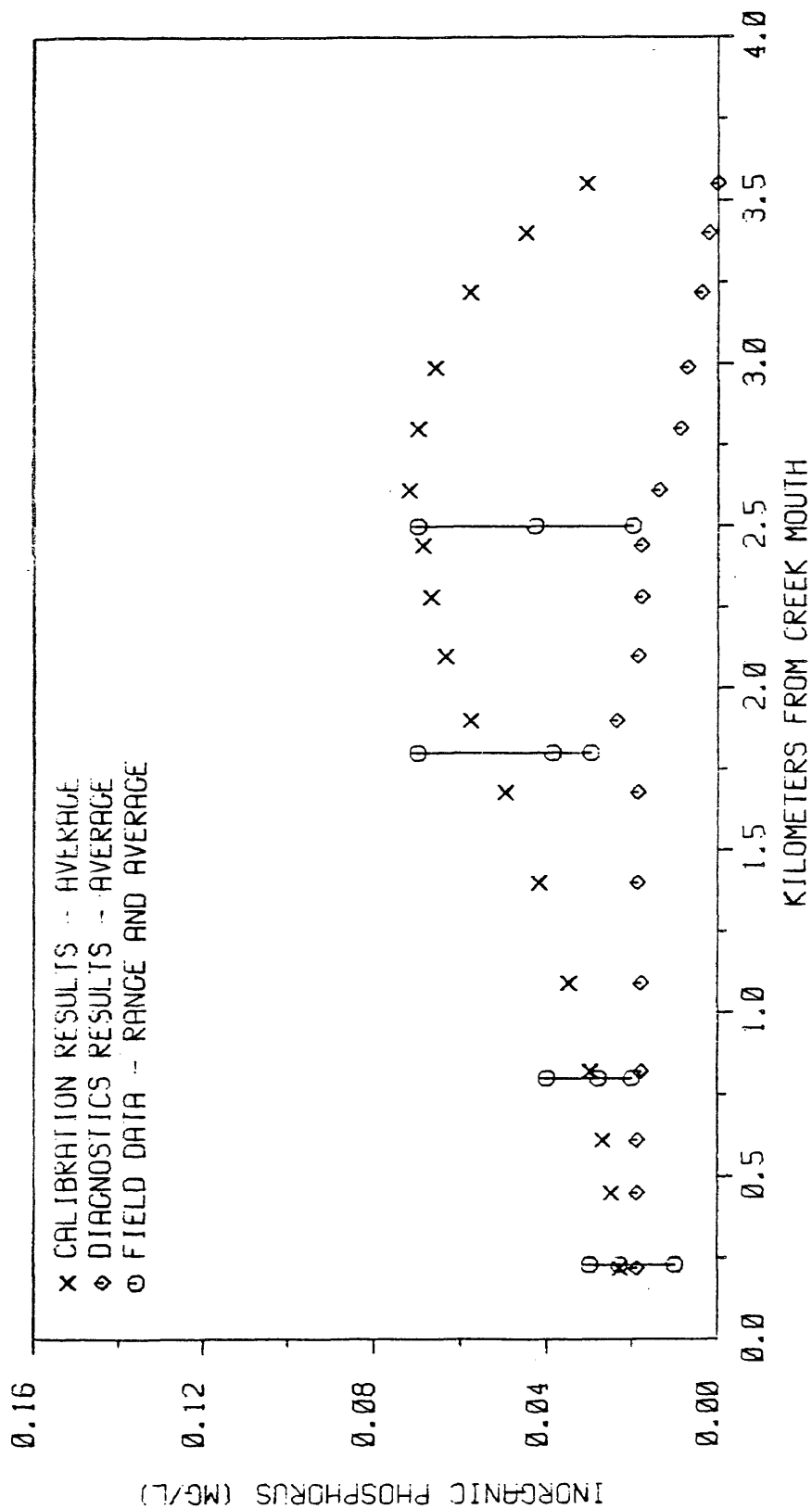


Figure 41. Results for inorganic (ortho) phosphorus - nonpoint source inputs set to zero.

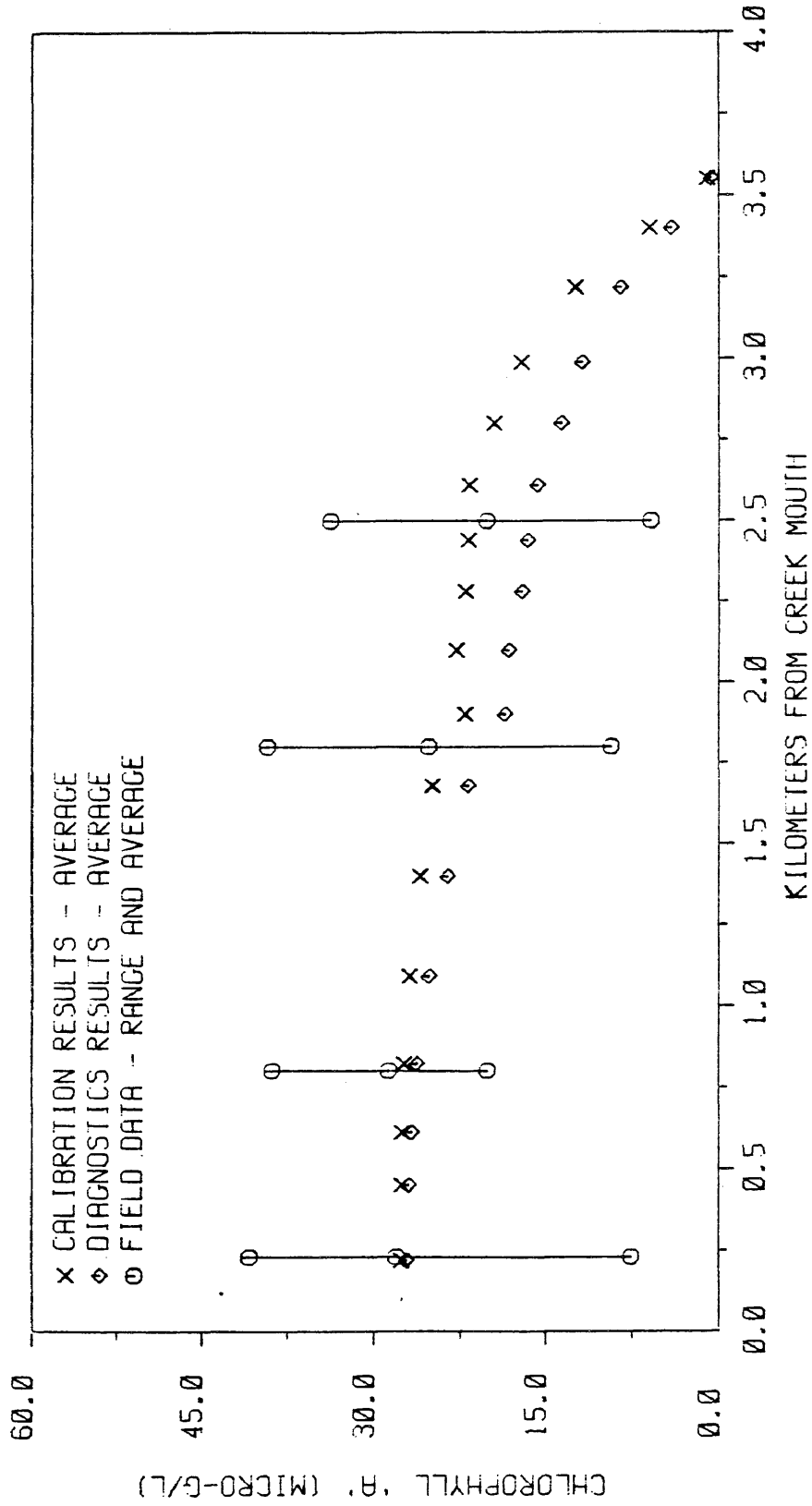


Figure 42. Results for chlorophyll 'a' - point source inputs set to zero.

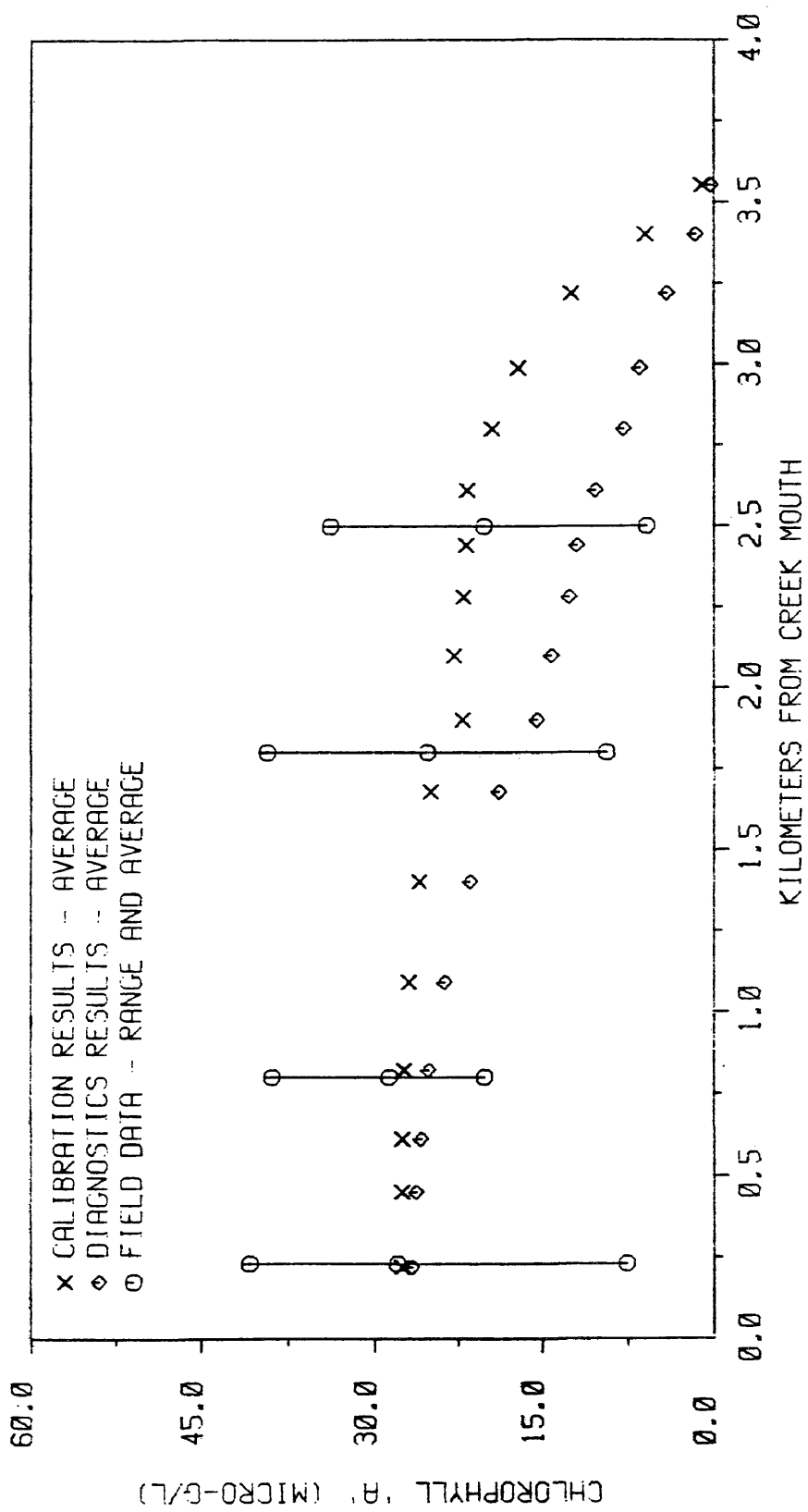


Figure 43. Results for chlorophyll 'a' - nonpoint source inputs set to zero.

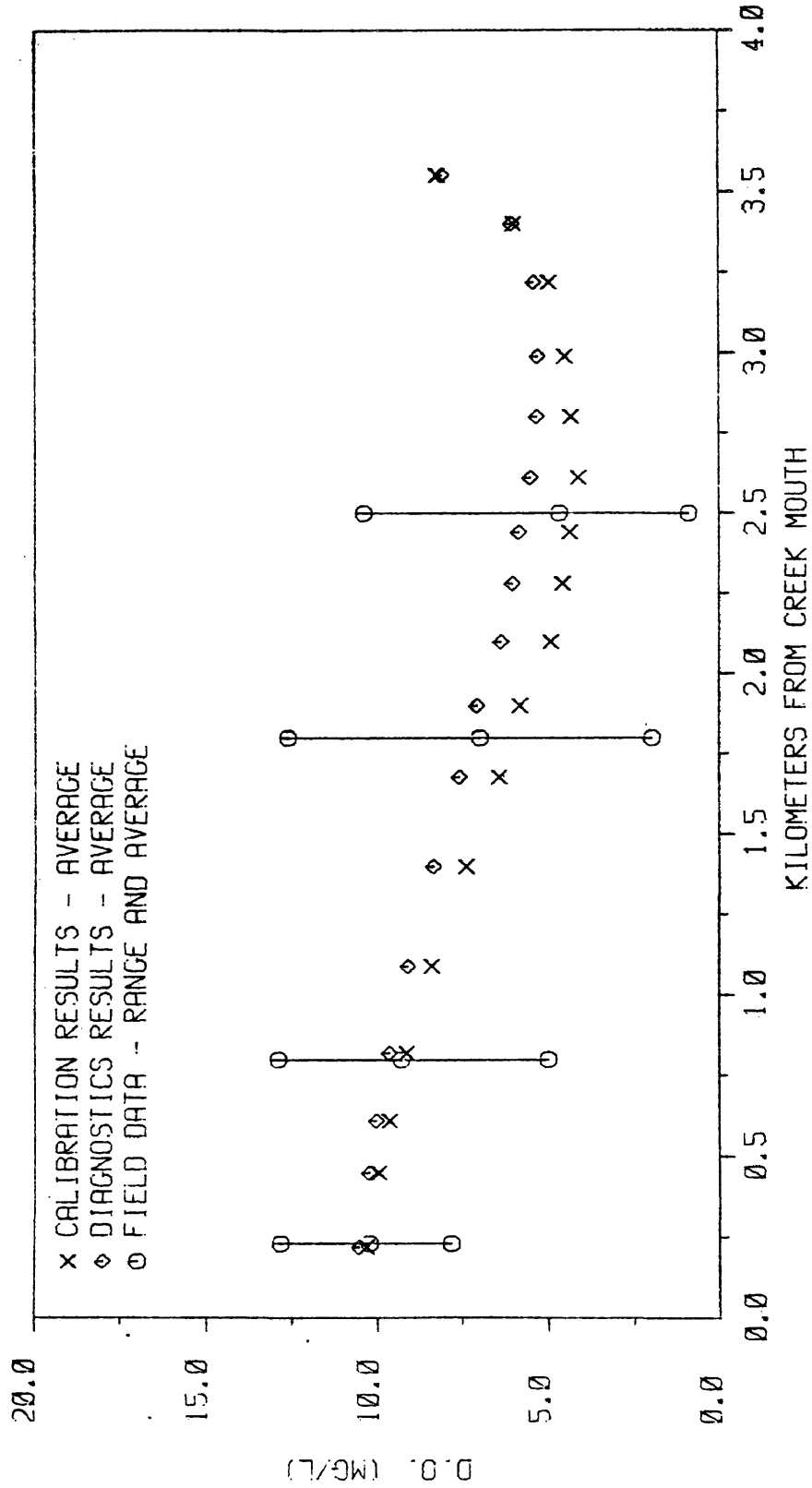


Figure 44. Results for dissolved oxygen - point source inputs for nitrogen, phosphorus and CBOD set to zero.

DO concentrations can be attributed to a sharp reduction in oxidizable matter - CBOD and ammonia nitrogen. The reduction in CBOD and ammonia more than outweigh the effects of reduced phytoplankton growth.

On the other hand, the elimination of nonpoint inputs led to a decline in average dissolved oxygen concentrations throughout the creek. The average DO value for two tidal cycles decreased by 0.6 mg/l at the sag point (Figure 45). This result can be attributed to the reduced phytoplankton growth which is due to the drastic decrease in ortho-phosphorus input.

A separate model run was made to assess the role of sediment oxygen demand (SOD). Setting SOD to zero resulted in an increase of 3.5 mg/l at the minimum point of the DO distribution curve (Figure 46).

Two model runs were made in which the downstream boundary conditions for all parameters except dissolved oxygen were set to zero to assess the importance of inputs from the Potomac River. These runs indicated that the downstream boundary conditions for CBOD, the nitrogen parameters and the phosphorus parameters have little effect on conditions upstream of the STP outfall (reach 11) where the water quality problem exists. Setting the chlorophyll 'a' boundary condition to zero had a significant effect for some distance upstream of the STP outfall (Figure 47). This result is due to the relatively high boundary condition for chlorophyll obtained from field data and used in model calibration.

Two model runs were made in which it was assumed that the Potomac River was perfectly clean - no nitrogen, phosphorus, CBOD or phytoplankton. For one of these runs the DO boundary condition was left at the oversaturated level indicated by field measurements. The

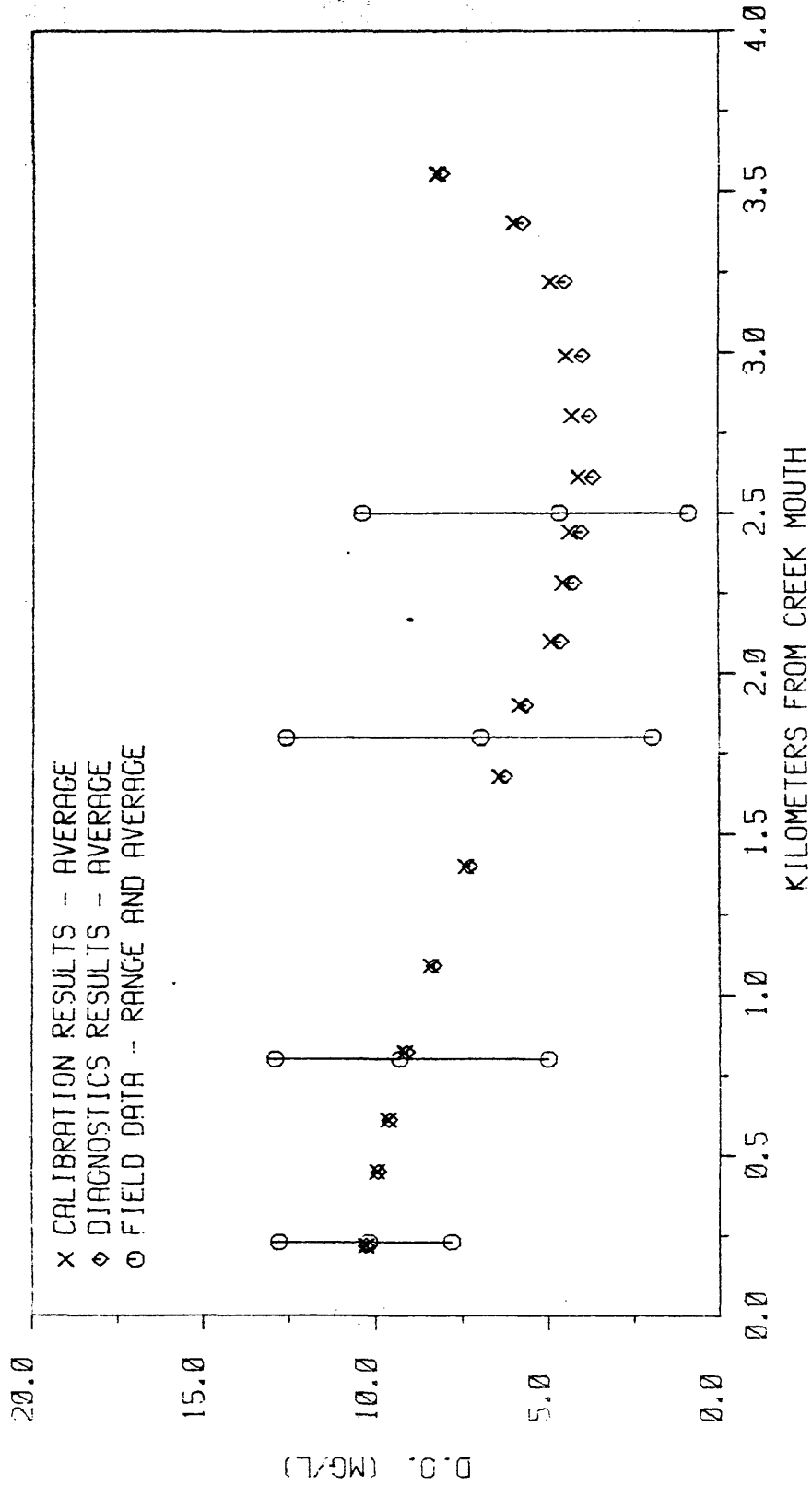


Figure 45. Results for dissolved oxygen - nonpoint source inputs for nitrogen, phosphorus and CBOD set to zero.

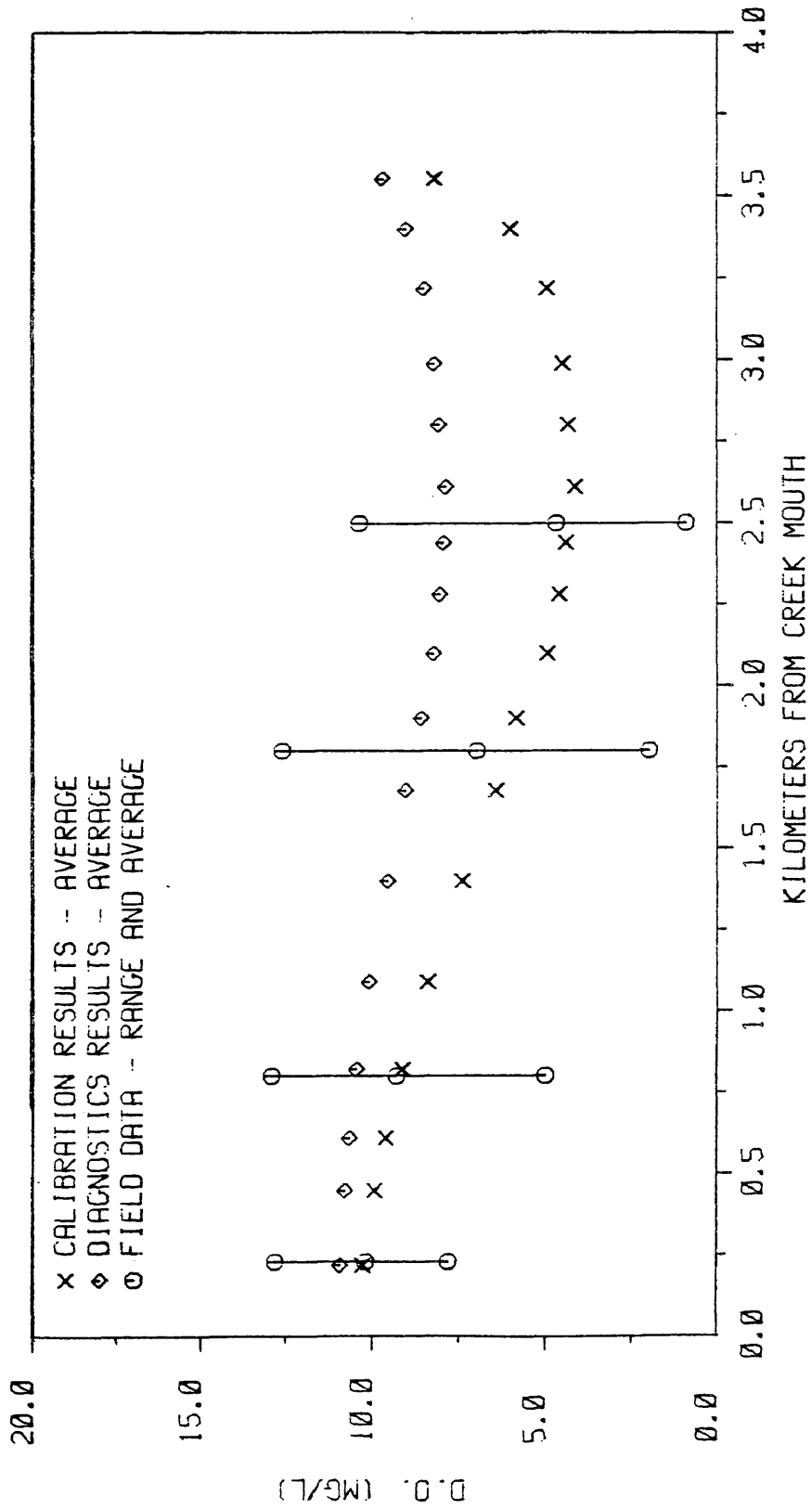


Figure 46. Results for dissolved oxygen - sediment oxygen demand set to zero.

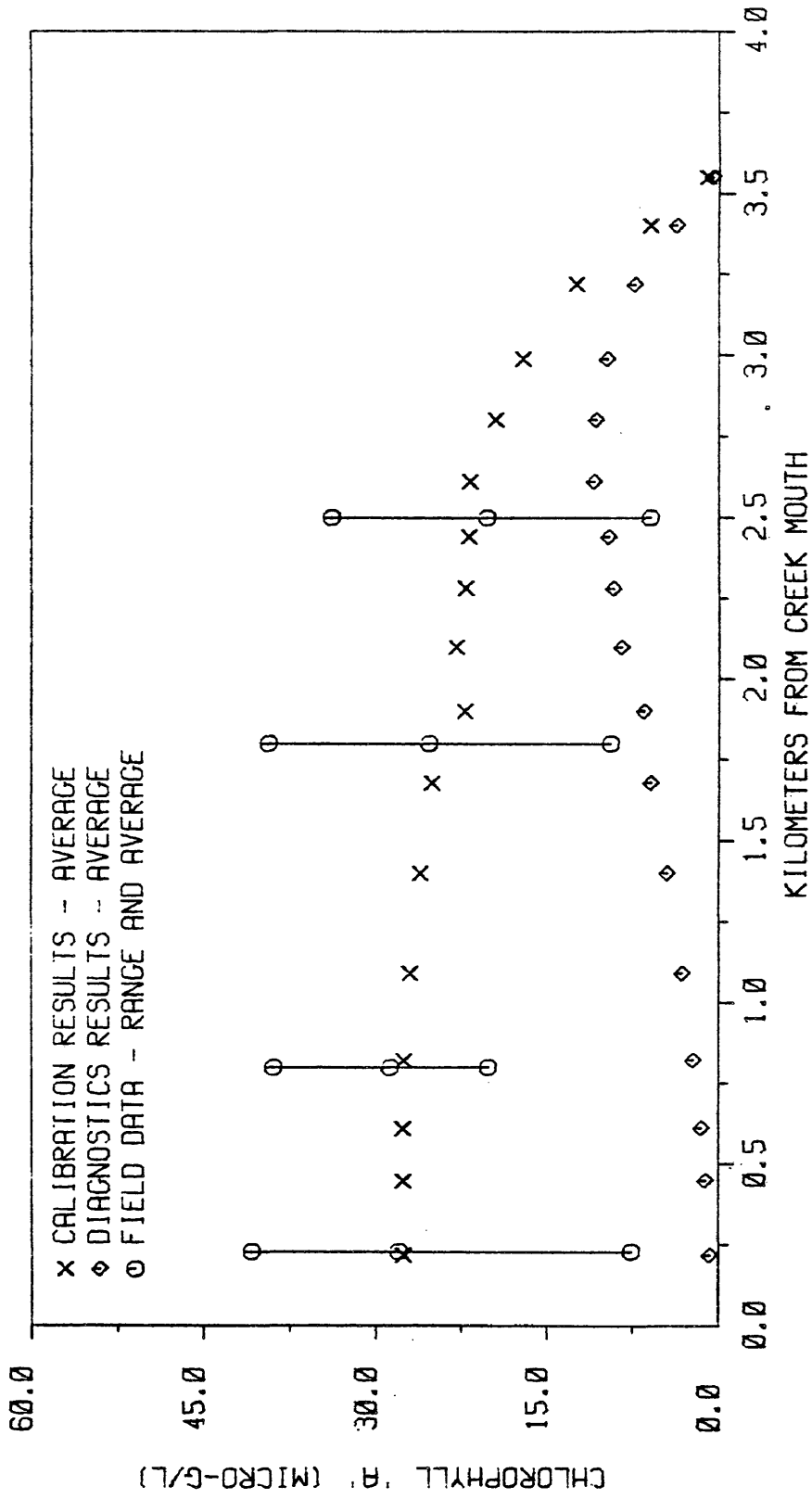


Figure 47. Results for chlorophyll 'a' - downstream boundary conditions set to zero.

run under these conditions resulted in a slight depression of average DO concentrations throughout the creek due to the lower phytoplankton concentrations mentioned above. In the second run the dissolved oxygen concentration of the Potomac was assumed at saturated level while all other boundary conditions were maintained at zero. The lowering of the DO boundary condition had significant effect on DO concentrations only in that portion of the creek downstream of the STP outfall.

V. SUMMARY AND CONCLUSIONS

An intra-tidal, real-time mathematical model based on the one-dimensional forms of the momentum, continuity and mass-balance equations has been developed to simulate hydrodynamic behavior and water quality conditions in a tidal system. The model is composed of two submodels. In the hydrodynamic submodel a semi-implicit finite difference scheme is used to solve the one-dimensional continuity and momentum equations simultaneously for the velocity and surface elevation as functions of time and longitudinal distance. This dynamic approach to modeling hydrodynamic behavior insures that the interaction between tides and freshwater inflows is adequately addressed. The information provided by the hydrodynamic submodel is used as input to the water quality submodel. The water quality submodel consists of a series of one-dimensional mass-balance equations describing the longitudinal and temporal distribution of eight interacting dissolved or suspended substances. The mass-balance equations are solved via an implicit finite difference method.

The mathematical model developed here has been applied to the Little Hunting Creek, a small tidal creek off the Potomac River. It has effectively reproduced both the short-term (intra-tidal and diurnal) variations and long-term (seasonal) variations of water quality in the creek. The model's capabilities in predicting longitudinal and temporal changes in the concentrations of dissolved

substances due to the changes in wasteloadings or variations in the physical transport processes has been demonstrated in the results of the long-term validation simulation.

The model's usefulness as a diagnostic tool has also been demonstrated by the case study. Model results indicate that sediment oxygen demand has the largest influence on the dissolved oxygen distribution in Little Hunting Creek, causing a deficit of over 3 mg/l at the sag point. In comparison, point source loadings of oxidizable materials, second to SOD in influence, causes a deficit of approximately 1 mg/l at the sag. Model results indicate that chlorophyll concentrations in the creek are strongly influenced by flux across the downstream boundary. Population fluctuations influenced by prevailing conditions in the creek are superimposed on the relatively large boundary condition effect. Model results also suggest that phytoplankton growth in the creek is phosphorus limited and that phosphorus is primarily contributed by nonpoint runoff. The elimination of nonpoint source loadings would further inhibit phytoplankton growth by significantly reducing the inorganic phosphorus available for uptake. On the other hand, the elimination of point source loadings would drastically reduce the concentrations of inorganic nitrogen throughout the creek, resulting in phytoplankton growth being nitrogen limited.

The hydrodynamic submodel satisfactorily simulates the interaction between tides and upstream inflows during periods of heavy runoff as well as during dryer periods. With a very few changes in inputs the hydrodynamic submodel can be used to simulate either a freshwater tidal stream, as in the case study presented, or a system

where salinity gradients exist.

The water quality submodel combines the influences exerted by point source and nonpoint source wasteloadings, exchanges between the surroundings and the water column, and biochemical transformations, together with information on advection and dispersion generated by the hydrodynamic submodel. The model can easily be adapted to include additional dissolved or suspended substances.

The real-time approach employed allows for the investigation of important water quality measures in terms of maximum and minimum values occurring within a tidal or a diurnal cycle. Utilization of this model to simulate long-term changes in water quality is made economically viable through the use of an efficient numerical scheme. The time increment for the Little Hunting Creek case study is set as 0.01 tidal cycles. It takes approximately 2.8 minutes to simulate ten tidal cycles using the Prime 750 computer.

While the model satisfactorily simulates the intra-tidal, diurnal and seasonal variations in water quality in the case study, there are some differences between model predictions and measurements made in the field. Model predictions for intra-tidal variations exhibit a reduced range of concentrations in comparison to field measurements. Some reduction in concentration ranges is an expected result of the one-dimensional finite-difference scheme which produces average concentrations over the total volume of a segment, while field data represents measurements taken at a single point along the channel.

It has been shown that the model developed here satisfactorily predicts the variations in water quality within the limitations imposed by the one-dimensional representation and by the use of estimated

loadings, inflows and boundary conditions. The accuracy of model predictions of future water quality will depend on the accuracy of predicted inputs and driving forces. The importance of an adequate data base cannot be overstressed.

VI. DISCUSSION AND RECOMMENDATIONS

Where possible, it is desirable to model small tidal systems up to the limit of tidal influence. This allows for easier definition of upstream boundary conditions. However, model simulation will break down if at any time local surface elevation falls below the channel depth specified. This is most likely to occur in the upstream portion of the creek and may be the result of describing the creek geometry by specifying average mean tide depths for model transects and reaches. A possible solution to this problem may lie in more detailed approach in describing change in cross-sectional areas with change in surface elevation.

The model's predictive capability is restricted by the necessity of specifying boundary conditions. The downstream boundary condition of surface elevation necessary for the hydrodynamic submodel may be addressed by using information available from tide tables or tide gauge records. Unfortunately, such sources do not exist for use in determining downstream boundary conditions for dissolved or suspended substances. Lack of information on changes in downstream boundary conditions may seriously affect model predictions, at least in the lower portion of the system.

Similar uncertainties are introduced in terms of upstream inflows and loadings. Nonpoint source field data, when available, is usually sketchy. Nonpoint source loadings will generally be in the

form of predictions generated by a nonpoint source model. Although such models employ information on local land use to achieve predictions, important differences between the various drainage basins may not be adequately addressed. More research and development in nonpoint source modeling is essential for successful application of water quality models.

Sediment oxygen demand is often an important influence on dissolved oxygen concentrations in an estuary and its determination through field techniques is becoming more routine. However, techniques for measuring the effects of sediments and benthic organisms on other dissolved substances are not yet well developed. Aside from the difficulty in measurement, in systems with extensive shallows there is the question of where to measure in order to determine truly representative values for benthic fluxes. It is not likely that measurements made along the channel will be useful in quantifying a process that for the most part occurs in the shallow areas. Some average of measurements made in deep and shallow areas would be more appropriate for use in a model of the system.

Rooted aquatic plants are often abundantly present in small tidal streams during certain times of the year. Where nutrients are sufficient the surfaces of the shallow portions of the stream may essentially be covered by vegetation. The effects of these plants on water quality, through photosynthesis, respiration, shading and the uptake of nutrients, are not well known. For these reasons, including rooted aquatic vegetation in a mathematical model is not yet practical. However, information on the influence of such plants would be useful in assessing model performance.

A mathematical model is an important tool in the decision making process of water quality management. Models are an aid to researchers in identifying factors affecting water quality and in assessing their relative importance. Models permit evaluation of proposed changes in wasteload allocations and changes in system use or geometry. Utilizing models to assess appropriate in-stream water quality standards and in evaluating the maximum allowable wasteloading that still meets these standards affords the best hope for man to gain optimum use of estuarine systems. All too often, however, this powerful tool is laid aside after the decisions are made and is never taken up again. This is unfortunate in that useful information can be lost when there is no comparison between model predictions and the ensuing results of program implementation. Ideally, such a comparison would result in a reaffirmation of the model's capabilities allowing the model to be employed with confidence in the study of other similar systems.

APPENDIX. RESULTS OF MODEL VALIDATION

— model

○ slackwater survey
measurements

● intensive or diurnal
survey - average

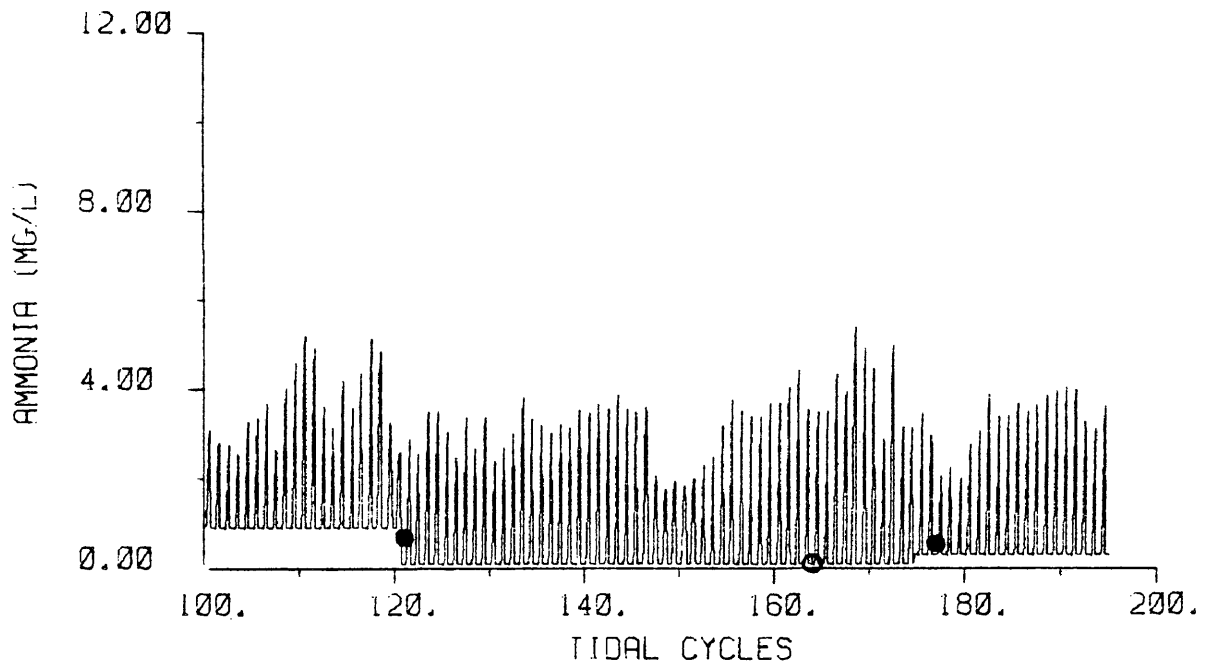
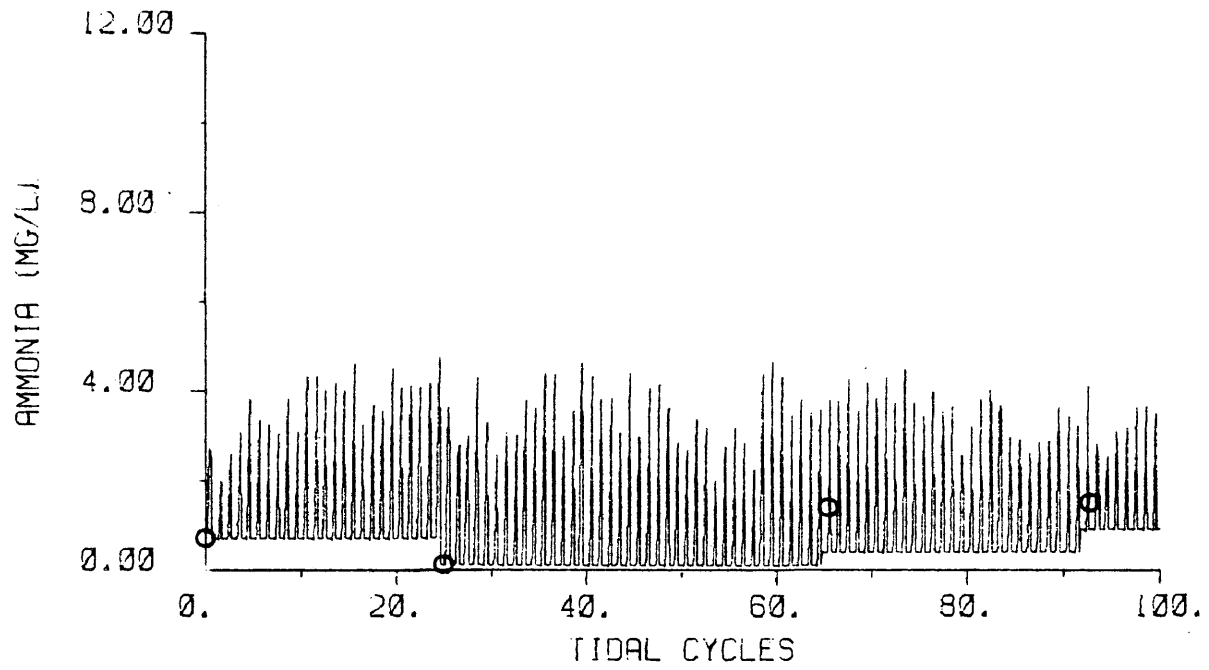


Figure A1. Validation results for ammonia - station 2.

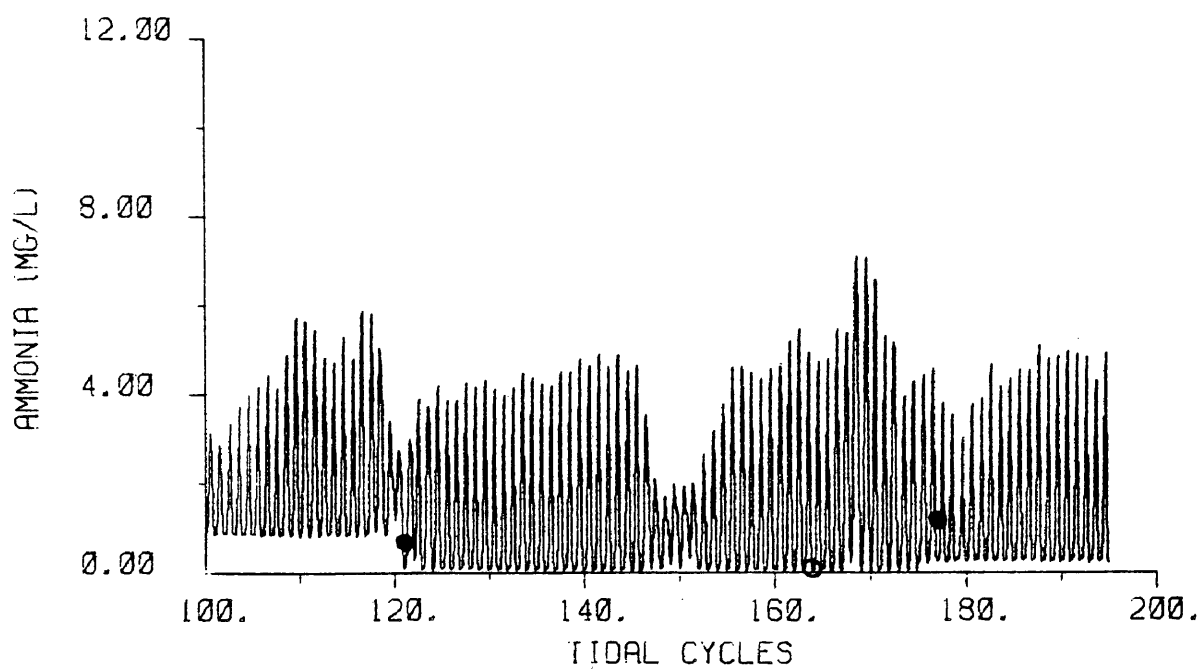
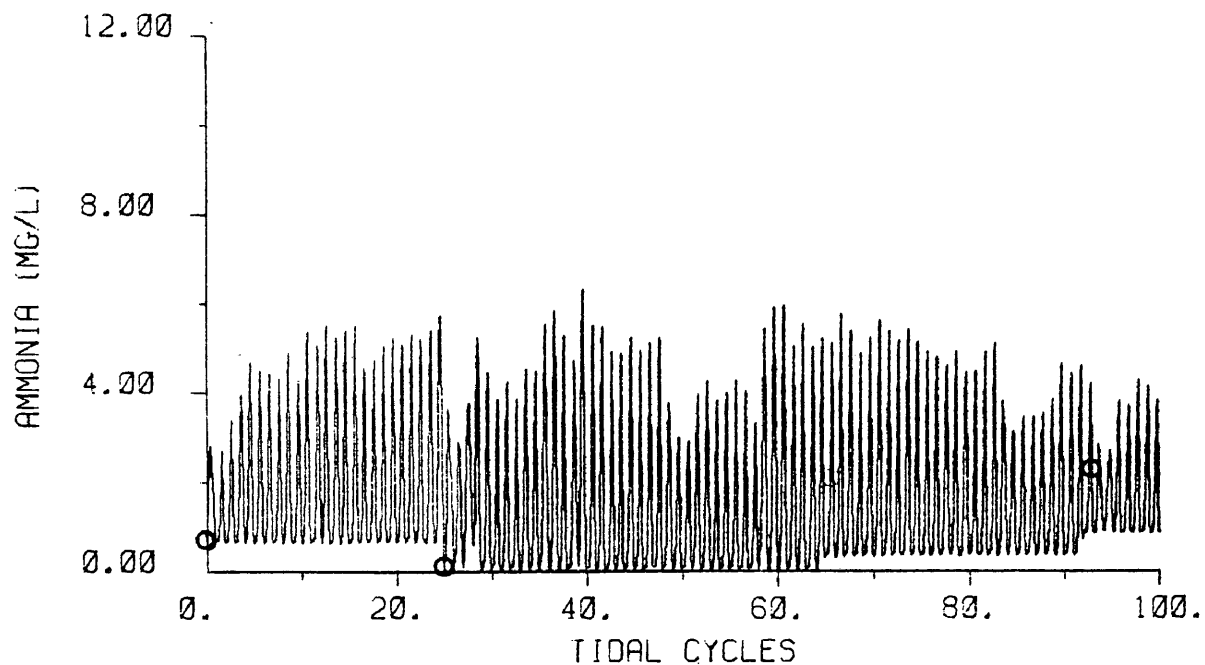


Figure A2. Validation results for ammonia - station 3.

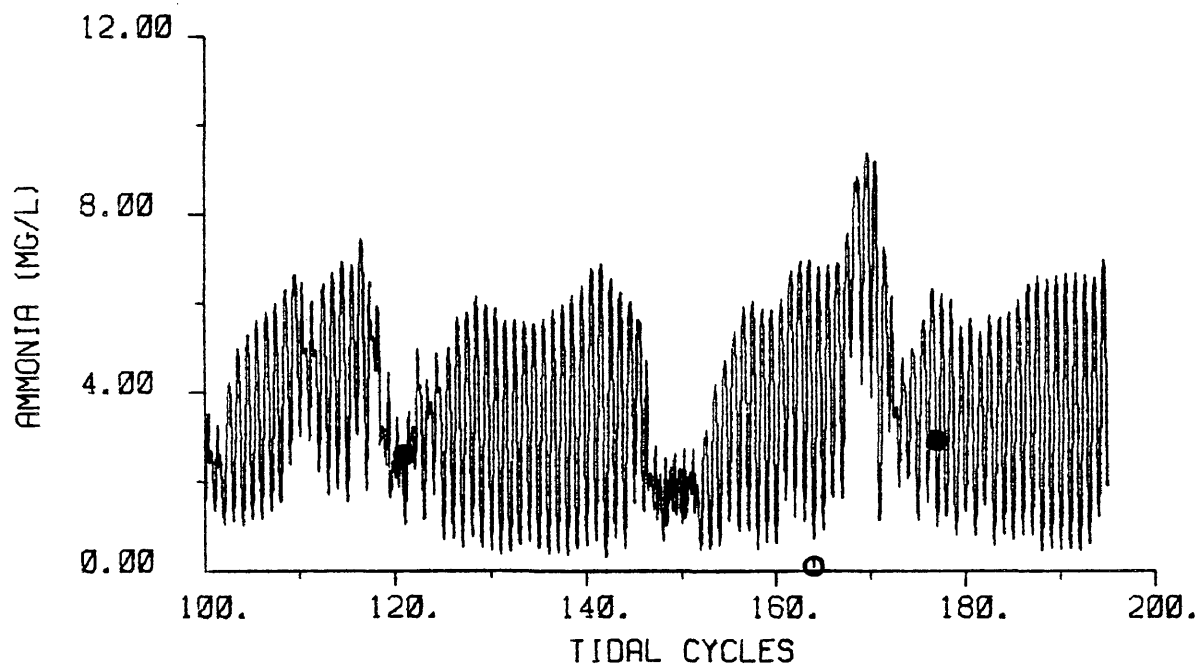
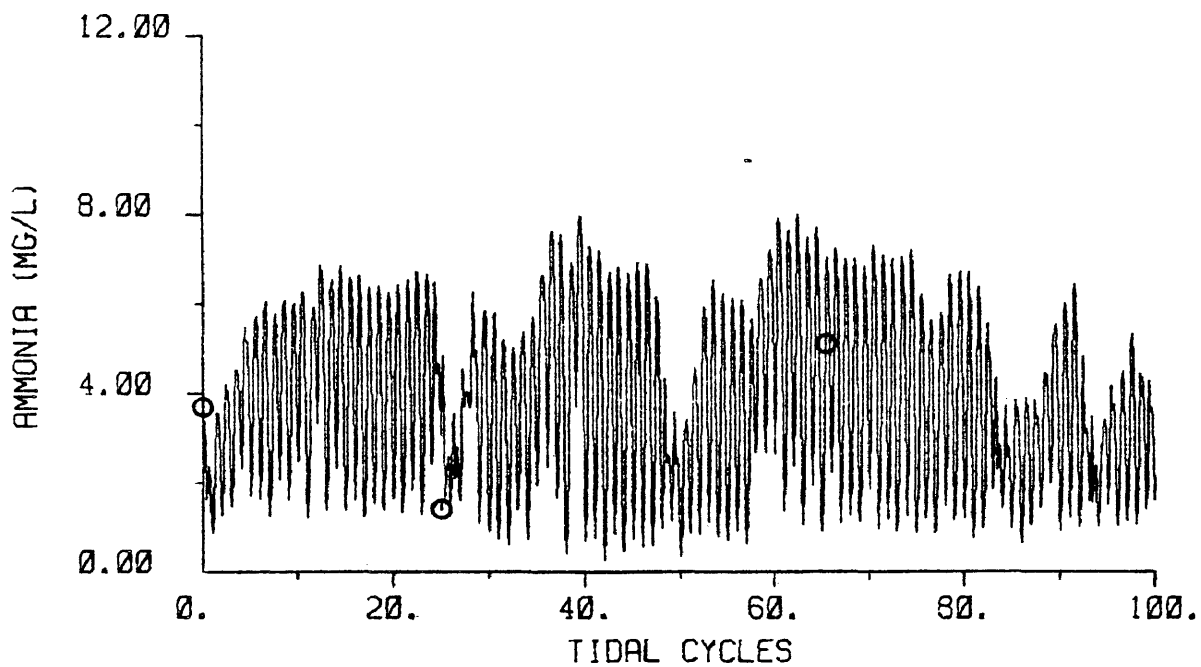


Figure A3. Validation results for ammonia - station 4.

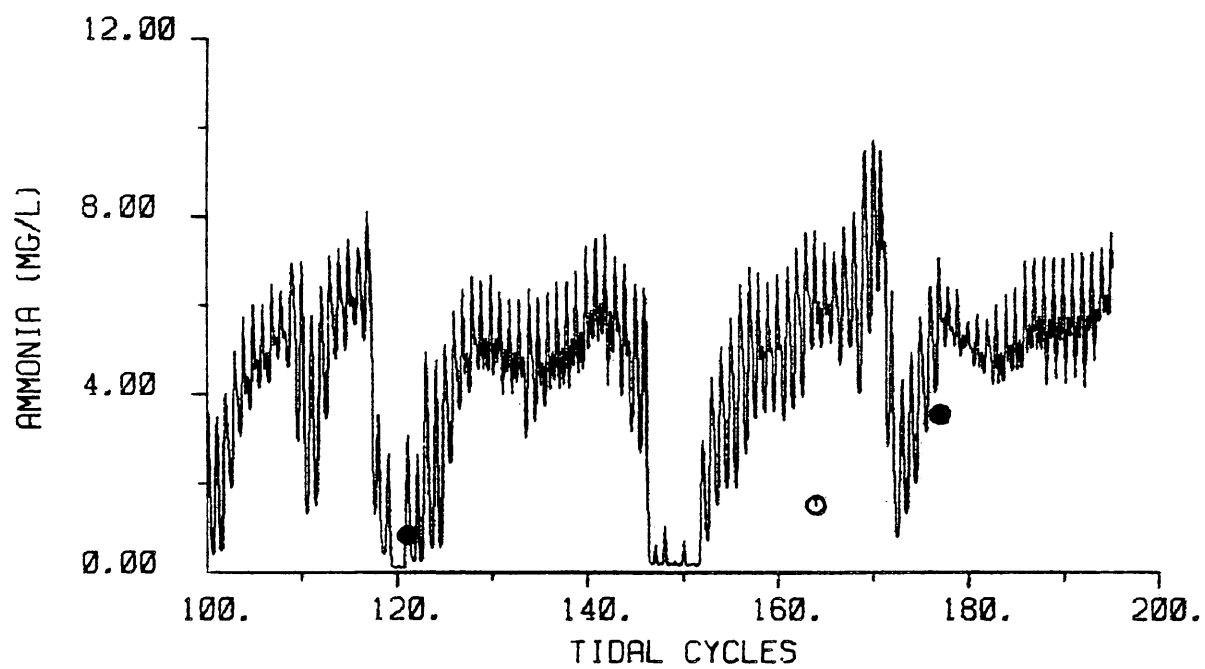
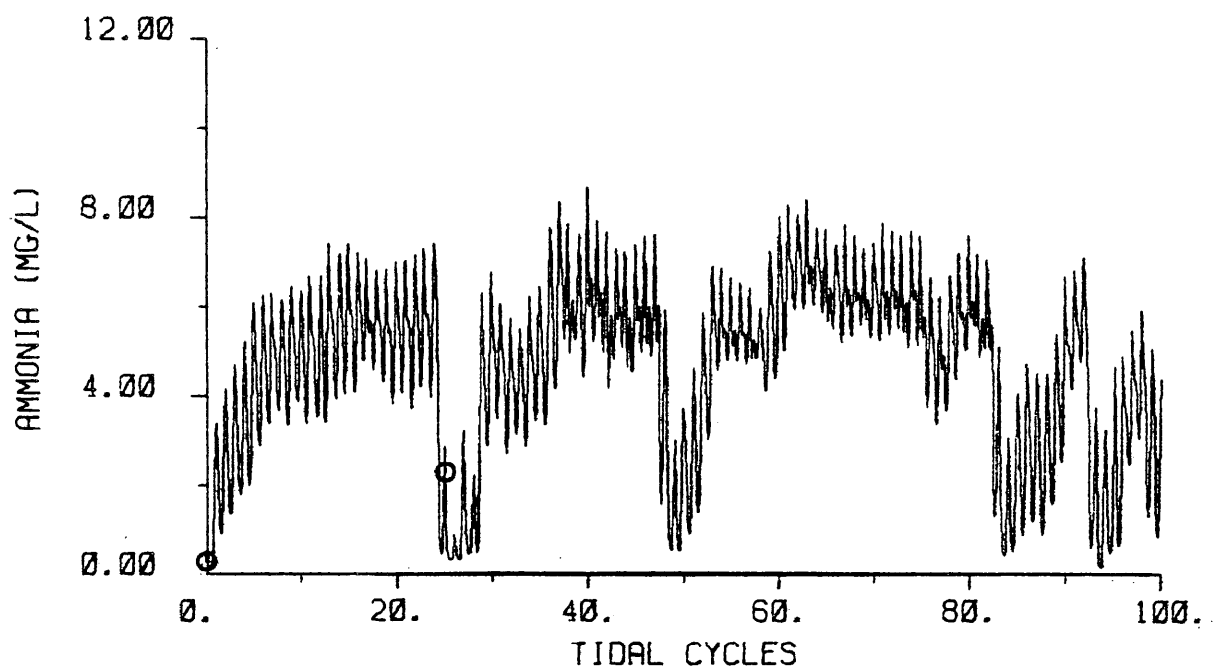


Figure A4. Validation results for ammonia - station 5.

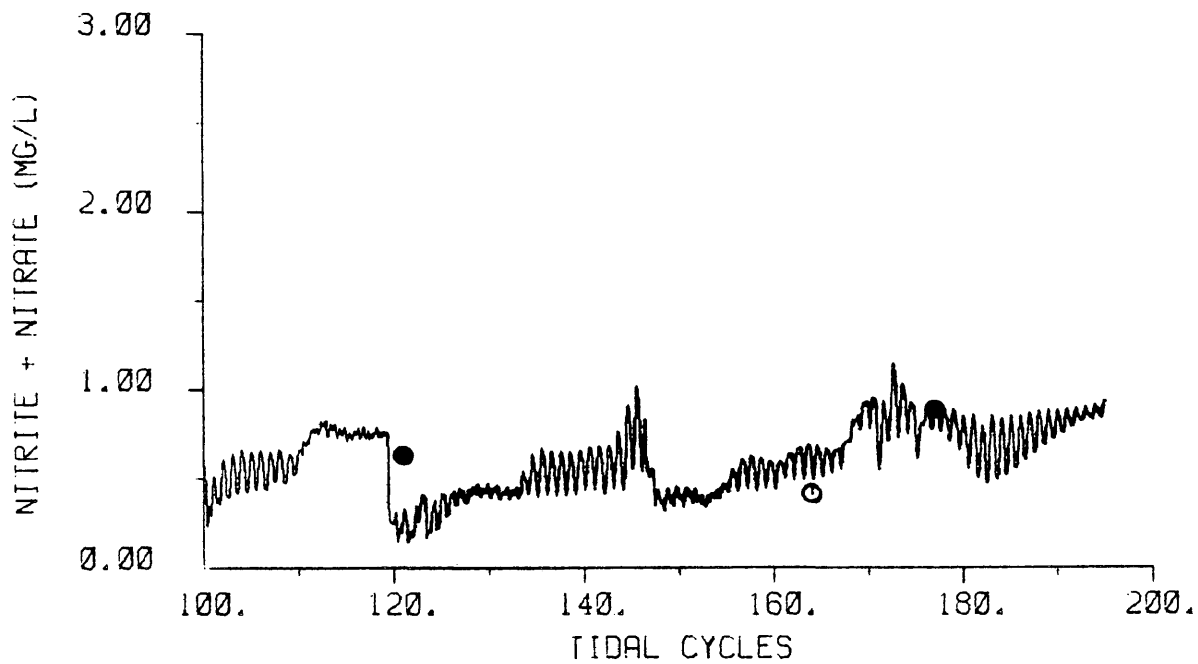
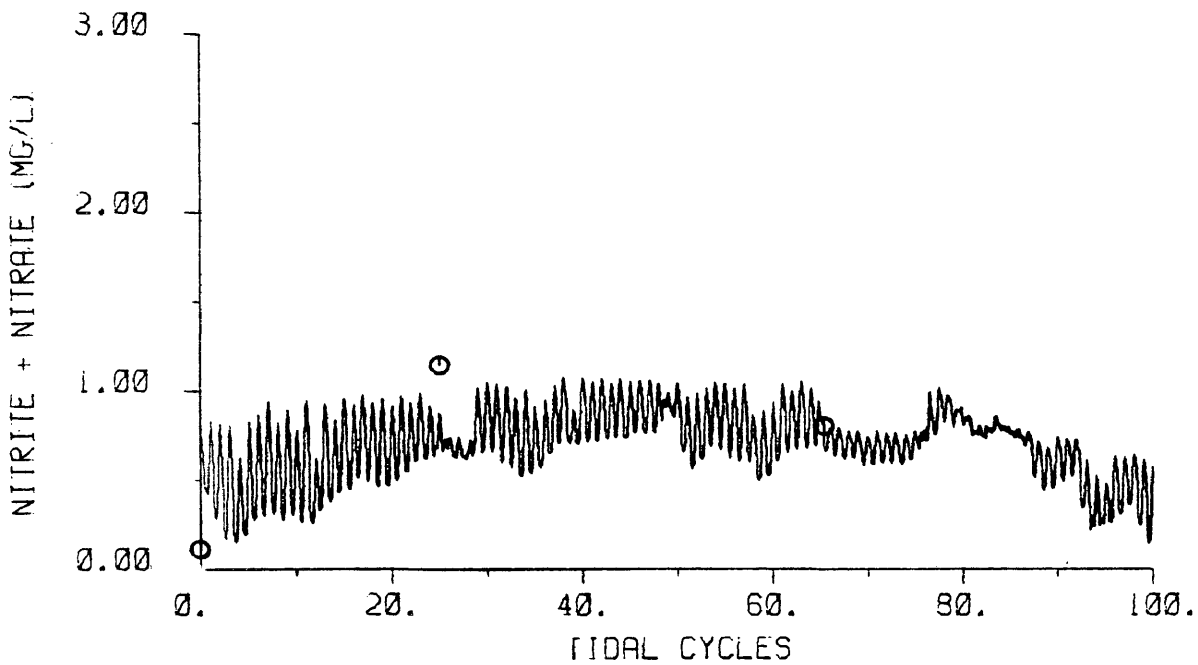


Figure A5. Validation results for nitrite-nitrate nitrogen - station 4.

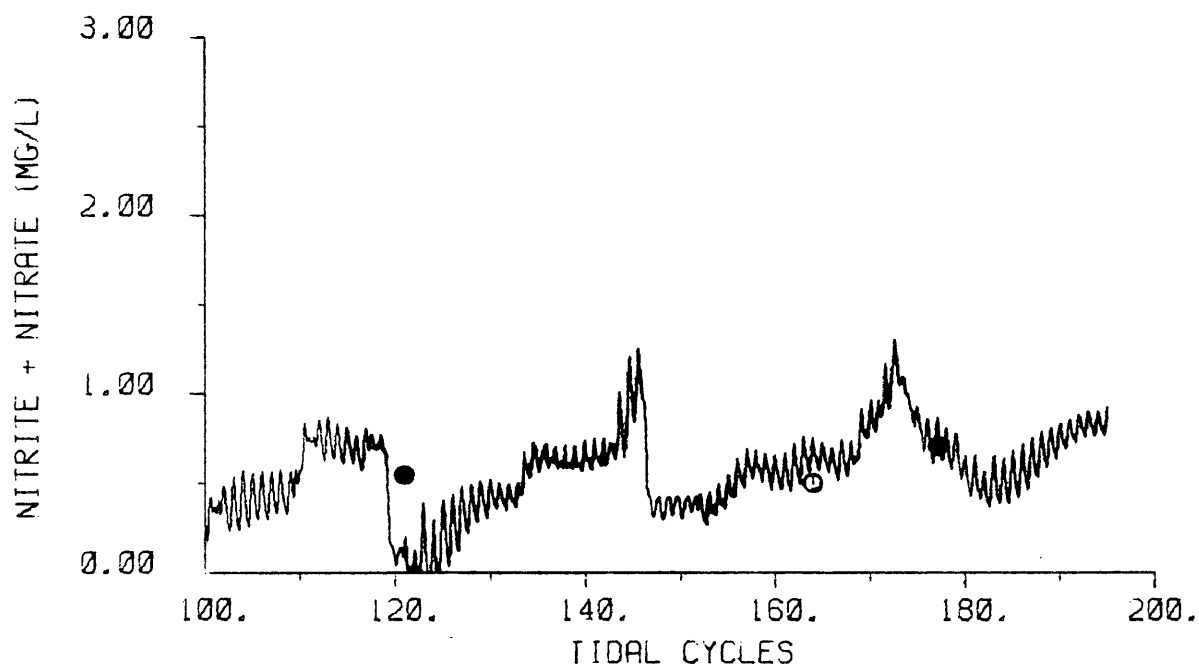
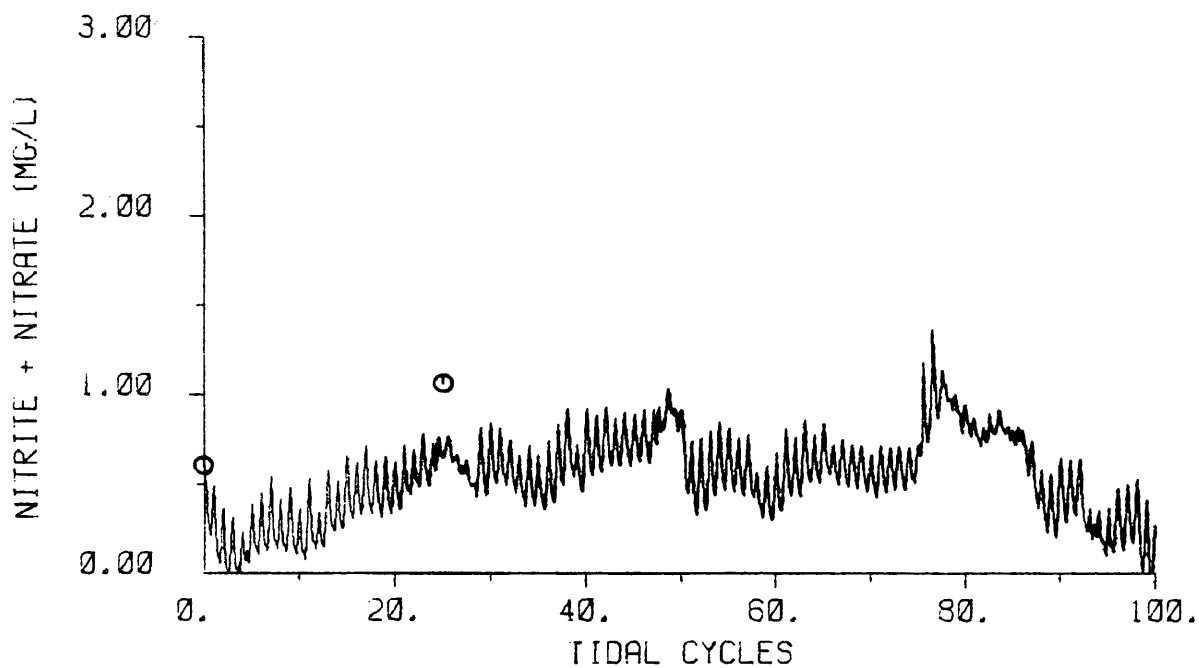


Figure A6. Validation results for nitrite-nitrate nitrogen - station 5.

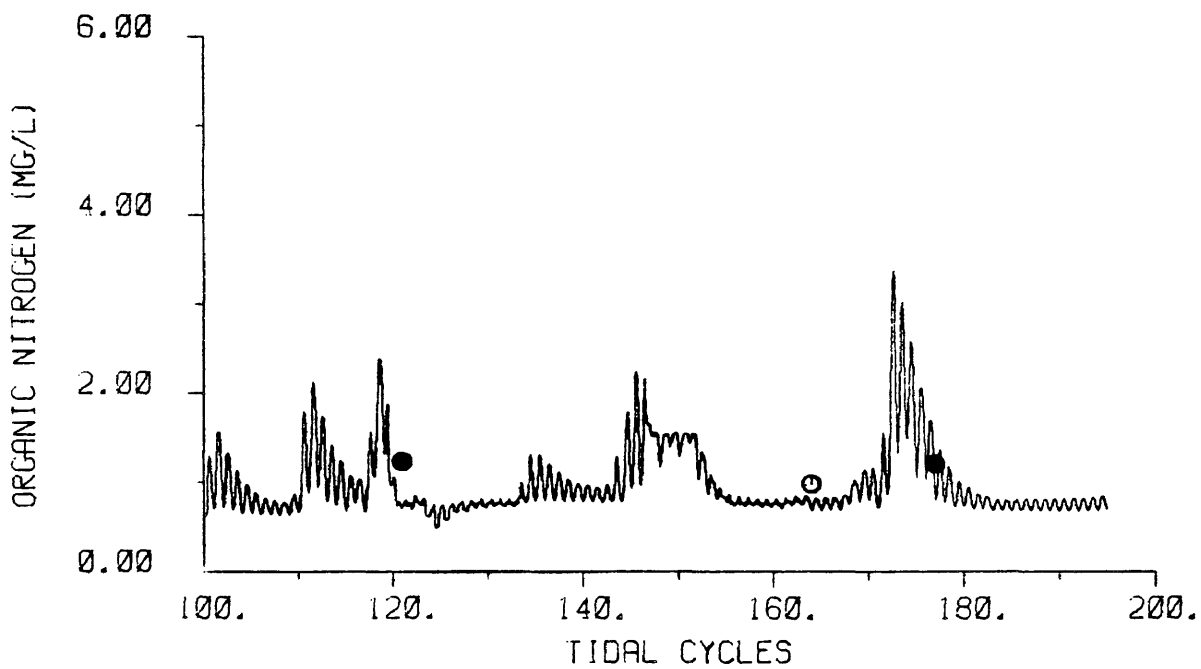
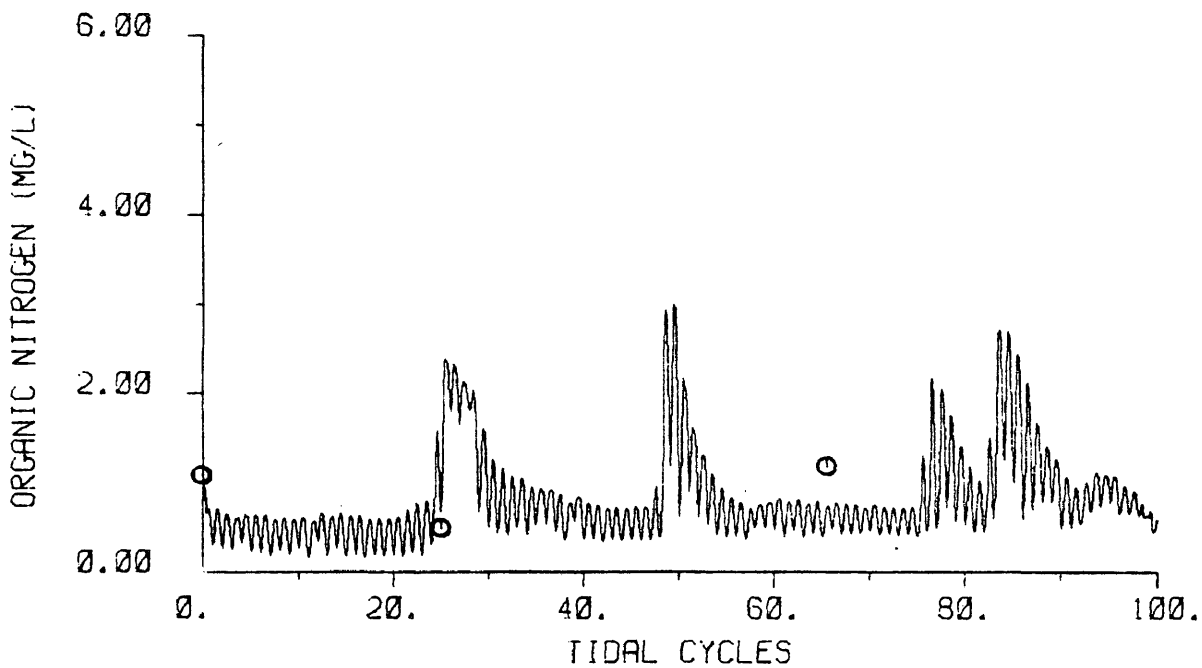


Figure A7. Validation results for organic nitrogen - station 4.

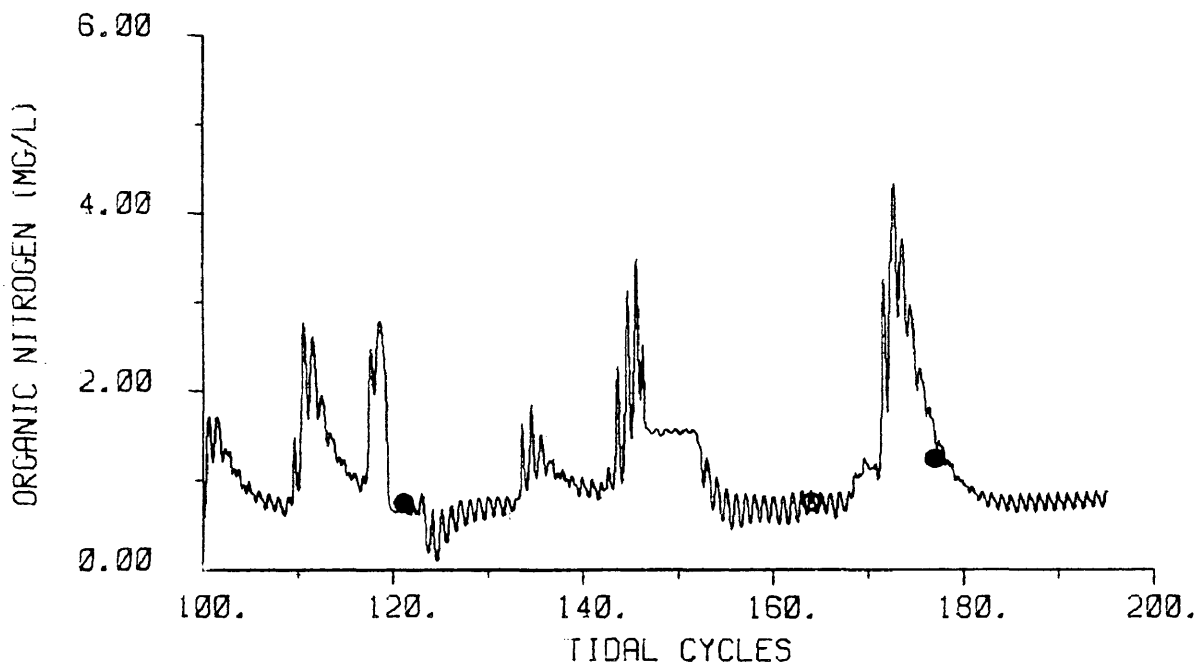
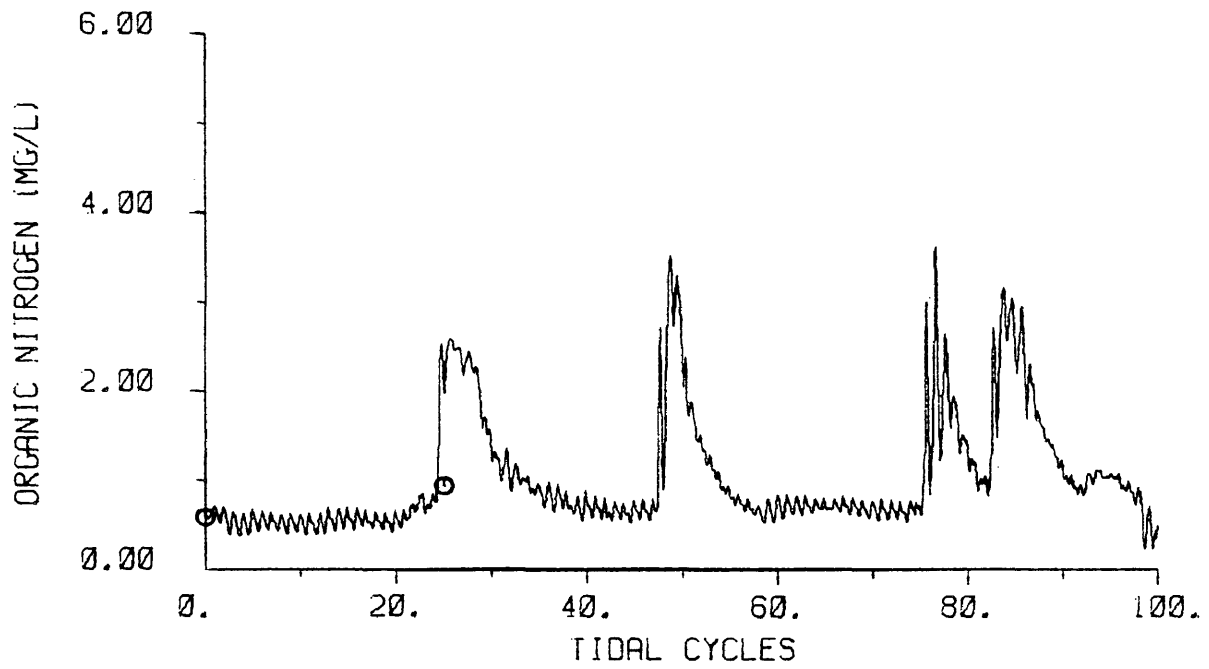


Figure A8. Validation results for organic nitrogen - station 5.

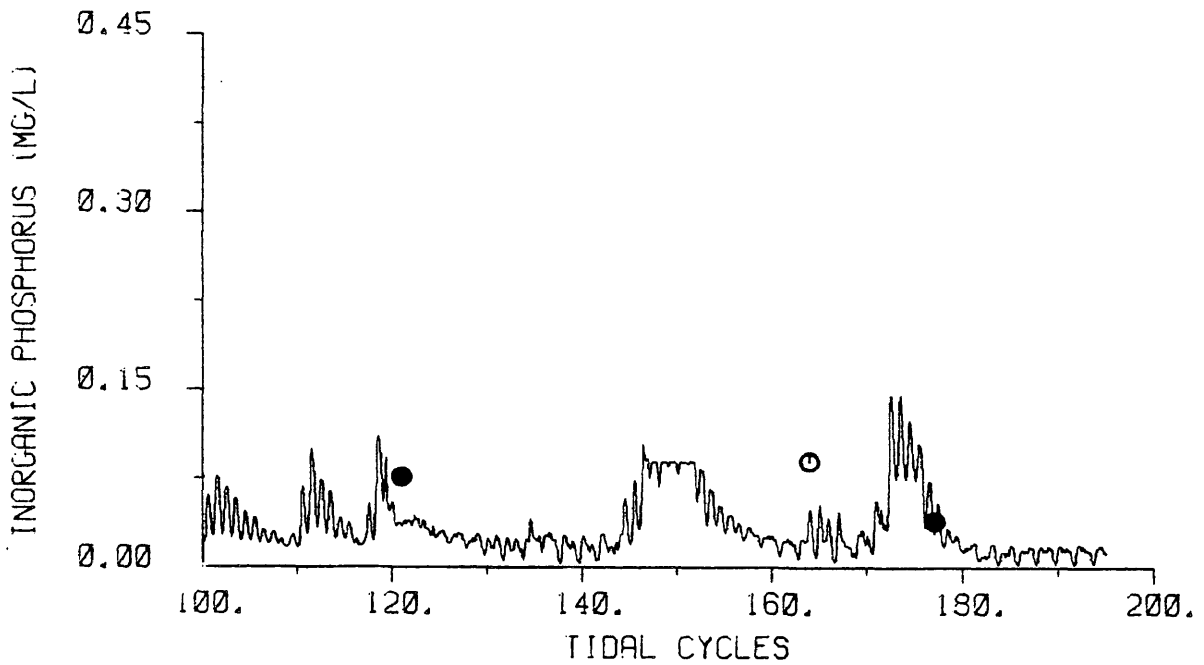
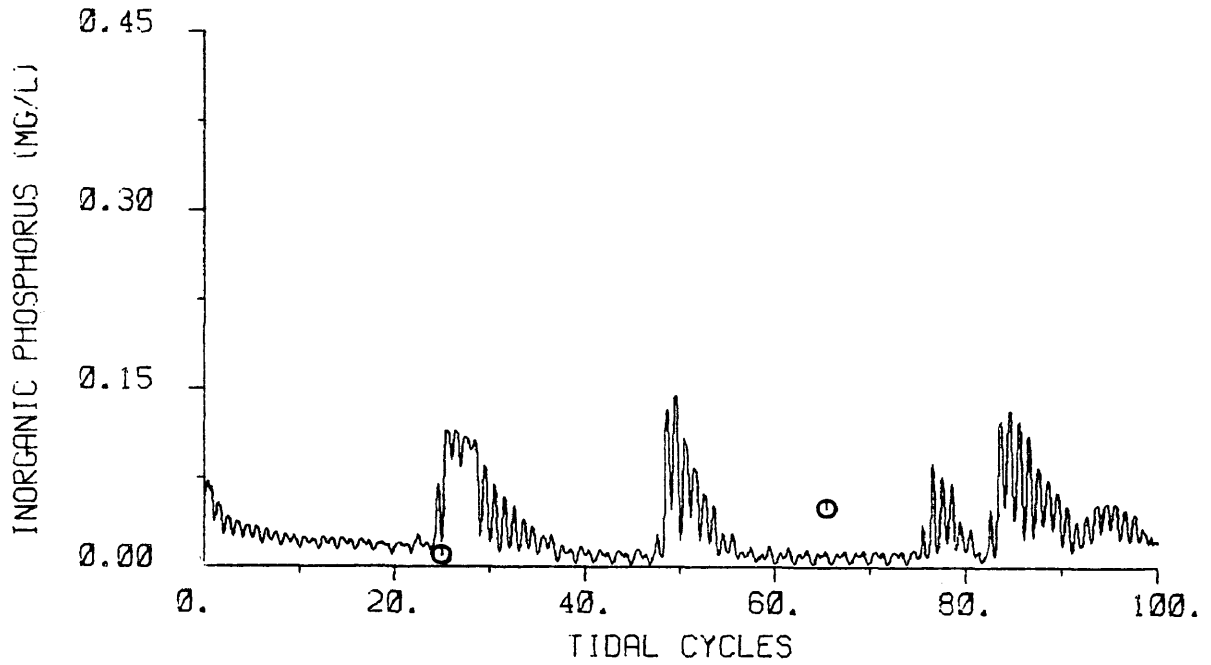


Figure A9. Validation results for inorganic phosphorus - station 4.

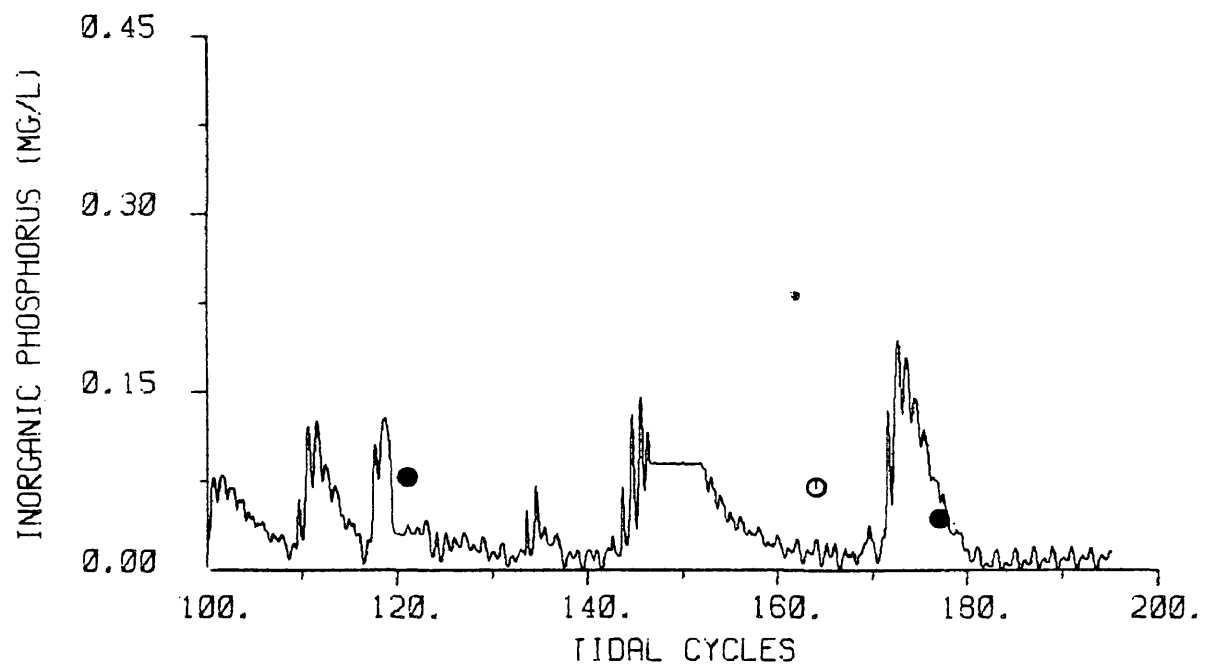
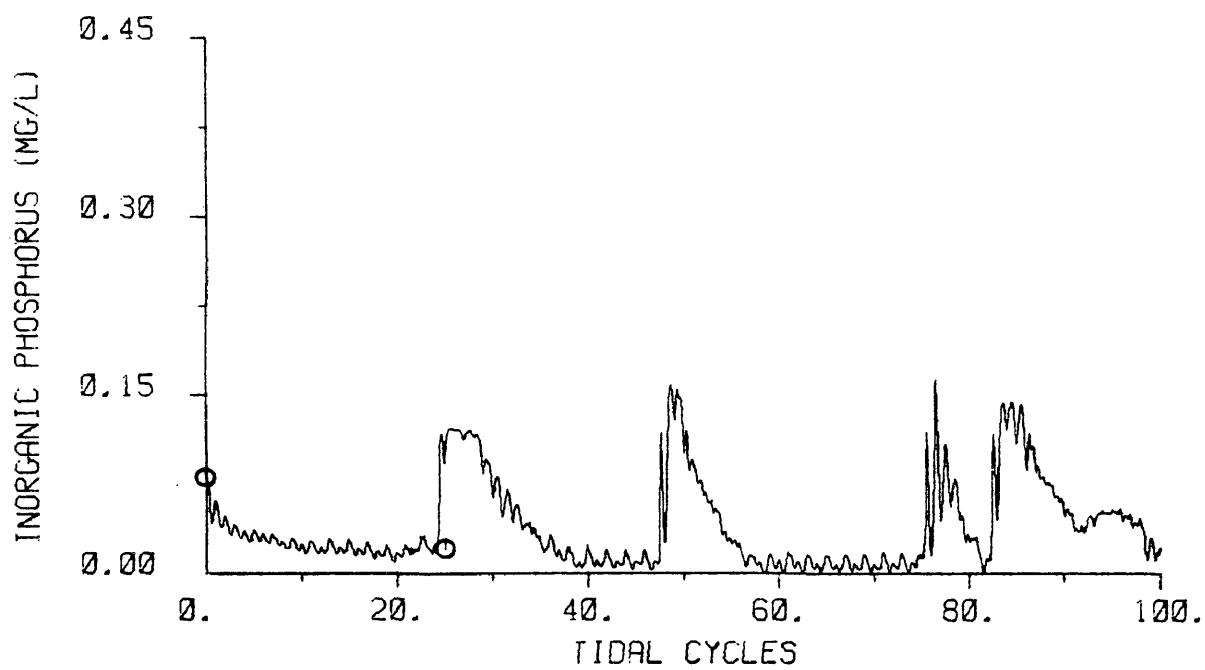


Figure A10. Validation results for inorganic phosphorus - station 5.

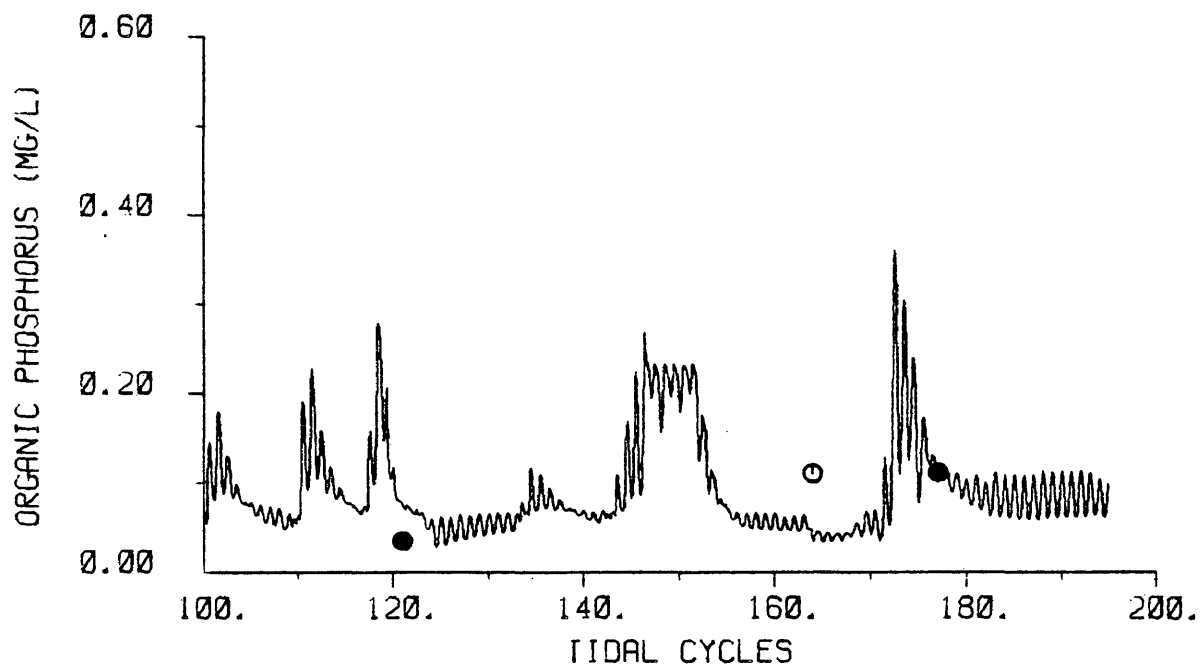
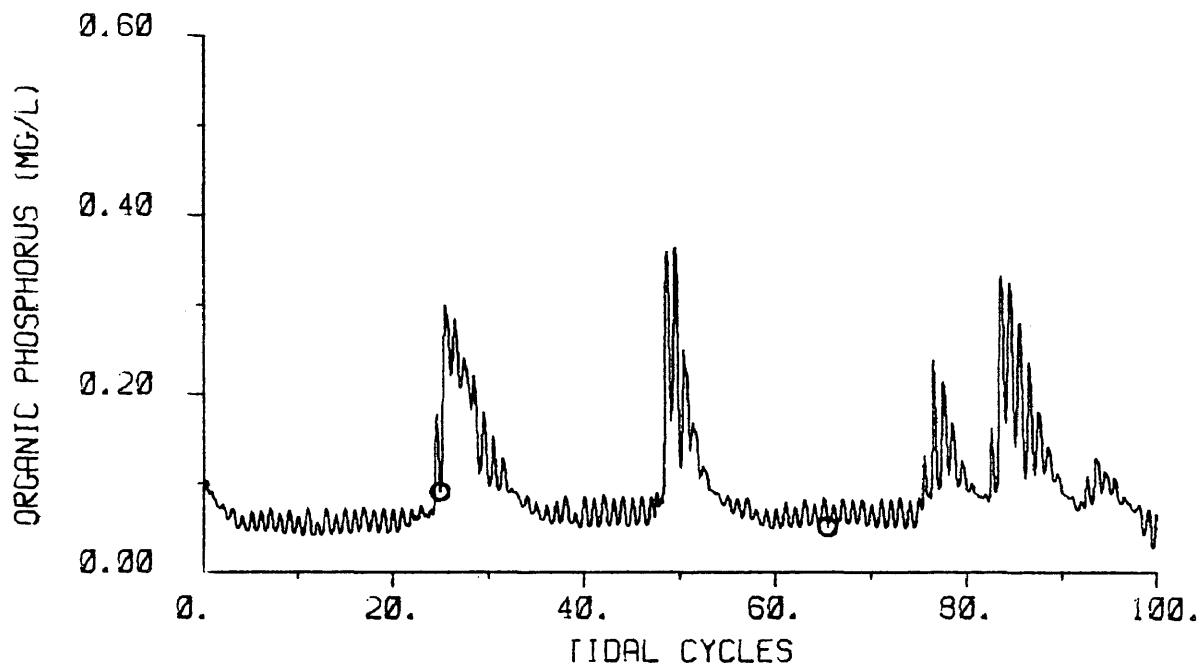


Figure A11. Validation results for organic phosphorus - station 4.

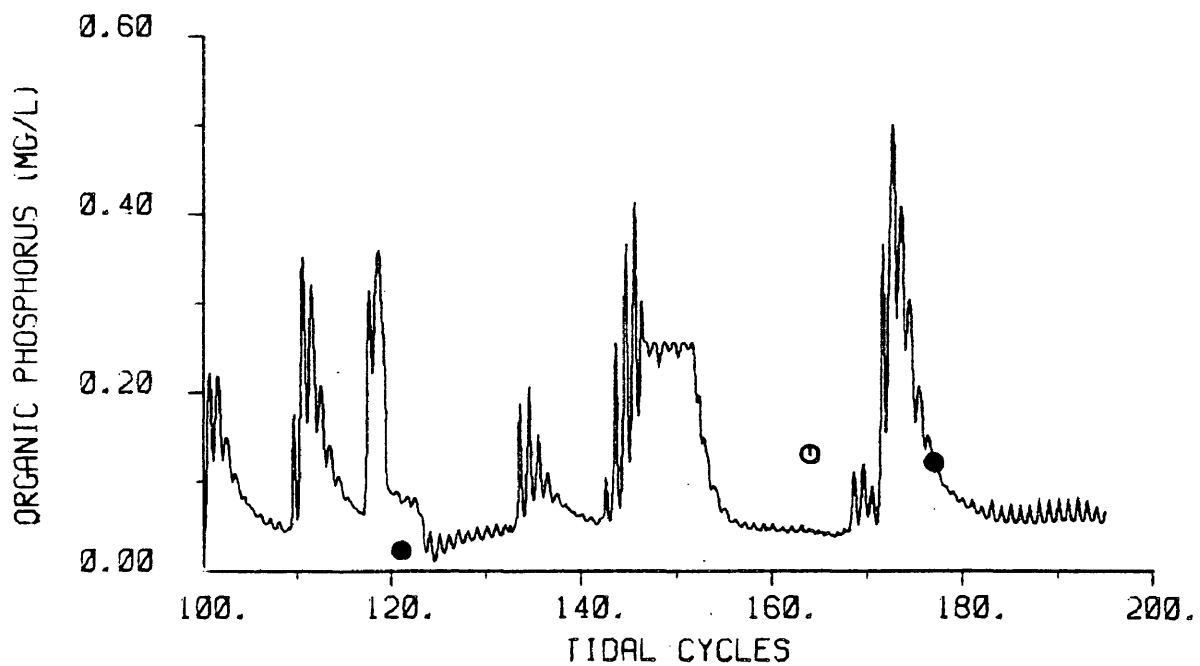
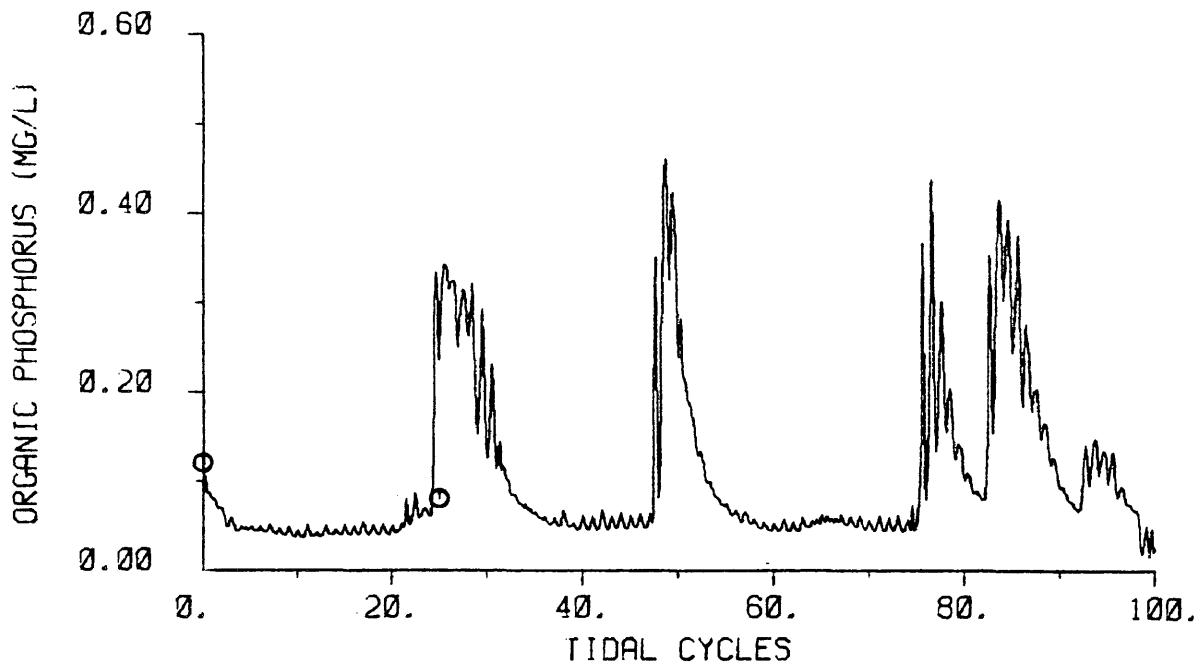


Figure A12. Validation results for organic phosphorus - station 5.

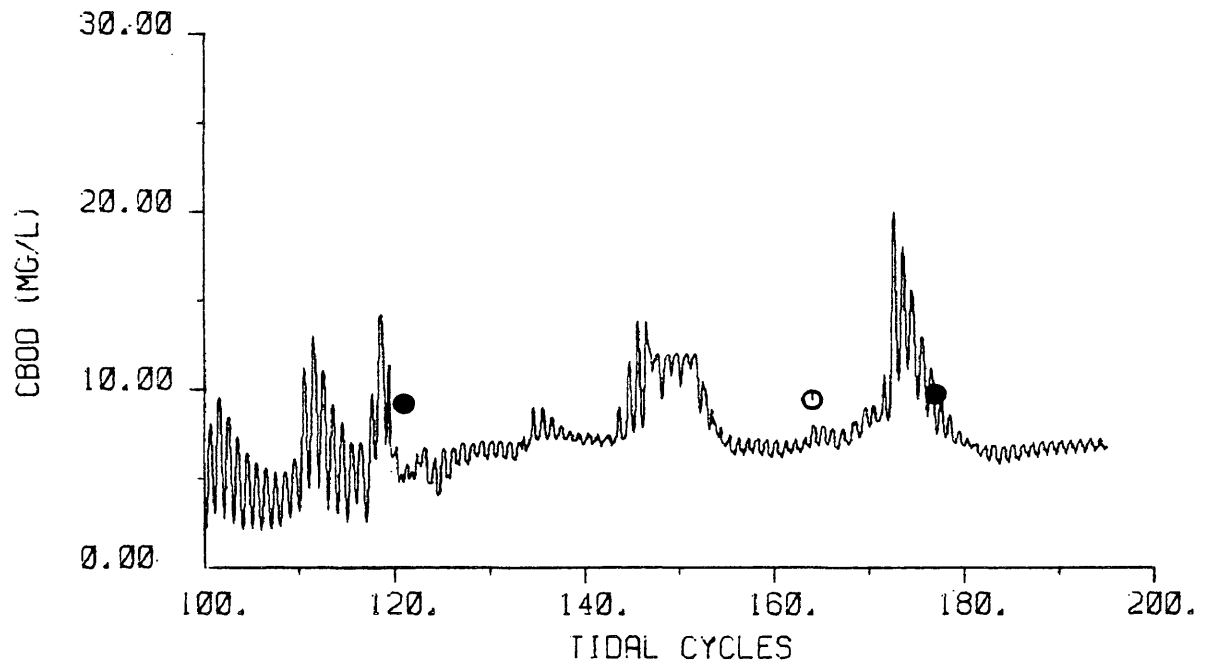
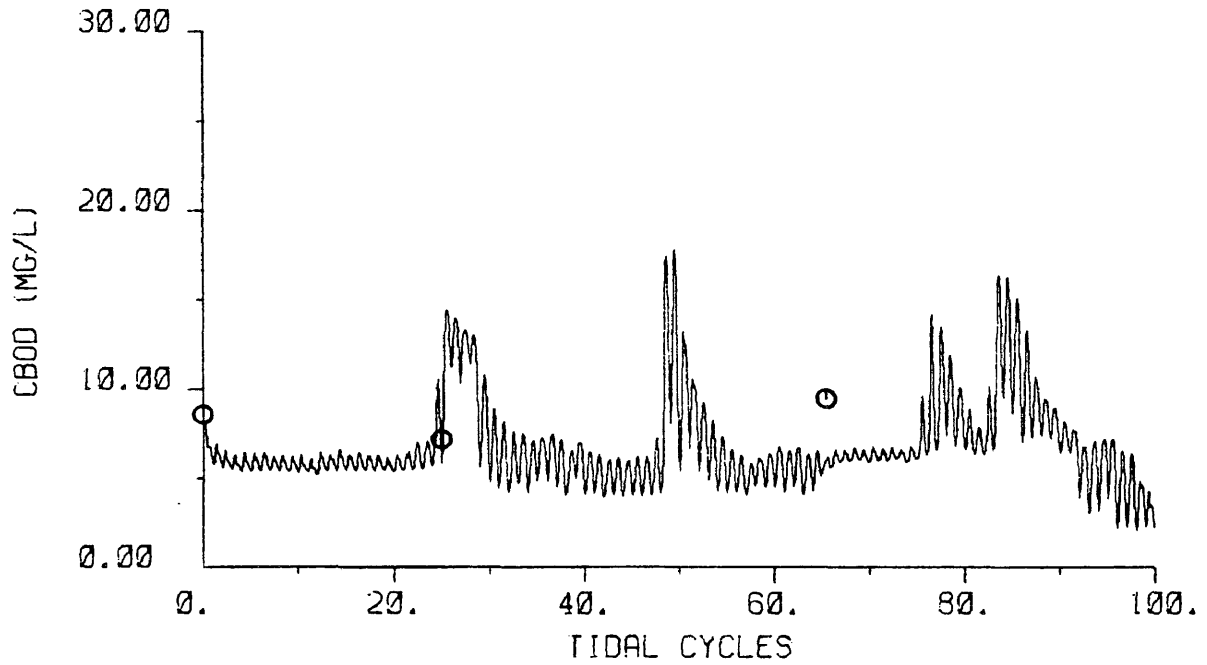


Figure A13. Validation results for CBOD - station 4.

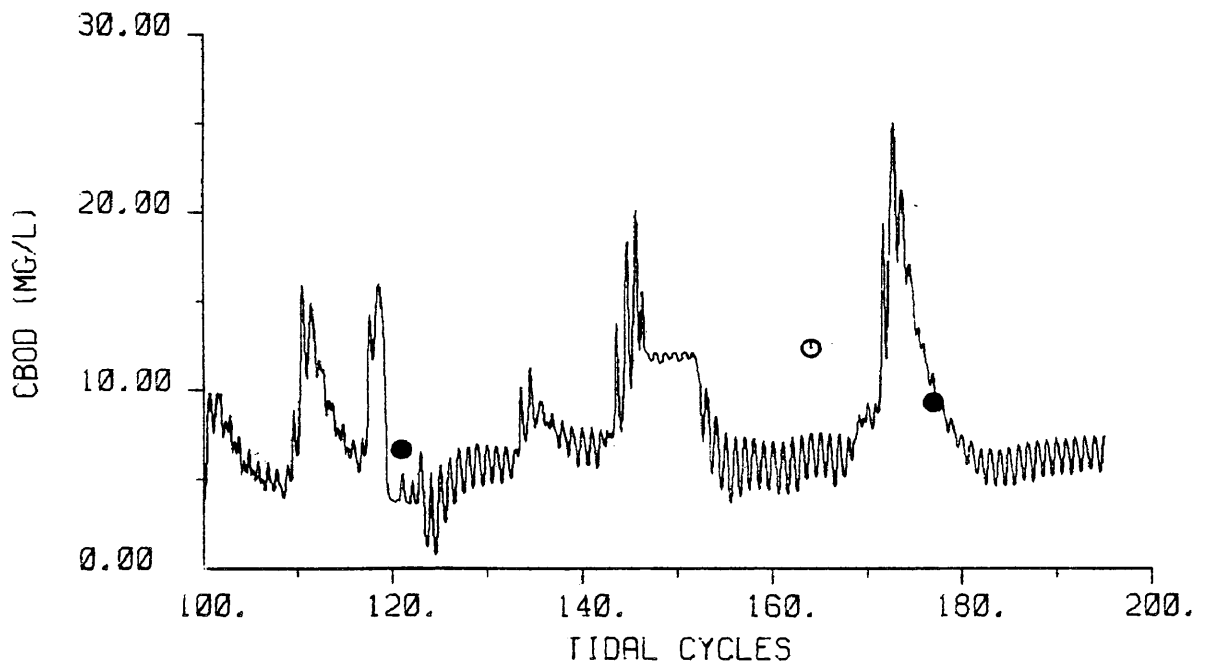
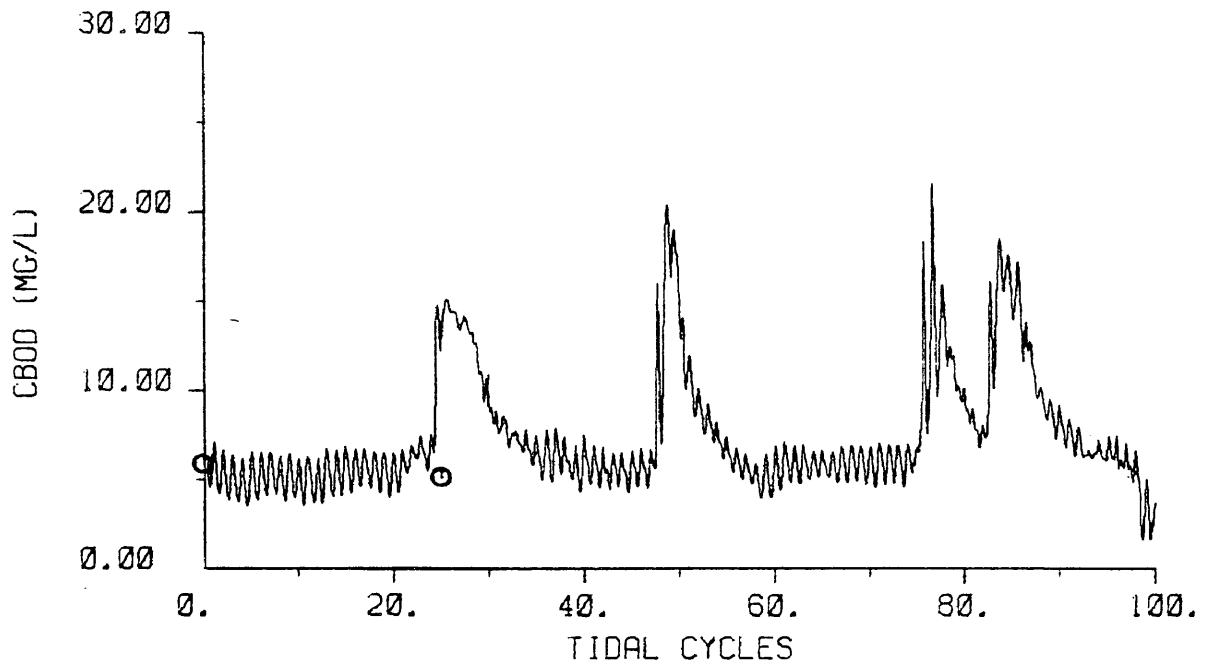


Figure A14. Validation results for CBOD - station 5.

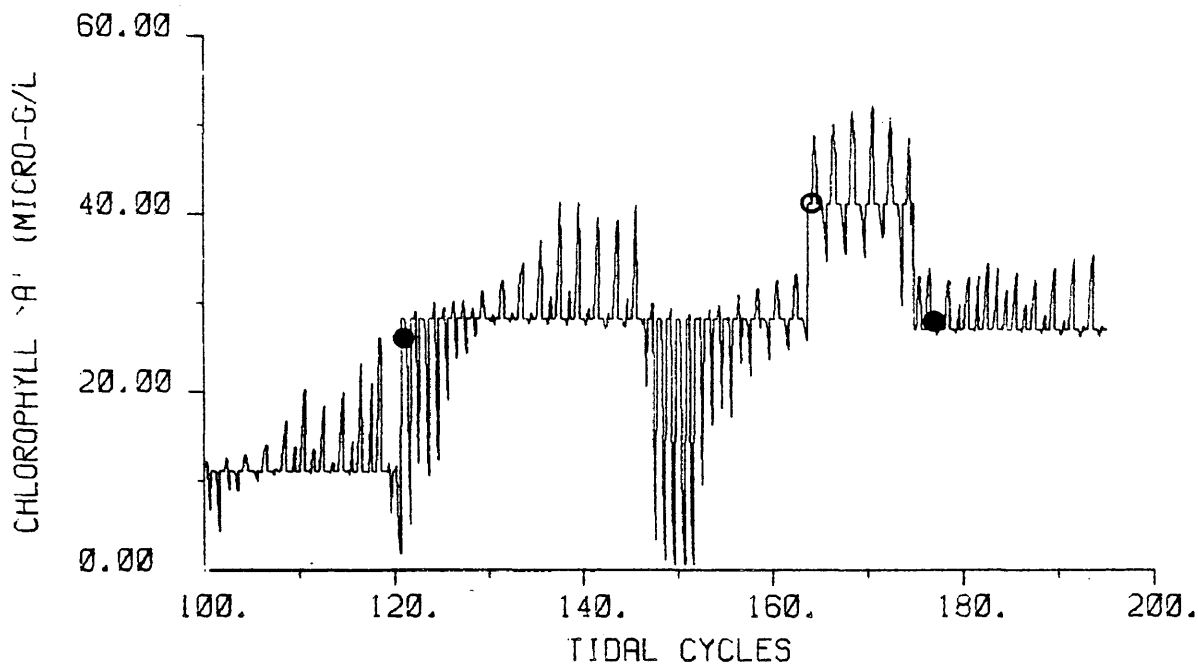
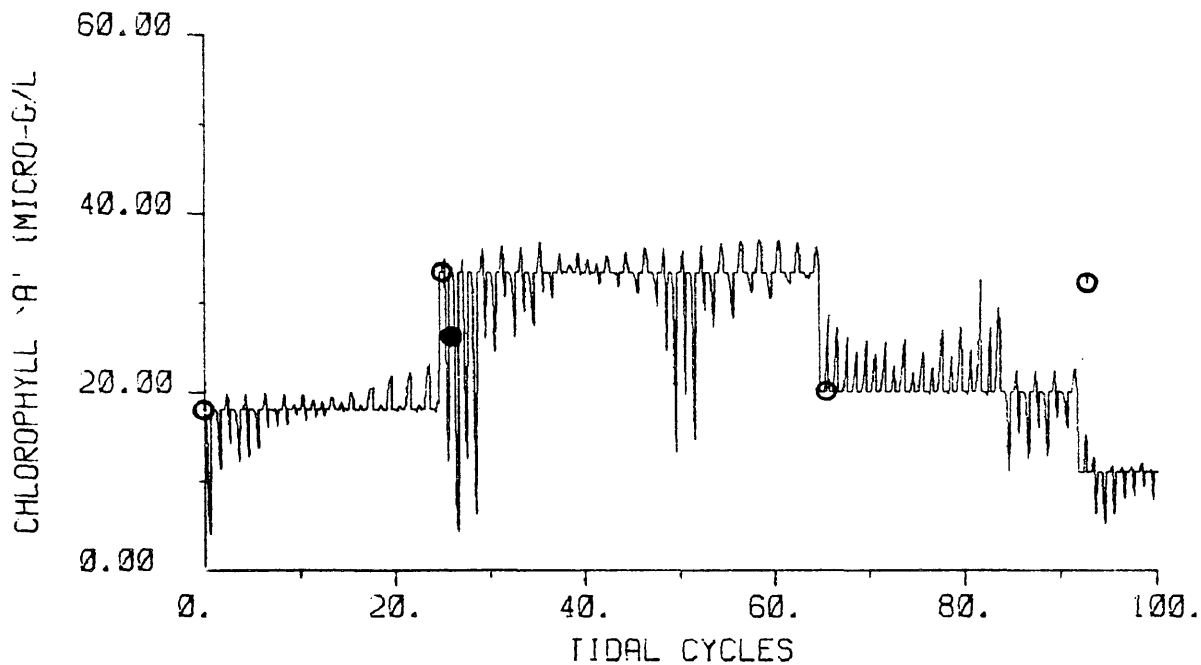


Figure A15. Validation results for chlorophyll 'a' - station 2.

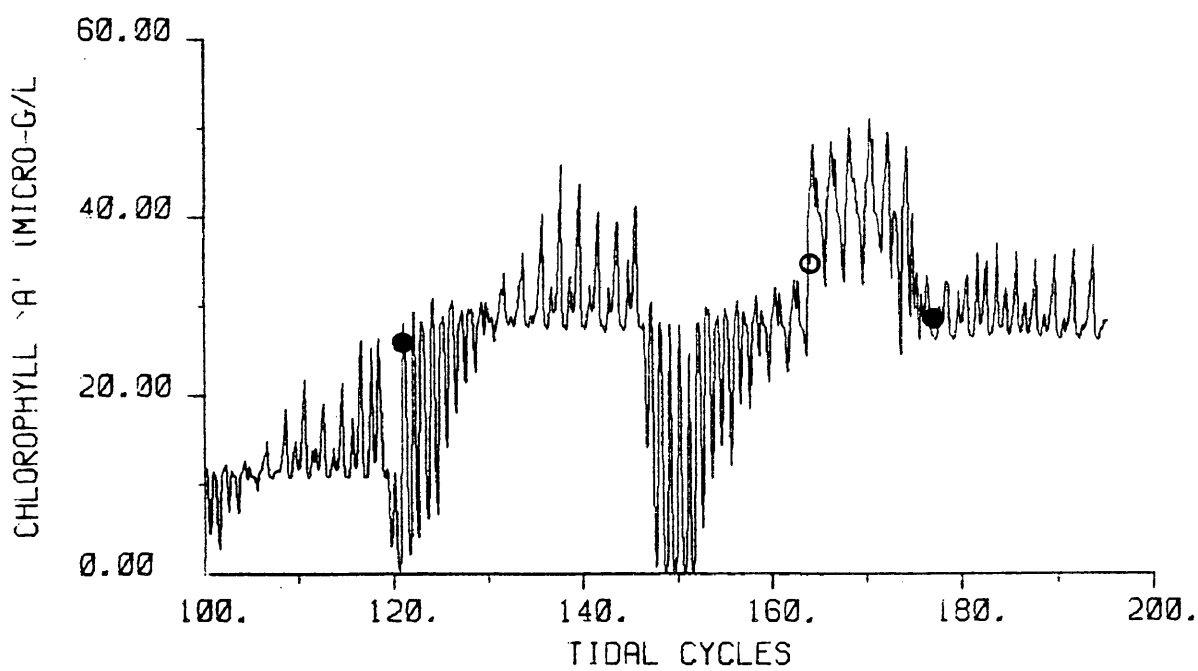
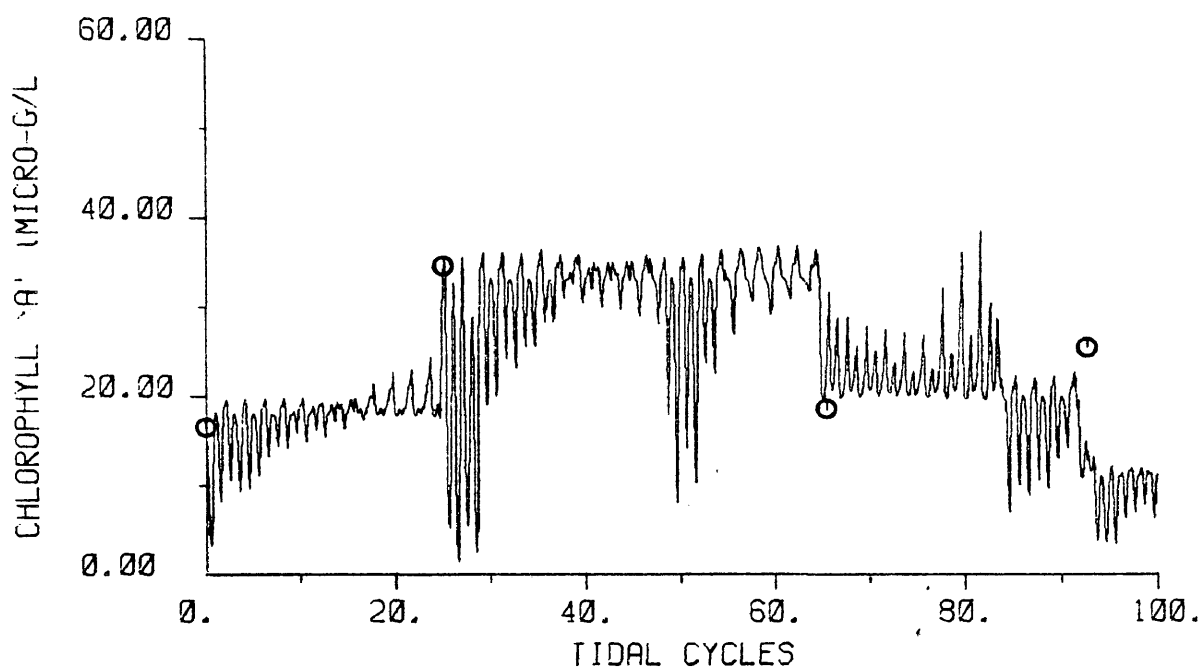


Figure A16. Validation results for chlorophyll 'a' - station 3.

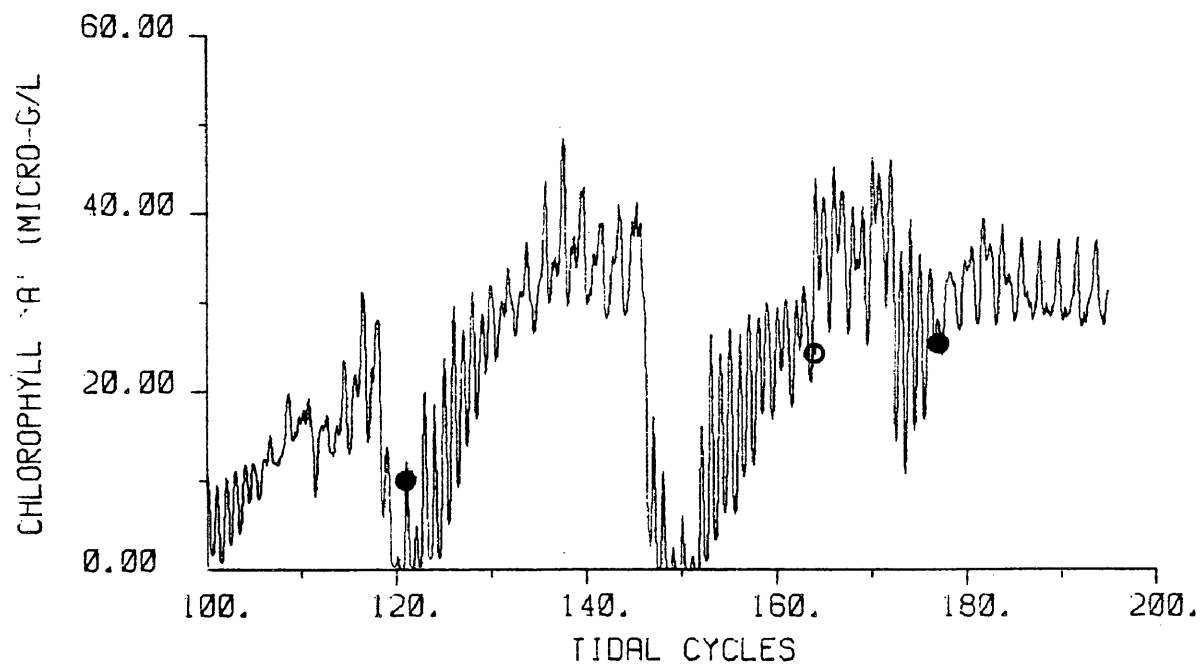
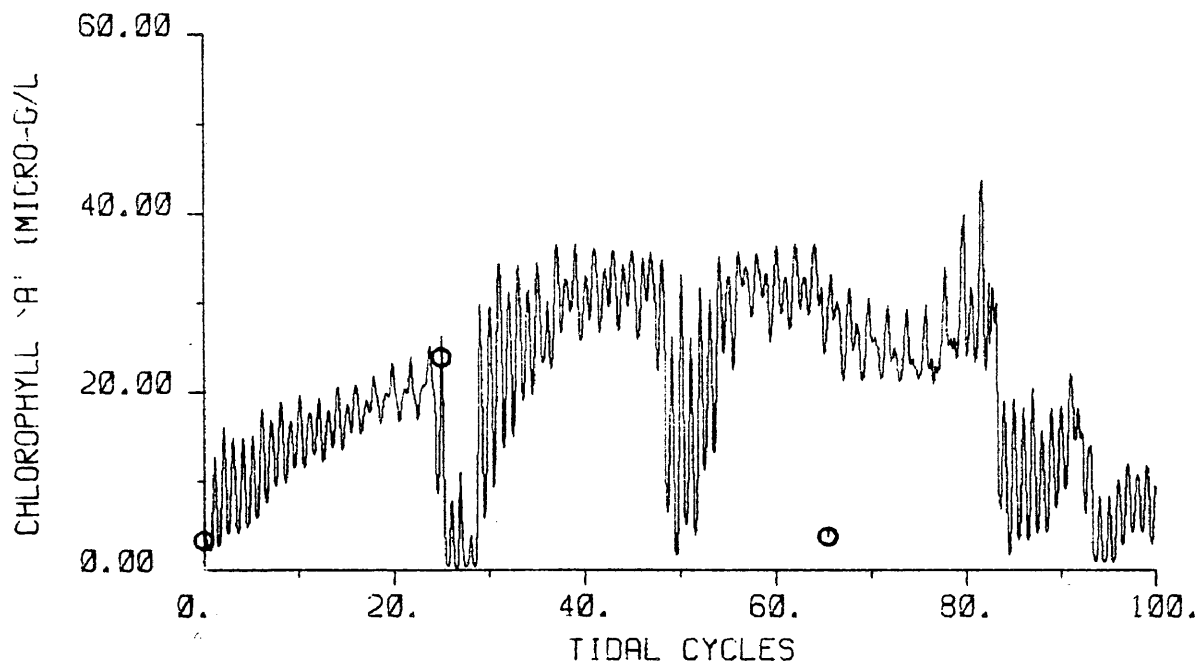


Figure A17. Validation results for chlorophyll 'a' - station 4.

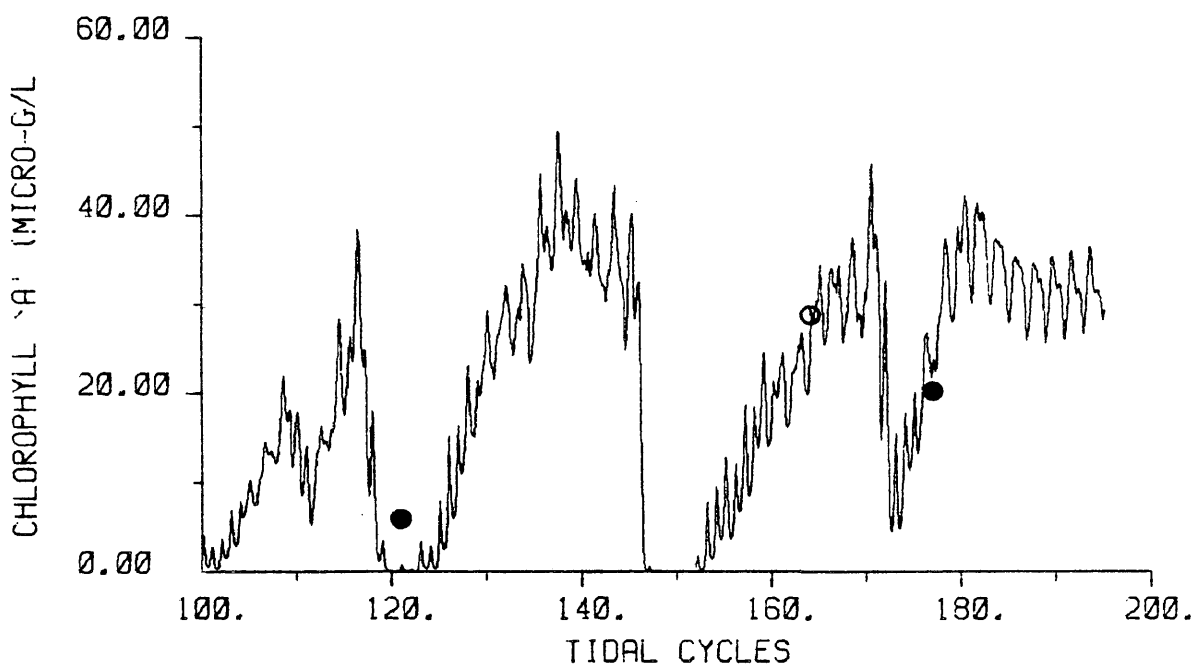
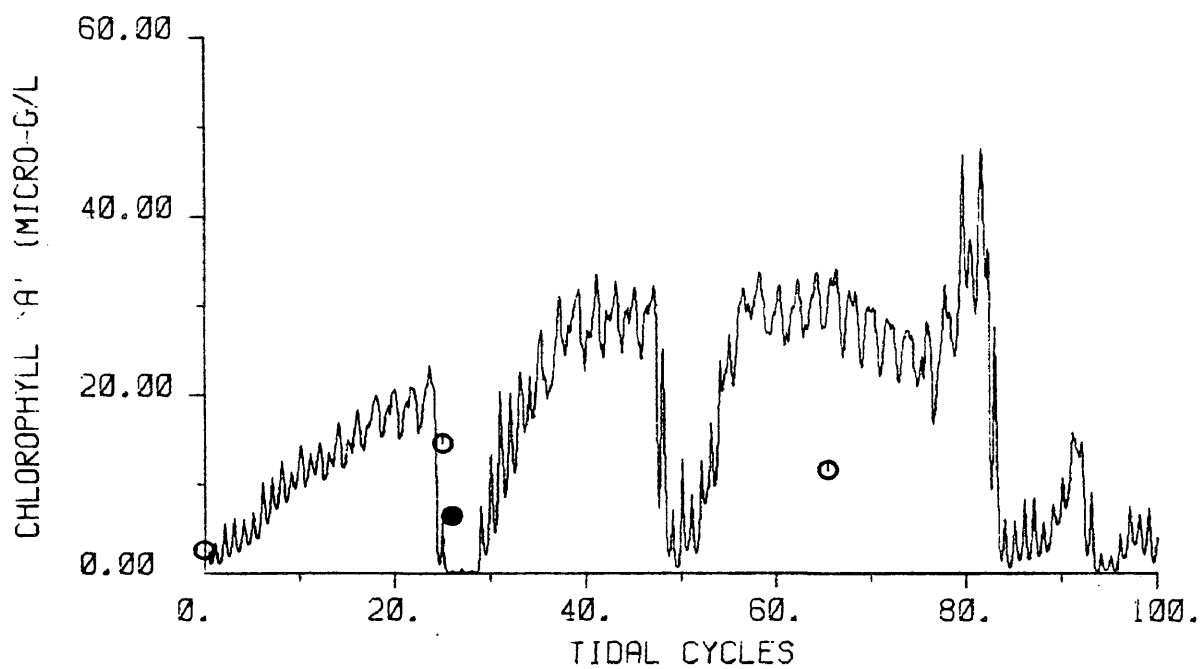


Figure A18. Validation results for chlorophyll 'a' - station 5.

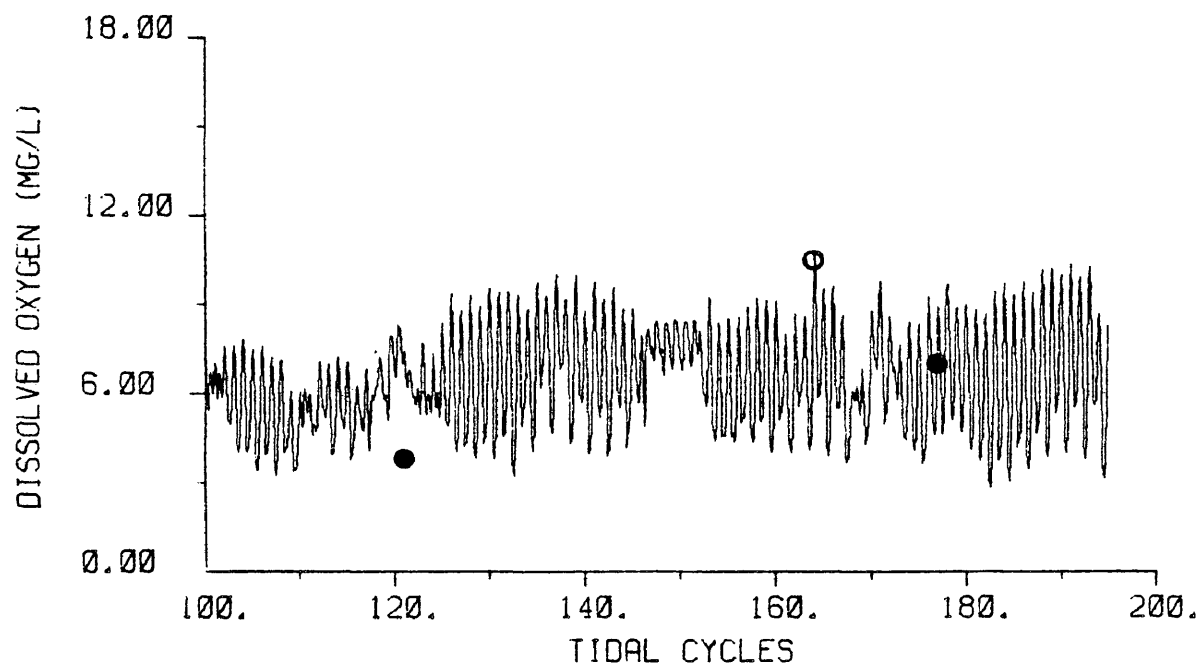
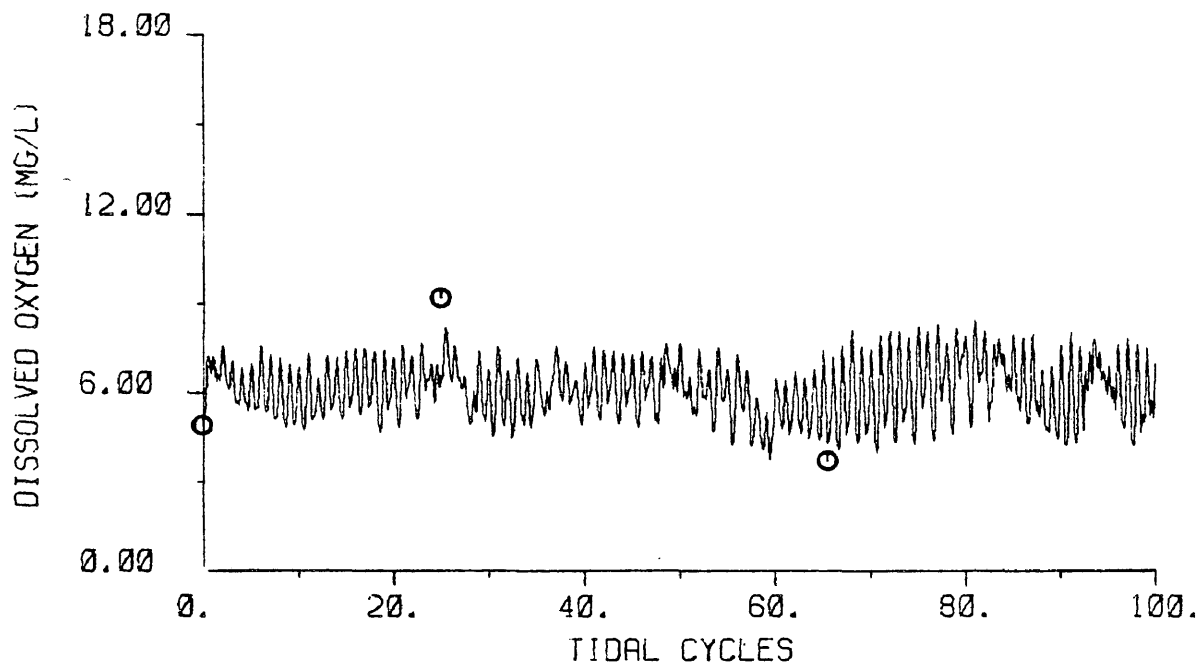


Figure A19. Validation results for dissolved oxygen - station 4.

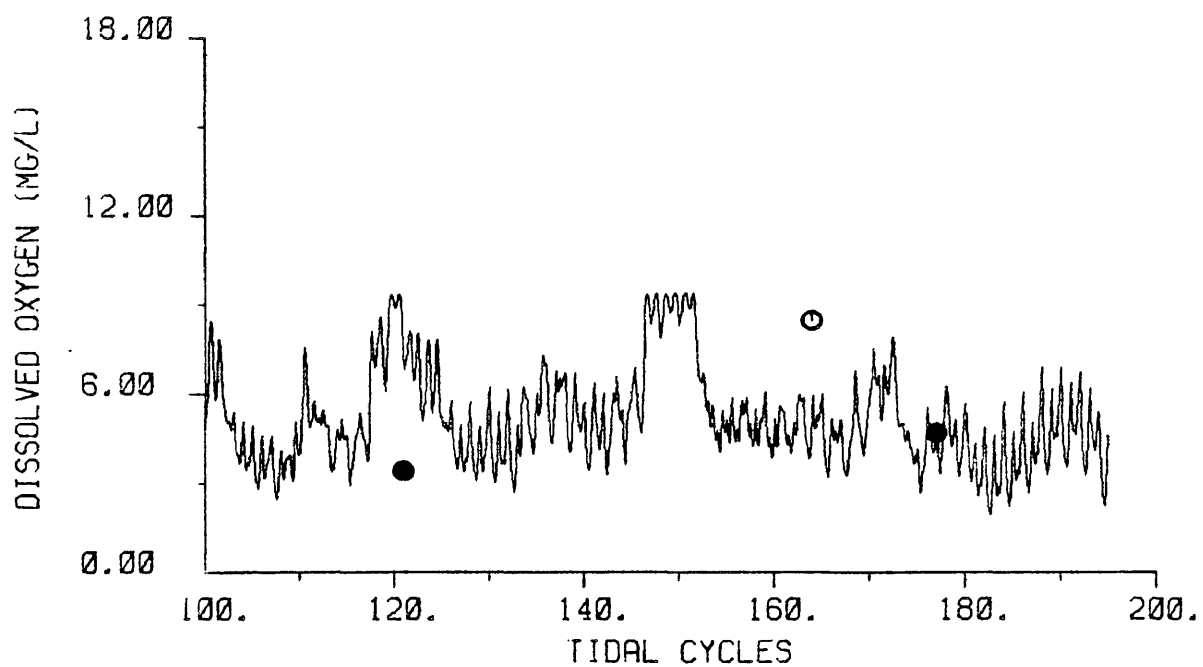
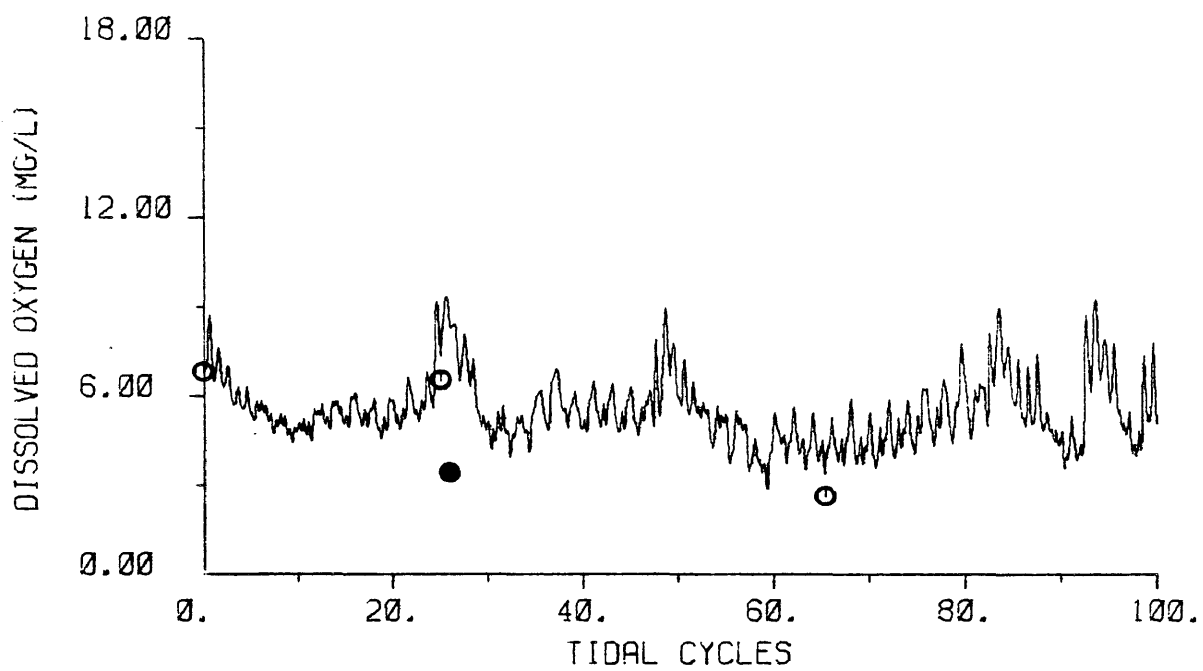


Figure A20. Validation results for dissolved oxygen - station 5.

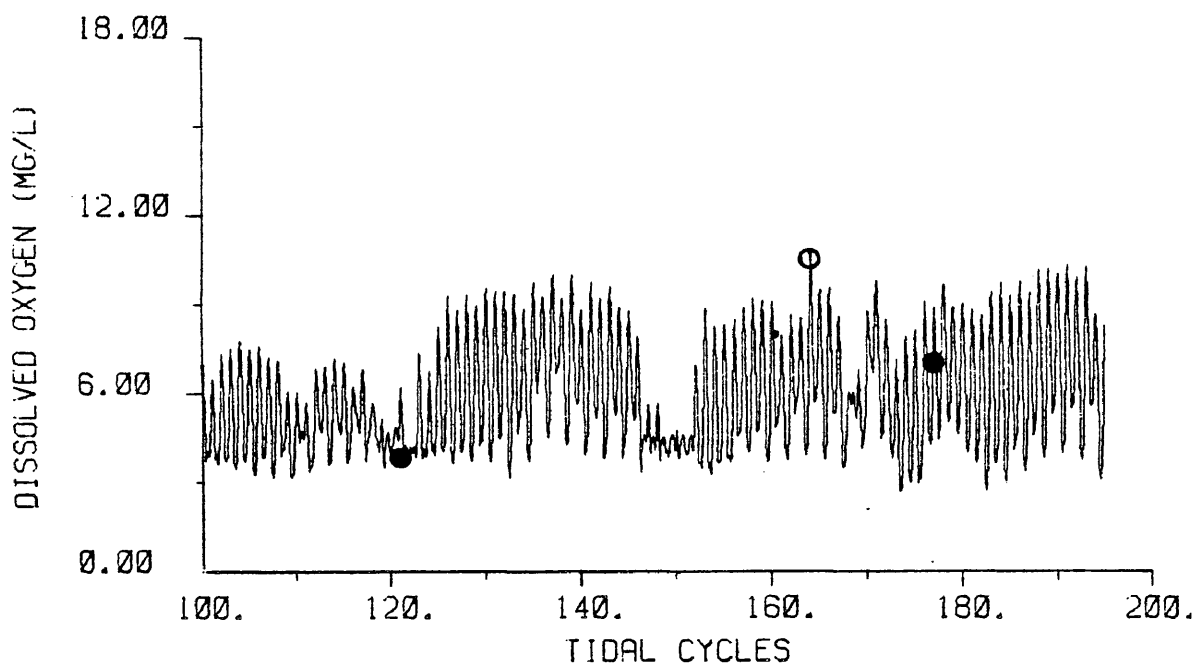
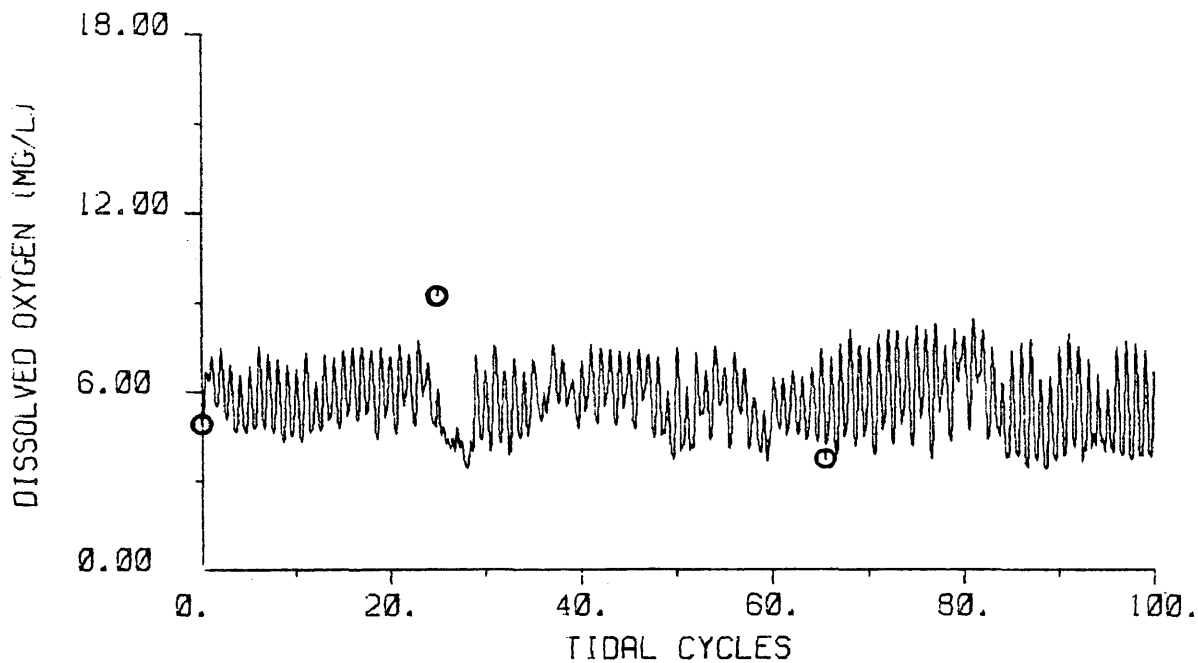


Figure A21. Long-term simulation: nonpoint DO concentrations set to 4.2 mg/l - station 4.

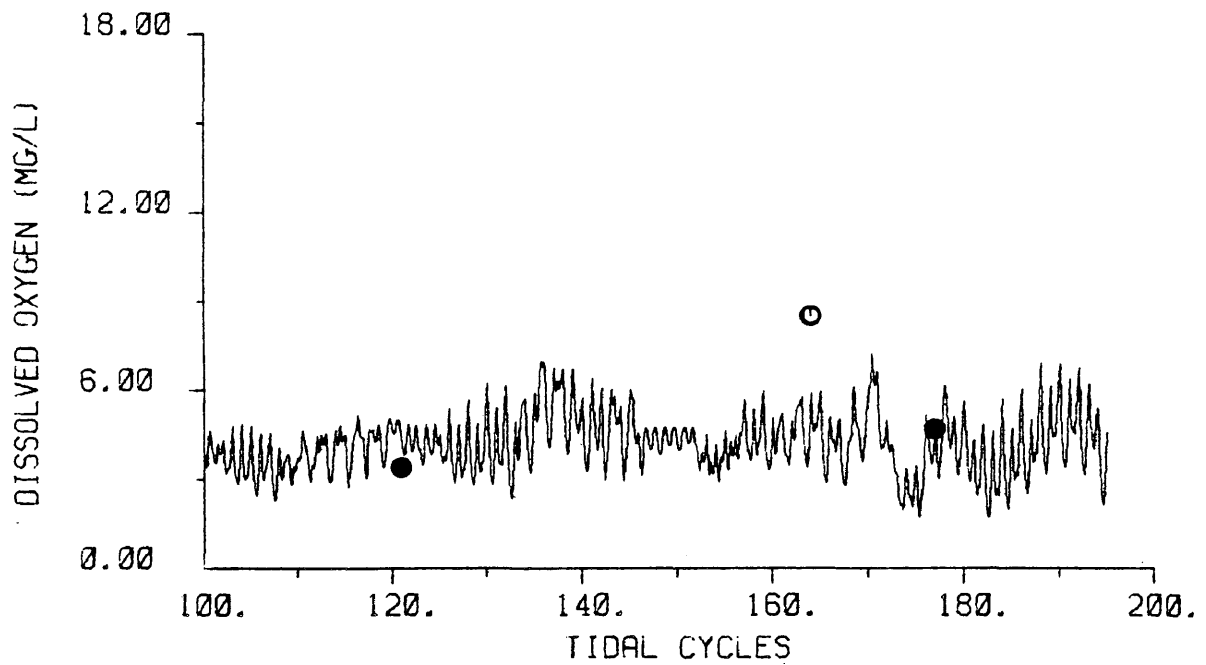
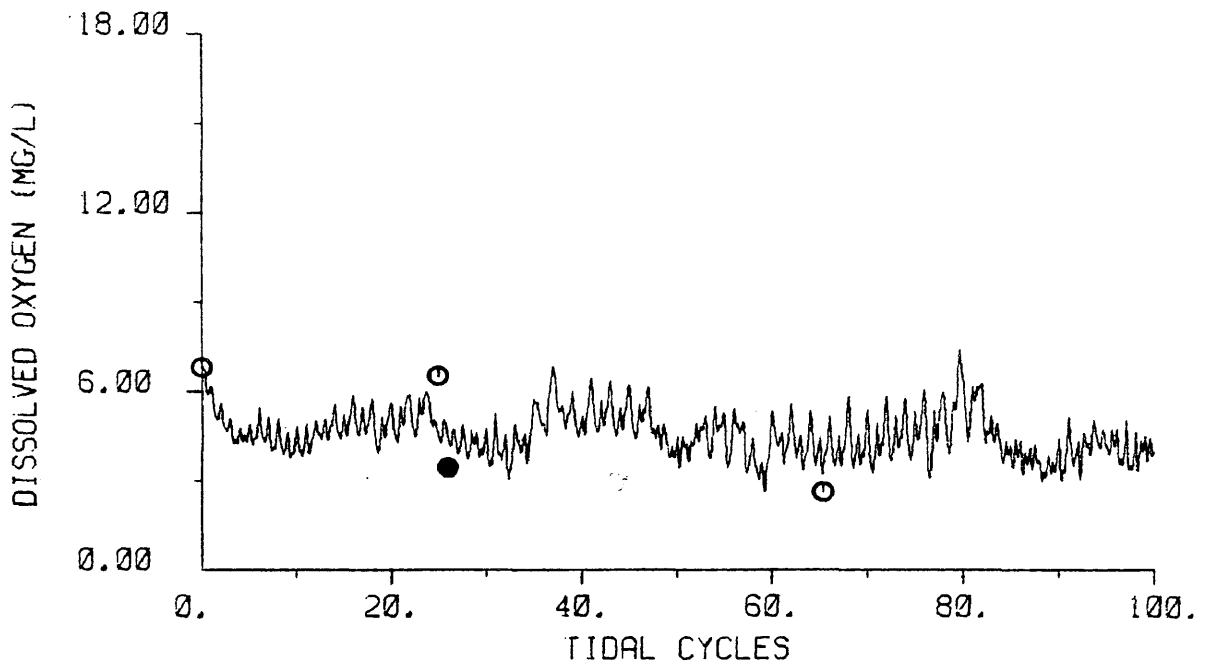


Figure A22. Long-term simulation: nonpoint DO concentrations set to 4.2 mg/l - station 5.

REFERENCES

- Aris, R., 1956. "On the dispersion of a solute flowing through a tube." Proc. Roy. Soc. London (A), 235. April, 1956.
- Carritt, D. E. and E. J. Green, 1967. "New Tables for Oxygen Saturation in Seawater." J. of Mar. Res., Vol. 25, No. 2.
- Cerco, C. F. and A. Y. Kuo, 1981. Water Quality in a Virginia Potomac Embayment: Hunting Creek - Cameron Bay. Special Rep. No. 244, Va. Inst. of Mar. Sci.
- Champ, M. A., O. Villa and R. C. Bubeck, 1981. "Historical overview of the freshwater inflow and sewage treatment plant discharges to the Potomac River Estuary with resultant nutrient and water quality trends." Proc. of the Nat. Symp. on Freshwater Inflow to Estuaries. USDO I, GPO-FWS/OBS-8104.
- Cox, G. C. and S. A. Macola, 1967. "Predicting salinity in an estuary." ASCE Conference Preprint No. 433, Env. Eng. Conf., Dallas, Texas. February, 1967.
- DiToro, D. M., D. J. O'Conner and R. V. Thomann, 1970. A dynamic model of phytoplankton populations in natural waters. Env. Eng. and Sci. Prog., Manhattan College, Bronx, N.Y.
- DiToro, D. M., D. J. O'Conner and R. V. Thomann, 1971. "A Dynamic Model of the Phytoplankton Population in the Sacramento - San Joaquin Delta." Adventures in Chemistry Series, No. 106, Amer. Chem. Soc.
- Dobbins, W. E., 1964. "BOD and oxygen relationships in streams." Proc. ASCE, 95, No. HY4 (July).
- Dronkers, J. J., 1964. Tidal Computation in Rivers and Coastal Waters. New York, Interscience North-Holland Publ. Co.
- Edwards, R. W. and H. L. J. Rolley, 1965. "Oxygen Consumption of River Muds." J. Ecol., 53.
- Elmer, H. L. and W. F. West, 1961. "Effect of Water Temperature on Stream Reaeration." Proc. ASCE, 87 (SA6).

- Fang, C. S., A. Y. Kuo, P. V. Hyer and W. J. Hargis, Jr., 1973. Hydrography and Hydrodynamics of Virginia Estuaries IV. Mathematical Model Studies of Water Quality in the James River Estuary. Special Rep. 41, Va. Inst. of Mar. Sci.
- Harleman, D. R. F., 1971. "One-Dimensional Models." In Estuarine Modelling: An Assessment. Tracor, Inc.
- Harleman, D. R. F. and G. Abraham, 1966. One-dimensional analysis of salinity intrusion in the Rotterdam Waterway. Publ. No. 44, October, Delft Hydraulics Laboratory, Raam 61, Delft, The Netherlands.
- Harleman, D. R. F. and C. H. Lee, 1969. The Computation of Tides and Currents in Estuaries and Canals. Tech. Bull. No. 16, Committee on Tidal Hydraulics, Corp. of Eng., U. S. Army.
- Holley, E. R. and D. R. F. Harleman, 1965. Dispersion of pollutants in estuary type flows. Tech. Rep. No. 74, Hydraulics Lab., MIT.
- Hydrocomp, Inc., 1977. Hydrocomp Simulation Programming: Water Quality Simulations Operations Manual. Palo Alto, Calif.
- Hyer, P. V., A. Y. Kuo, and B. J. Nielson, 1977. Water Quality Models of Back and Poquoson Rivers, Virginia. Special Rep. No. 144, Va. Inst. of Mar. Sci.
- Ippen, A., 1966. Estuary and Coastline Hydrodynamics. McGraw-Hill Book Co., Inc., N. Y.
- Ketchum, B. H., 1951. "The flushing of tidal estuaries." Sewage and Industrial Wastes, Vol. 23.
- Koh, R. C. Y. and L. N. Fan, 1970. Mathematical Models for the Prediction of Temperature Distribution Resulting From the Discharge of Heated Water into Large Bodies of Water. USEPA, Water Quality Office, WPCR Series 16130 DWO 10/70, Washington, D. C.
- Kremer, J. N. and S. W. Nixon, 1978. A Coastal Marine Ecosystem - Simulation and Analysis. Springer-Verlag, Germany.
- Kuo, A. Y., 1976. "A Model of Tidal Flushing for Small Coastal Basins." Proc. of the Conf. on Env. Modeling and Simulation. EPA 600/9-76-016 July, 1976, USEPA, Washington, D. C.
- Kuo, A. Y. and C. S. Fang, 1972. "A mathematical model for salinity intrusion." Proc. 13th Coastal Eng. Conf., Amer. Soc. Civil Eng.

- Kuo, A. Y., P. V. Hyer and C. S. Fang, 1975. Hydrography and Hydrodynamics of Virginia Estuaries VI. Mathematical Model Studies of Water Quality of the Rappahannock Estuary. Special Rep. No. 102, Va. Inst. of Mar. Sci.
- Kuo, A. Y., P. V. Hyer and C. S. Fang, 1979. Manual of Water Quality Models for Virginia Estuaries. Special Rep. No. 214, Va. Inst. of Mar. Sci.
- Lin, F., 1975. "A one-dimensional mathematical model of tidal hydraulics and salt intrusion in estuarine rivers." Masters Thesis, Va. Inst. of Mar. Sci.
- Nielson, B. J., 1977. A Layman's Guide to Models of the Tidal Waters of Virginia. Special Rep. No. 150, Va. Inst. of Mar. Sci.
- Northern Virginia Planning District Commission, 1979. Occoquan Basin Computer Model: Summary of Calibration Results. Falls Church, Va.
- O'Conner, D. J., 1966. "An analysis of the dissolved oxygen distribution in the East River." J. WPCF, 38, No. 11 (November).
- O'Conner, D. J. and D. M. DiToro, 1964. "The solution of the continuity equation in cylindrical coordinates with dispersion and advection for an instantaneous release." Proc. Sym. in Diffusion in Ocean and Fresh Waters, Lamont Geol. Obs., Columbia Univ., Palisades, N. Y.
- O'Conner, D. J. and W. E. Dobbins, 1958. "Mechanism of Reaeration in Natural Streams." Trans. Am. Soc. of Civil Eng., Vol. 123.
- Okubo, A., 1964. "Equations describing the diffusion of an introduced pollutant in a one-dimensional estuary." Studies on Oceanography, Univ. of Tokyo Press.
- Onishi, Y. and S. E. Wise, 1978. "Mathematical Modeling of Sediment and Contaminant Transport in the James River Estuary." Proc. 26th Annual ASCE Hydraulics Division Speciality Conf. on Verification of Mathematical and Physical Models in Hydraulic Eng., College Park, Md.
- Pritchard, D. W., 1952. "Salinity distribution and circulation in the Chesapeake Bay estuarine system." J. Mar. Res., 11, No. 2.
- Pritchard, D. W., 1954. "A study of the salt balance in a coastal plain estuary." J. Mar. Res., 13, No.1.

- Streeter, H. W. and E. B. Phelps, 1925. A study of the pollution and natural purification of the Ohio River. U. S. Public Health Service, Public Health Bull. 146.
- Taylor, G. I., 1954. "The dispersion of matter in turbulent flow through a pipe." Proc. Roy. Soc. London (A), 223 (May, 1954).
- Thatcher, M. L. and D. R. F. Harleman, 1972. A Mathematical Model for the Prediction of Unsteady Salinity Intrusion in Estuaries. Ralph M. Parson Lab. Rep. 144, MIT.
- Thomann, R. V., 1963. "Mathematical Model for Dissolved Oxygen." J. Sanit. Eng. Div., Proc. ASCE, 83, SA5 (October, 1963).
- Thomann, R. V., 1972. Systems Analysis and Water Quality Management. Environmental Science Services Div., Environmental Research and Applications, Inc., New York.
- Thomann, R. V., D. J. O'Conner and D. M. DiToro, 1970. "Modeling of the nitrogen and algal cycles in estuaries." Proc. 5th Int. Water Poll. Res. Conf., San Francisco, Ca.
- Tracor, Inc., 1971. Estuarine Modeling : An Assessment. EPA 1607DZV 02/71.
- Tully, J. P., 1949. Oceanography and Prediction of Pulp Mill Pollution in Alberni Inlet. Bull. No. LXXXIII, Fisheries Research Board of Canada.
- van Kessel, J. F., 1977. "Removal of Nitrate from Effluent Following Discharge on Surface Water." Water Research, Vol. 11.

VITA

Stephen Anthony Williams

Born in New Bern, North Carolina on April 24, 1952. Attended public schools in Gaffney, South Carolina. Obtained a Bachelor of Science in Marine Science from the University of South Carolina - Coastal Carolina Campus, Conway, South Carolina (1979). Entered graduate studies at the College of William and Mary, School of Marine Science in September, 1979. Graduate Assistant, Department of Physical Oceanography and Hydraulics, School of Marine Science until April, 1983.